9

Ground Water in the Hydrologic Cycle

Ground water is water under positive (i.e., greater than atmospheric) pressure in the saturated zone of earth materials. The water table is the fluctuating upper boundary of the ground-water zone at which pressure is atmospheric (denoted on diagrams by the **hydrat** symbol, ⏚). Figure 9.1 shows the general relations between ground water and surface water. Most water enters the ground-water reservoir when infiltrated water arrives at the **water table** as **recharge**; recharge can also occur by horizontal or vertical seepage from surface-water bodies. Under natural conditions ground water eventually discharges into rivers or lakes or, in coastal areas, directly into the ocean; water can also leave the ground-water reservoir by moving upward from the water table into the capillary fringe and thence into the unsaturated zone, where it is subject to evapotranspiration.

Ground water constitutes about 30% of the world's total fresh water and 99% of its total stock of liquid fresh water (table 2.5). As with all hydrologic stocks, ground water is in continual motion, albeit slow (typically much less than 1 m/d). Using the values from figure 2.20 in equation (1.25), one can calculate that the overall residence time for the global ground-water reservoir is about 235 yr; for moderate- to large-scale regional flow systems in various parts of the world residence time varies from a few years to 1,000 years or more. In spite of its slow pace, ground water is a crucial link in the hydrologic cycle because it is the source of most of the water in rivers and lakes.

Ground water is, of course, also important as the direct source of water withdrawn for domestic water use, irrigation, and industrial uses worldwide. In the United States, about one-fourth of the water used for these purposes comes from ground water, and the proportion is much higher for many regions; concern about the quantity and quality of ground water is one of the major water-resource issues in many parts of the world.

The material properties of porous media were described in sections 7.1 and 7.2, and the basic physics of ground-water flow were developed in section 7.3. For convenience, the basic equations and concepts of ground-water flow are summarized in box 9.1 on p. 391.

Our focus in this chapter is on ground water as a link in the hydrologic cycle. We will examine the effects of topography and geology on natural ground-water flows in drainage basins; how ground water in-

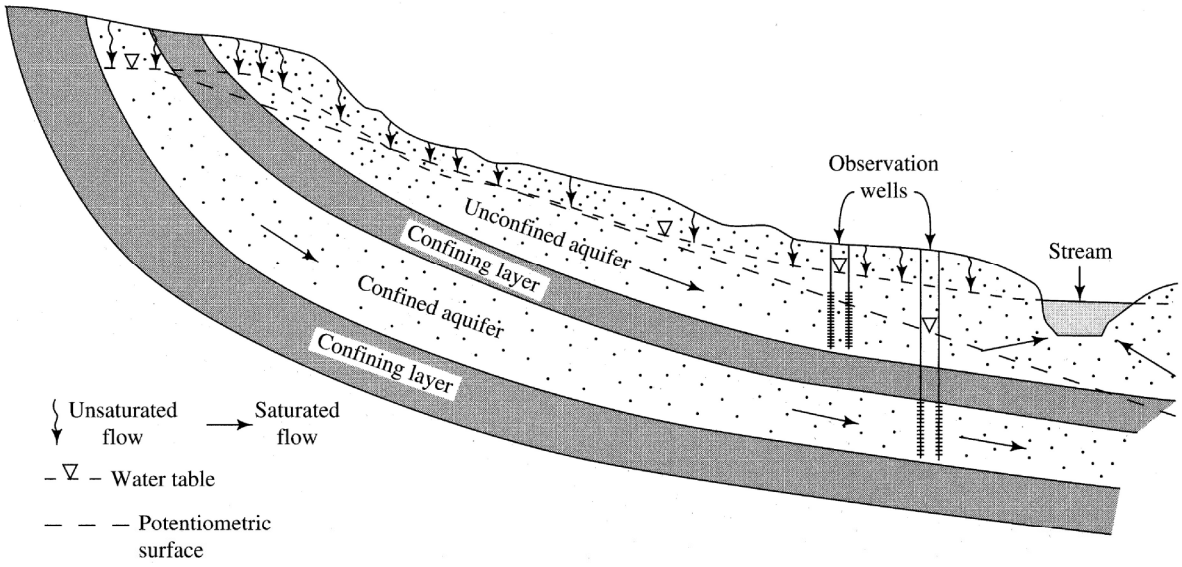

Figure 9.1 Unconfined and confined aquifers in a region of folded sedimentary rocks. Note relations of water levels in wells penetrating unconfined and confined aquifers.

teracts with streams, lakes, wetlands, and the ocean; the role of ground water in the drainage-basin water balance; and approaches to the quantitative evaluation of components of the ground-water budget. We will also briefly examine the hydraulics of wells, how human use of ground water affects the basin water balance, and the concept of "safe yield." We do not explore the chemical evolution of ground water or its relation to geotechnical problems or geologic processes; these topics are well covered in many texts devoted exclusively to hydrogeology (e.g., Freeze and Cherry 1979; Fetter 2001).

9.1 Aquifers and Aquitards

9.1.1 Definitions

A **geologic formation** is a regionally extensive, mappable geologic unit with a characteristic lithology. For our purposes, an **aquifer** is a formation that can store enough water and transmit it at a rate fast enough to be hydrologically significant. A given aquifer has reasonably uniform water-storage and transmitting properties, and the ground-water movement within it can be considered to be the flow field induced by a single coherent potential-energy field.

Formations that do not transmit water at hydrologically significant rates are called **aquitards**. The term **aquiclude** is sometimes used to describe an "impermeable" formation, but it is now recognized that few, if any, geologic materials are strictly impermeable.

Note that the definitions of aquifer and aquitard are relative, and depend on the particular regional context: In an area of interbedded sands and silts, the sands would be considered aquifers and the silts aquitards; in an area of interbedded silts and clays, the silts would be aquifers and the clays aquitards. In the context of runoff generation, the aquifer of interest may be a thin surficial layer capable of conducting infiltrated water to streams. In the context of water resources, an aquifer is a geologic unit that is a significant source of water.

9.1.2 Unconfined and Confined Aquifers

Figure 9.1 illustrates the two major classes of ground-water flows, which are distinguished by the nature of the upper boundary of the flow:

1. **Unconfined aquifers**: If the upper boundary of a ground-water flow is a water surface at atmospheric pressure (the water table), the flow and the aquifer in which it occurs are **unconfined**. At the water table, the pressure is atmospheric, the gauge pressure $p = 0$, and the total head is equal to its elevation above the selected datum, z. The elevation of the water table can be determined as that of the water surface in a well open along its length and extending just deep enough to encounter standing

Box 9.1 Basic Ground-Water Definitions and Equations

Hydraulic Head

The total potential energy per unit weight of a fluid at a point is given by the **total head**, h [L], which is the sum of the **gravitational head**, z [L], and the **pressure head**, ψ [L]:

$$h = z + \psi. \qquad \textbf{(9B1.1)}$$

Pressure head is the local fluid gauge pressure, p [F L^{-2}], divided by the weight density of the fluid, γ [F L^{-3}]:

$$\psi \equiv \frac{p}{\gamma}. \qquad \textbf{(9B1.2)}$$

Total head at a point in a saturated porous medium is measured as the elevation of the water surface in a **piezometer**, which is a tube connecting the point to the atmosphere (see figure 7.8).

Gravitational head at the point is measured as the elevation of the point above an arbitrary datum. Pressure head at the point can be determined as $\psi = h - z$.

Darcy's Law

At any point, ground-water flow rate in coordinate direction x equals the product of the local total head gradient and the local **hydraulic conductivity** of the medium in direction x, K_{hx} [L T^{-1}]:

$$q_x \equiv \frac{Q_x}{A_x} = -K_{hx} \cdot \frac{dh}{dx}, \qquad \textbf{(9B1.3)}$$

where q_x [L T^{-1}] is the **Darcy velocity**, Q_x is the volumetric flow rate [L^3 T^{-1}], and A_x [L^2] is the cross-sectional area of the medium through which flow occurs. Darcy's law is valid for laminar (viscous) flow, which occurs when

$$Re \equiv \frac{q_x \cdot d}{\nu} < 1, \qquad \textbf{(9B1.4)}$$

where Re is the **Reynolds number** [1], d is the characteristic (average) grain size of the porous medium [L], and ν is the fluid kinematic viscosity [L^2 T^{-1}].

Permeability and Hydraulic Conductivity

Intrinsic permeability k_I [L^2] is determined by properties of the medium,

$$k_I = C \cdot d^2, \qquad \textbf{(9B1.5)}$$

where C [1] is a parameter that depends on grain shape, size distribution, and packing of the medium. Hydraulic conductivity K_h is determined by properties of the medium and of the fluid:

$$K_h = C \cdot d^2 \cdot \frac{\rho \cdot g}{\mu} = k_I \cdot \frac{\rho \cdot g}{\mu} = k_I \cdot \frac{g}{\nu}, \qquad \textbf{(9B1.6)}$$

where ρ is fluid mass density [M L^{-3}], g is gravitational acceleration [L T^{-2}], and μ is fluid dynamic viscosity [M L^{-1} T^{-1}]. Grain diameters of geologic materials range over more than six orders of magnitude ($< 10^{-6}$ m to > 1 m); at near-surface conditions, viscosity varies approximately twofold as a function of temperature, and water density is essentially constant. Thus K_h of granular geologic materials varies over 12 orders of magnitude (figure 7.9).

Specific Storage

Specific storage, S_s [L^{-1}], is defined as

$$S_s \equiv \frac{\text{volume of water entering or leaving control volume [L}^3\text{]}}{\text{increase or decrease in head [L]} \times \text{control volume [L}^3\text{]}} \qquad \textbf{(9B1.7)}$$

General Equation of Ground-Water Flow

$$\frac{\partial}{\partial x}\left(K_{hx} \cdot \frac{\partial h}{\partial x}\right) + \frac{\partial}{\partial y}\left(K_{hy} \cdot \frac{\partial h}{\partial y}\right) + \frac{\partial}{\partial z}\left(K_{hz} \cdot \frac{\partial h}{\partial z}\right) = S_s \cdot \frac{\partial h}{\partial t}, \qquad \textbf{(9B1.8)}$$

where x, y, z are Cartesian coordinate directions and t is time.

water (Freeze and Cherry 1979). Recharge to unconfined aquifers usually occurs from infiltrated water percolating vertically to the water table over a significant portion of the upper surface. The elevation of the water table changes as the flow through the aquifer varies; thus flow and storage in unconfined aquifers are correlated, as in streams.

2. **Confined aquifers**: If an aquifer is saturated throughout and bounded above and below by formations with significantly lower hydraulic conductivity, the flow and the aquifer are **confined**; the bounding aquitards are called **confining layers**. The pressure throughout is greater than atmospheric, and the water level in an observation well penetrating a confined aquifer will rise above the upper boundary to coincide with the **potentiometric surface**, an imaginary surface analogous to the water table. Major recharge to a confined aquifer occurs from water infiltrating at its "upstream" end, where the flow is not confined and a water table is present.

The boundary of the flow in a confined aquifer does not change with time; thus flow and storage in confined aquifers are not correlated, as in pipes.

It is important to recognize that the unconfined/confined categories are idealizations, and that the three-dimensional spatial variability of geologic conditions produces flows that may have some of the characteristics of both types. As noted, most confining layers can transmit some ground water, and if the amount transmitted is significant such layers are called **leaky aquitards**.

9.1.3 Storage Properties of Aquifers

9.1.3.1 Specific Storage and Storage Coefficient

The volume of water stored in a saturated porous medium per unit volume of medium equals the porosity, ϕ [equation (7.4)], and the degree of saturation, θ^* [equation (7.8)], equals unity.[1] However, the actual volume of water in a unit volume of porous medium may change in response to changes in head; these changes are reflected in the values of the *specific storage* and the *specific head*.

Consider a small unit area (say 1 m^2) on the earth's surface above an aquifer. The saturated thickness of the aquifer beneath that area is designated H [L]. When the hydraulic head in the aquifer increases or decreases, water is taken into or released from storage. The increase or decrease in volume of water stored beneath the unit area per unit increase or decrease in head is the **specific storage**, S_s [L^{-1}], of the aquifer [equation (9B1.7)].

We can also define a dimensionless measure of storage, equal to the change in volume of stored water per unit aquifer surface area per unit change in head; this is the **storage coefficient**, S [1]:

$$S \equiv \frac{\text{Increase or decrease in volume of water stored } [L^3]}{\text{Surface area of aquifer } [L^2] \times \text{Increase or decrease in head } [L]} \qquad \textbf{(9.1)}$$

Specific storage and storage coefficient are related as

$$S = H \cdot S_s. \qquad \textbf{(9.2)}$$

The mechanisms relating changes in head and changes in storage, and the relative magnitudes of these changes, differ for unconfined and confined aquifers, as described in the following sections (figure 9.2).

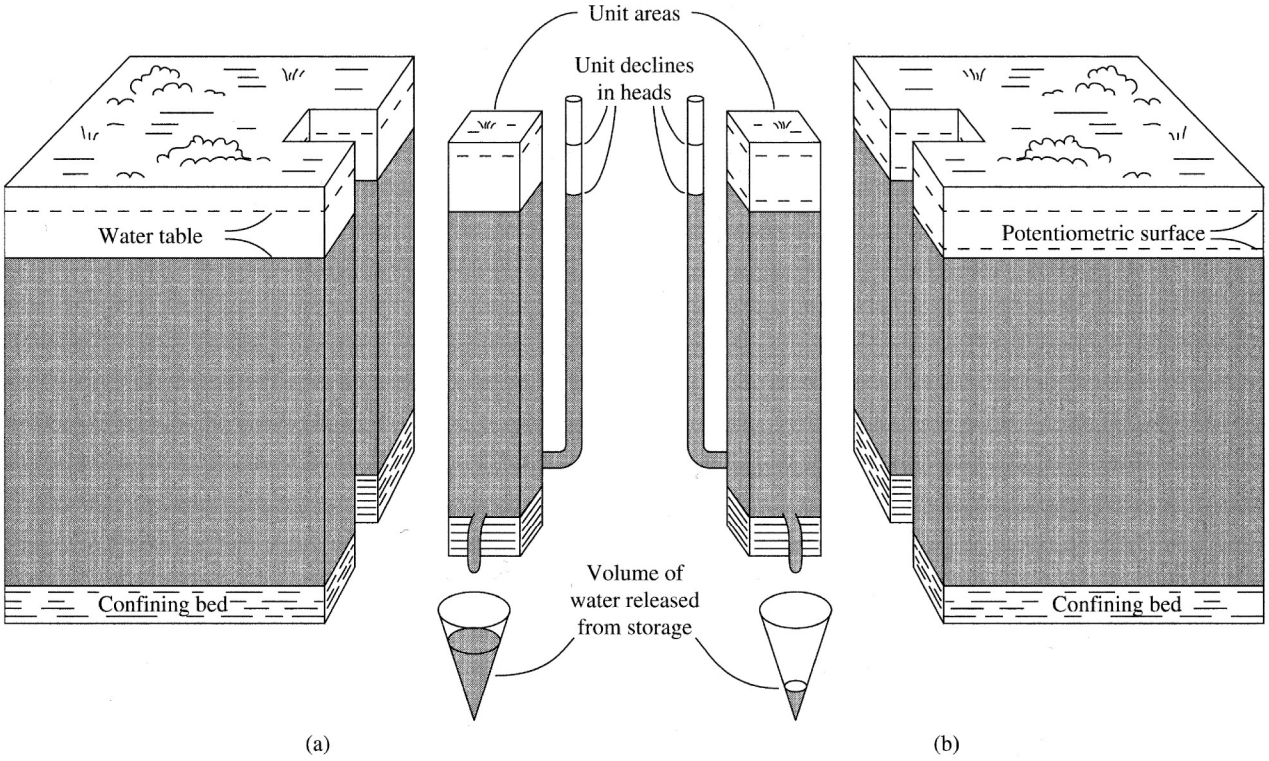

Figure 9.2 Definition of storativity in (a) unconfined and (b) confined aquifers. See equation (9.1) [Heath (1982)].

9.1.3.2 Unconfined Aquifers

In an unconfined aquifer, a change in head produces a change in the volume of water in the medium (figure 9.2a). A decrease in head is reflected in the lowering of the water table and a concomitant decrease in water content of the portion of the aquifer through which the water table descends and in the overlying unsaturated zone (figure 9.3). The opposite occurs for an increase in head. The amount of water-content change is characterized by the **specific yield**, S_y, defined as the volume of water released per unit surface area per unit decline of water table (figure 9.2a). Thus for an unconfined aquifer,

$$S = S_y. \tag{9.3}$$

Typical values of S_y are shown in table 9.1.

The relative volume of water retained in the portion of the aquifer experiencing a head decline is the **specific retention**, S_r. Thus

$$\phi = S_y + S_r. \tag{9.4}$$

The water remaining in the portion of the medium experiencing a water-table decline is held by surface-tension against gravity, so specific retention is essentially identical to field capacity (section 8.1.1). Recall also that soil drainage is not instantaneous, and many days may be required for water content to decline to S_r in a draining aquifer (figure 8.1).

9.1.3.3 Confined Aquifers

In a confined aquifer, a decrease in head is reflected in a lowering of the piezometric surface, but the aquifer beneath the unit surface area remains saturated (figure 9.2b). In this case, the decrease of storage accompanying the head decrease is due to: (1) compaction of the aquifer as part of the weight of the overlying material is transferred from the liquid to the solid grains, resulting in an increase in **effective stress** and a slight decrease in porosity and (2) expansion of the water due to the lowered pressure (box 9.2 on p. 395). The changes are reversed for an increase in head.

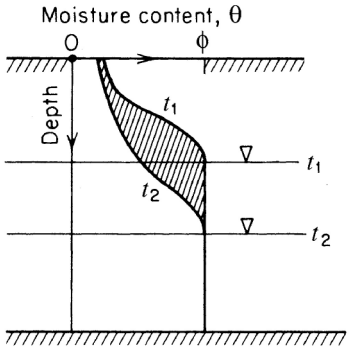

Figure 9.3 Specific yield (shaded area) in an unconfined aquifer [reproduced from Freeze and Cherry (1979), *Groundwater*, with permission from Prentice Hall].

Following Freeze and Cherry (1979), when a volume V_T of a saturated aquifer is subjected to an increase in effective stress $d\sigma_{eff}$, it is compacted by an amount $-dV_T$, and an equal volume of water dV_w is expelled. Thus from equations (9B2.5) and (9B2.6),

$$dV_w = -dV_T = \alpha \cdot V_T \cdot d\sigma_{eff} = -\alpha \cdot V_T \cdot \gamma \cdot dh, \tag{9.5}$$

where α [$L^2\ F^{-1}$] is the aquifer compressibility and γ [$F\ L^{-3}$] is the weight density of water. Thus for a unit volume ($V_T = 1$) and a unit head decline ($dh = -1$), the volume of water expelled becomes

$$dV_w = \alpha \cdot \gamma. \tag{9.6}$$

The increase in effective stress produces a decrease in fluid pressure and head [equations (9B2.3) and (9B2.4)], which produces an expansion in the water. From equation (9B2.1), this is given by

$$dV_w = -\beta \cdot V_w \cdot dp. \tag{9.7}$$

The total volume of water in the unit volume of medium is $\phi \cdot V_T$, where ϕ is porosity. Thus using equation (9B2.4), equation (9.7) becomes

$$dV_w = \beta \cdot \phi \cdot \gamma. \tag{9.8}$$

Thus the specific storage for a confined aquifer is the sum of the water-volume changes due to compaction/expansion of the medium [equation (9.6)] and of the water [equation (9.8)]:

$$S_s = (\alpha + \phi \cdot \beta) \cdot \gamma. \tag{9.9}$$

The dimensionless storage coefficient, S, for a confined aquifer is often called the **storativity**; combining equations (9.2) and (9.9) gives

$$S = (\alpha + \phi \cdot \beta) \cdot \gamma \cdot H. \tag{9.10}$$

Storativities for confined aquifers are usually in the range 5×10^{-5} to 5×10^{-3}; i.e., at least an order of magnitude less than the specific yield for unconfined aquifers.

Table 9.1 Porosities, Specific Yields, and Specific Retentions of Geologic Materials.[a]

Material	Porosity			Specific Yield			Specific Retention		
	Min.	Avg.	Max.	Min.	Avg.	Max.	Min.	Avg.	Max.
Unconsolidated Alluvial Deposits									
Clay	0.34	0.42	0.57	0.01	0.06	0.18	0.25	0.38	0.47
Silt	0.34	0.46	0.61	0.01	0.20	0.39	0.03	0.28	0.45
Fine sand	0.26	0.43	0.53	0.01	0.33	0.46	0.03	0.08	0.43
Medium sand	0.29	0.39	0.49	0.16	0.32	0.46	0.01	0.04	0.18
Coarse sand	0.31	0.39	0.46	0.18	0.30	0.43	0.05	0.07	0.18
Fine gravel	0.25	0.34	0.39	0.13	0.28	0.40	0.00	0.07	0.17
Medium gravel	0.24	0.32	0.44	0.17	0.24	0.44	0.01	0.07	0.15
Coarse gravel	0.24	0.28	0.37	0.13	0.21	0.25	0.03	0.09	0.14
Unconsolidated Glacial Deposits									
Silty till	0.30	0.34	0.41	0.01	0.06	0.13	0.23	0.28	0.33
Sandy till	0.22	0.31	0.37	0.02	0.16	0.31	0.03	0.14	0.29
Gravelly till	0.22	0.26	0.30	0.05	0.16	0.34	0.01	0.12	0.25
Unconsolidated Aeolian Deposits									
Loess	0.44	0.49	0.57	0.14	0.18	0.22	0.22	0.27	0.30
Aeolian sand	0.40	0.45	0.51	0.32	0.38	0.47	0.01	0.03	0.06
Unconsolidated Biogenic Deposits									
Peat		0.92			0.44			0.44	
Weathered Rock (Saprolites)									
Granite	0.34	0.45	0.57						
Gabbro	0.42	0.43	0.45						
Clastic Sedimentary Rocks									
Fine sandstone	0.14	0.33	0.49	0.02	0.21	0.40	0.01	0.13	0.31
Med. sandstone	0.30	0.37	0.44	0.12	0.27	0.41	0.05	0.10	0.19
Siltstone	0.29	0.35	0.48	0.01	0.12	0.33	0.05	0.29	0.45
Claystone	0.41	0.43	0.45						
Shale	0.01	0.06	0.10						
Carbonate Rocks									
Limestone	0.07	0.30	0.56	0.02	0.14	0.36	0.05	0.13	0.29
Dolomite	0.19	0.26	0.33						
Igneous and Metamorphic Rocks									
Basalt	0.03	0.17	0.35						
Volcanic tuff	0.07	0.41	0.55	0.02	0.21	0.47	0.06	0.21	0.38
Schist	0.04	0.38	0.49	0.22	0.26	0.33	0.22	0.26	0.33

[a]Values measured in small samples by Morris and Johnson (1967).

Box 9.2 Effective Stress and the Compressibility of Water and Aquifers

Compressibility of Water

Consider a volume of water V_w at a pressure p. If the pressure is increased by an amount dp, the volume will decrease by an amount $-dV_w$. The compressibility of water, β, is defined as the relative decrease in volume per unit increase in pressure [$L^2\ F^{-1}$]:

$$\beta \equiv \frac{-dV_w / V_w}{dp}. \qquad \textbf{(9B2.1)}$$

This is a reversible process, so a decrease in pressure ($dp < 0$) causes a concomitant expansion ($dV_w > 0$). β for water is very small and is effectively constant at near-surface pressures and temperatures at $\beta = 4.4 \times 10^{-10}\ m^2/N$.

Effective Stress

Consider a horizontal plane within a saturated porous medium. The total stress (≡ force per unit area [$F\ L^{-2}$]) acting on the plane is due to the weight of the overlying mineral medium and water. Part of this stress is borne by the solid particles of the medium and part by the fluid, which is reflected in the fluid pressure. Thus

$$\sigma_T = p + \sigma_{eff}, \qquad \textbf{(9B2.2)}$$

where σ_T is total stress, p is fluid pressure, and σ_{eff} is the stress borne by the medium, which is called the **effective stress**.

In most hydrologic situations, the weight of the overlying rock and water do not change, so that $d\sigma_T = 0$ and

$$d\sigma_{eff} = -dp. \qquad \textbf{(9B2.3)}$$

Thus if pressure decreases, stress is transferred from the fluid to the medium, and effective stress increases. This increase causes the grains of the medium to become somewhat more densely packed, so the medium compacts. If pressure increases, the effective stress decreases, and the medium tends to expand. However, the process is not quantitatively reversible, and the expansion is less than the compaction in response to a given dp. This means that a medium tends to become increasingly compacted in response to repeated cycles of increasing and decreasing pressure changes.

Since

$$p = \gamma \cdot \psi = \gamma \cdot (h - z), \qquad \textbf{(9B2.4)}$$

and z is constant at any level,

$$d\sigma_{eff} = -\gamma \cdot d\psi = -\gamma \cdot dh; \qquad \textbf{(9B2.5)}$$

that is, changes in effective stress are determined by changes in hydraulic head.

Note that changes in effective stress do not respond immediately to changes in pressure; water flow in response to a change in pressure may take considerable time (months to years in some cases).

Compressibility of Porous Media

The compressibility of the medium, α [$L^2\ F^{-1}$], is defined analogously to that of water:

$$\alpha \equiv \frac{-dV_T / V_T}{d\sigma_{eff}}, \qquad \textbf{(9B2.6)}$$

where V_T is the total volume of the medium (solid plus pore space).

Because of the nonreversibility of porous-media compaction, α is a function of the applied stress and of the history of stress changes. The table below gives ranges of α values for porous media. Note that these are generally much larger than for water, especially for unconsolidated materials.

Table 9B2.1

Medium	Compressibility, α (m^2/N)
Clay	10^{-8} to 10^{-6}
Sand	10^{-9} to 10^{-7}
Gravel	10^{-10} to 10^{-8}
Jointed rock	10^{-10} to 10^{-8}
Sound rock	10^{-11} to 10^{-9}

Source: Freeze and Cherry (1979).

9.1.4 Transmission Properties of Aquifers

The fundamental transmission property of a porous medium is its saturated hydraulic conductivity, K_h, which is the volume rate of flow per unit area transmitted through the medium by a unit hydraulic-head gradient [equation (9B1.2)]. Methods of measurement and ranges of values of K_h were described in section 7.3. As noted there, K_h has significant spatial variability, even within a given aquifer, and conductivity at a "point" may be different in different directions. Figure 9.4 illustrates the four possible combinations of anisotropy and heterogeneity: If K_h at a "point" is the

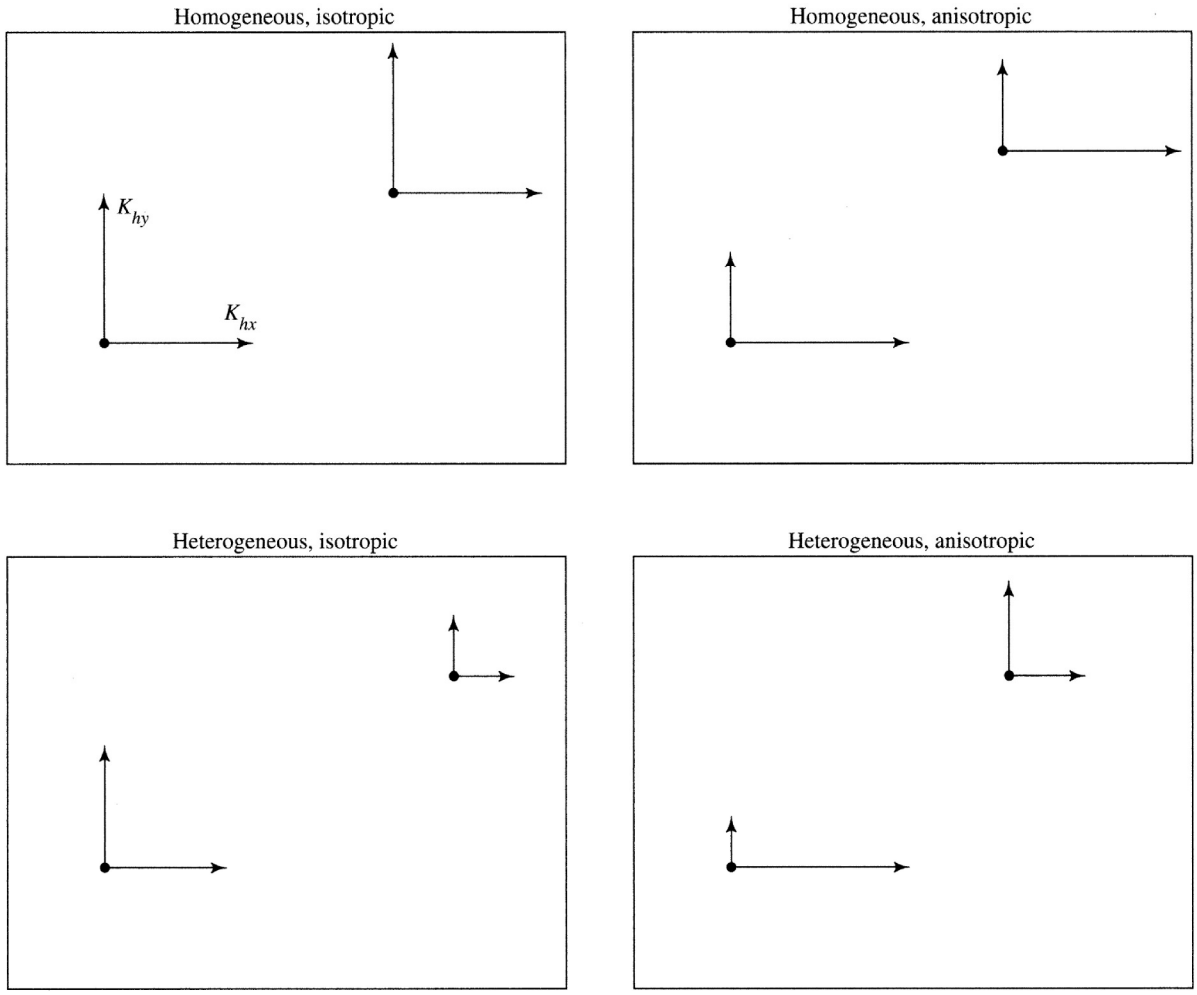

Figure 9.4 Four possible combinations of heterogeneity and anisotropy in saturated hydraulic conductivity [adapted from Freeze and Cherry (1979)].

same for all directions, the medium is **isotropic**; otherwise it is **anisotropic**. If the conductivity in all directions is the same at all "points," the medium is **homogeneous**; otherwise it is **heterogeneous**.

When dealing with flows to wells in confined aquifers in which K_h and the saturated thickness, H, are only slightly variable and the flow paths are approximately horizontal, ground-water hydrologists often use the concept of aquifer **transmissivity**, T [$L^2 T^{-1}$], defined as

$$T \equiv H \cdot K_h. \tag{9.11}$$

9.1.5 Aquifer Response Time and Residence Time

Unconfined aquifers are reservoirs in which outflow is related to storage [equation (1.23)], and storage is related to inflow and outflow. A relative measure of the time scale at which aquifer storage and outflow vary is given by

$$\tau \equiv \frac{L^2 \cdot S}{H \cdot K_h} = \frac{L^2 \cdot S}{T}, \tag{9.12}$$

where τ is **aquifer response time** [T], L is a measure of the horizontal extent of the aquifer [L], and the other symbols are as defined earlier. The inverse of τ is often called the **aquifer response rate** (Erskine and Papaioannou 1997). These response characteristics appear in various contexts later in this chapter.

As noted, the S values, and hence response times, for unconfined aquifers are orders of magnitude greater than those for confined aquifers, because changes in storage in unconfined aquifers reflect the

actual filling and emptying of soil pores rather than the very minor effects of water and aquifer compressibility. Unconfined aquifers may also be subject to recharge by infiltration and water loss in response to evapotranspiration over their entire extents. Thus

> Unconfined aquifers are much more interactively related to the regional hydrologic cycle than are confined aquifers,

and unconfined aquifers will be the sole focus of subsequent ground-water treatments in this text.

As discussed in section 1.10.3, the residence time of water in a reservoir is the average length of time a "parcel" of water spends in the reservoir. Aquifer residence time also characterizes the timing of aquifer responses to changes in recharge and the fate of contaminants that are subject to chemical and biological processes as they move through aquifers to surface-water bodies (Haitjema 1995). From equation (1.25), the general definition of residence time, T_R, is

$$T_R \equiv \frac{\text{average storage in reservoir } [\mathrm{L}^3]}{\text{average rate of input/output } [\mathrm{L}^3\ \mathrm{T}^{-1}]} \cdot \quad \textbf{(9.13)}$$

For an unconfined aquifer of average saturated thickness H, this becomes

$$T_R \equiv \frac{S_y \cdot H}{R}, \quad \textbf{(9.14)}$$

where R is average recharge rate per unit area [L T^{-1}].

9.2 Regional Ground-Water Flow

9.2.1 Equation for Steady Ground-Water Flow

Recall that the general ground-water flow equation [equation (9B1.8)] is derived by combining Darcy's law with the conservation of mass. To illustrate the essential features of regional ground-water flow systems, we will use solutions of that equation that represent *steady flow* in *two-dimensional* vertical slices through unconfined aquifers (like figure 9.1), imposing simple boundary conditions that represent idealized configurations of topography and geology. For these conditions, the general equation becomes

$$\frac{\partial}{\partial x}\left(K_{hx} \cdot \frac{\partial h}{\partial x}\right) + \frac{\partial}{\partial z}\left(K_{hz} \cdot \frac{\partial h}{\partial z}\right) = 0, \quad \textbf{(9.15a)}$$

where x is the horizontal coordinate and z is the vertical coordinate. In many of our examples, we assume that the hydraulic-conductivity field is isotropic (i.e., $K_{hx} = K_{hz}$), and the general equation reduces to the **Laplace equation**,

$$\frac{\partial^2 h}{\partial x^2} + \frac{\partial^2 h}{\partial z^2} = 0. \quad \textbf{(9.15b)}$$

As noted in section 7.3.4, solutions to these equations are shown as flow nets giving the pattern of equipotentials and streamlines that is consistent with the boundary conditions and the distribution of conductivity values. The spacing of the equipotentials is inversely related to the head gradient, so the relative intensity of the circulation is larger where the equipotentials are closely spaced. The rate of flow in the direction of the streamline at any point can be calculated by determining the head gradient in that direction and multiplying it by the local value of hydraulic conductivity.

In nature, topography, conductivity, and climate influence infiltration, recharge, evapotranspiration, and discharge of ground water to streams, and hence the water-table configuration. The water-table configuration in turn influences the distribution of recharge and discharge conditions, as discussed in section 9.5. These interactive processes are not incorporated in the solutions we examine here; instead, water-table configurations typical of those observed in nature are specified as imposed boundary conditions. However, if the general configuration of the water table does not greatly change through the year, and if the fluctuations of the water table at any point are small relative to the thickness of the saturated zone (as is often the case), equation (9.15) provides an instructive picture of the essential features of regional ground-water flow under various topographic and geologic conditions. Note that these features are independent of the scale of the flow system.

9.2.2 General Features of Regional Ground-Water Flow

Figure 9.5 shows the effects of overall aquifer geometry on solutions to equation (9.15). In both cases, the upper flow boundary is a gently sloping water table, the lower boundary is a horizontal impermeable layer, the right boundary is a **divide** where flow is vertically downward, and the left boundary is a valley where flow is vertically upward. In relatively thin aquifers, the flow is essentially horizontal except at

the divide and valley (figure 9.5a); in relatively thick aquifers the vertical components of the streamlines are much greater throughout (figure 9.5b).

The flowlines represent flow from *recharge areas* to *discharge areas*:

- **Recharge areas** are regions in which the ground-water flow is directed away from the water table.
- **Discharge areas** are regions in which the ground-water flow is directed toward the water table.
- The line separating recharge and discharge areas is called a **hinge line**.

The water table is usually at some depth in recharge areas and at or near the surface in discharge areas. Thus discharge areas are usually the sites of surface-water bodies: streams, lakes, wetlands, or, if highly localized, springs.

Note that basic water-balance considerations dictate that the average rate of discharge from a regional aquifer must be equal to the average rate of recharge. Since recharge rate (≈ precipitation less evapotranspiration) is determined largely by climate, topography and geology determine only the spatial distributions of discharge and recharge, not the absolute rates.

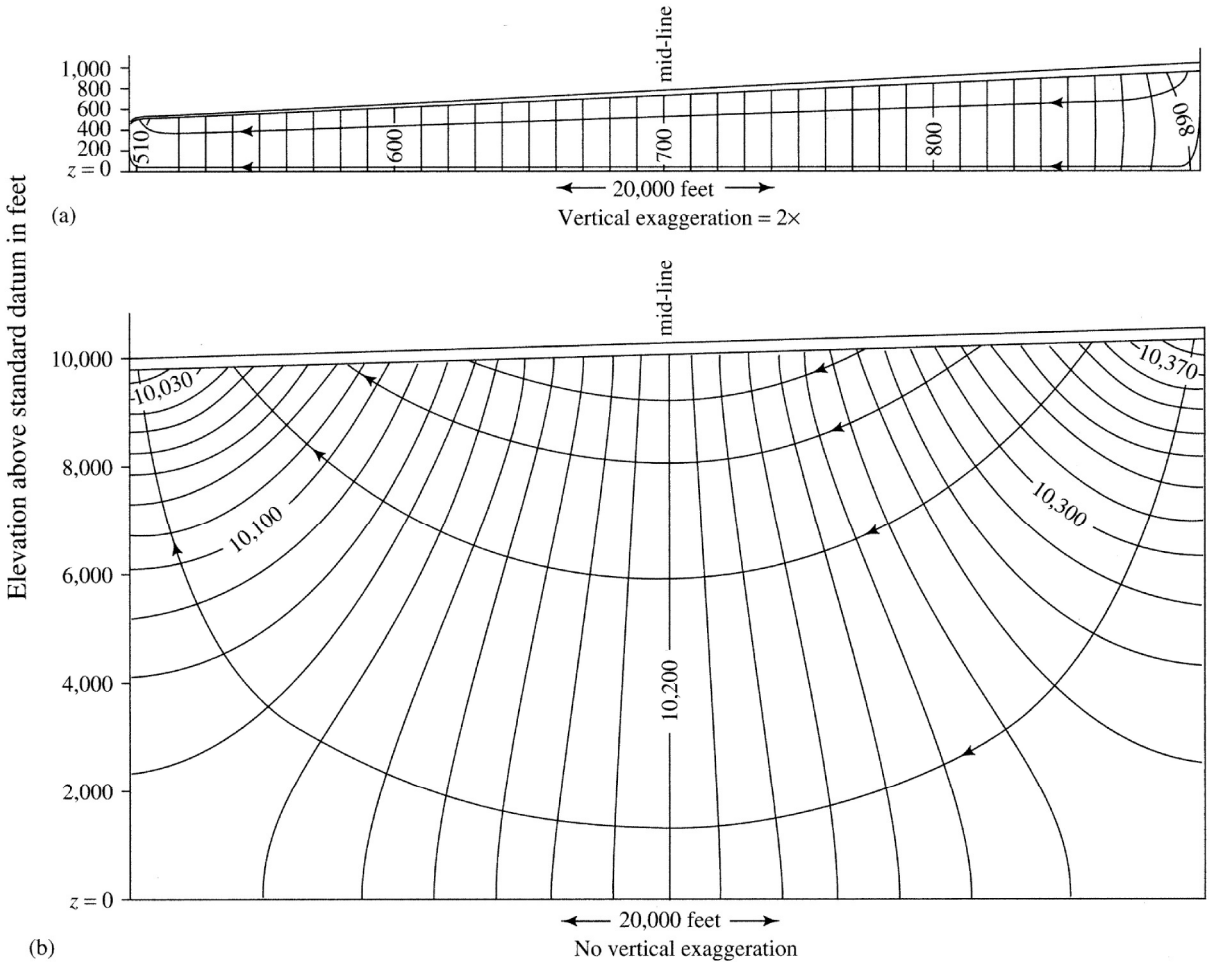

Figure 9.5 Flow-net configurations computed by applying the Laplace equation [equation (9.15b)] to idealized approximations of unconfined ground-water flow to a stream where: (a) the aquifer is relatively shallow (note flow is essentially horizontal) and (b) the aquifer is relatively deep (note flow has a significant vertical component, except near the mid-line). Contours are equipotentials; lines with arrows are streamlines [Tóth (1962). A theory of groundwater motion in small drainage basins in central Alberta, Canada. *Journal of Geophysical Research* 67:4375–4387, with permission of the American Geophysical Union].

9.2.3 Effects of Topography

Figure 9.6 shows a cross section through an idealized hilly upland area in a humid region, underlain by permeable deposits with homogeneous and isotropic conductivity resting on an impermeable base. Under these conditions, the solution of equation (9.15) results in a general head gradient from the divides toward the streams, with the flow moving downward and diverging near the divide and then upward and converging toward the valleys, where ground-water discharge produces streams. A boundary streamline flows vertically downward at the divides, horizontally along the impermeable base, and vertically upward under the streams. Thus in hilly humid areas,

- Surface divides and streams are usually the boundaries of ground-water flow systems;
- The balance between net vertical recharge and lateral ground-water flow produces a water table that is a subdued replica of the ground surface;
- The higher the ratio of recharge rate to hydraulic conductivity, the more closely the water table replicates the topography.

However, in arid regions or areas of asymmetric topography or heterogeneous geology, ground-water divides may not coincide with surface-water divides and surface-water bodies.

Figure 9.7 shows the flow nets for two situations of identical geology, depth to impermeable base, and lateral dimension. Both have a major valley on the left and an upland area toward the right, but the smaller-scale topography (as represented by the water table) differs. In figure 9.7a the water table is a gently sloping plane, such as might be found beneath a region of undeformed lake or coastal-plain sediments; the water table in figure 9.7b reflects a hilly upland superimposed on the general leftward-sloping topographic trend, such as might be found in a region of glacial deposits.

The plane water table of figure 9.7a results in a single flow system, with the recharge area extending down to the central valley. In figure 9.7b, on the other hand, each hill in the water table produces a small-scale recharge-discharge system that circulates above a larger-scale flow in the left half of the system, and both these systems circulate above a still larger-scale flow system extending from the major divide to the major valley.

Patterns like that in figure 9.7b led Tóth (1963) to conclude that, in many situations, one can identify **local flow systems**, in which water moves from a recharge area to the next adjacent discharge area; **regional flow systems**, in which the flow is from the recharge area farthest from the main valley to the discharge area in the main valley; and **intermediate flow systems**, in which the flow path is longer than local but shorter than regional (figure 9.8 on p. 401).

Regions with little local relief typically have only regional systems, and regions with pronounced local relief typically have only local systems. However, the pattern of development of flow systems of various scales is affected also by the overall system geometry: Development of local flow systems is favored where the depth to the impermeable layer is small relative to

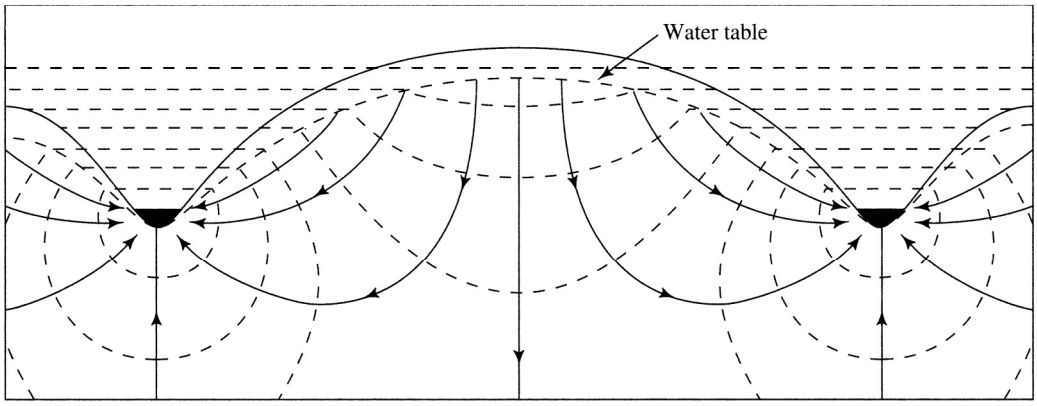

Figure 9.6 Ground-water flow net as given by solving the Laplace equation [equation (9.15b)] for a vertical section through idealized hills and valleys in a permeable material resting on an impermeable base. Dashed lines are equipotentials; arrows are streamlines. Streams, lakes, or wetlands are present in valleys where the water table intersects the land surface [adapted from Hubbert (1940)].

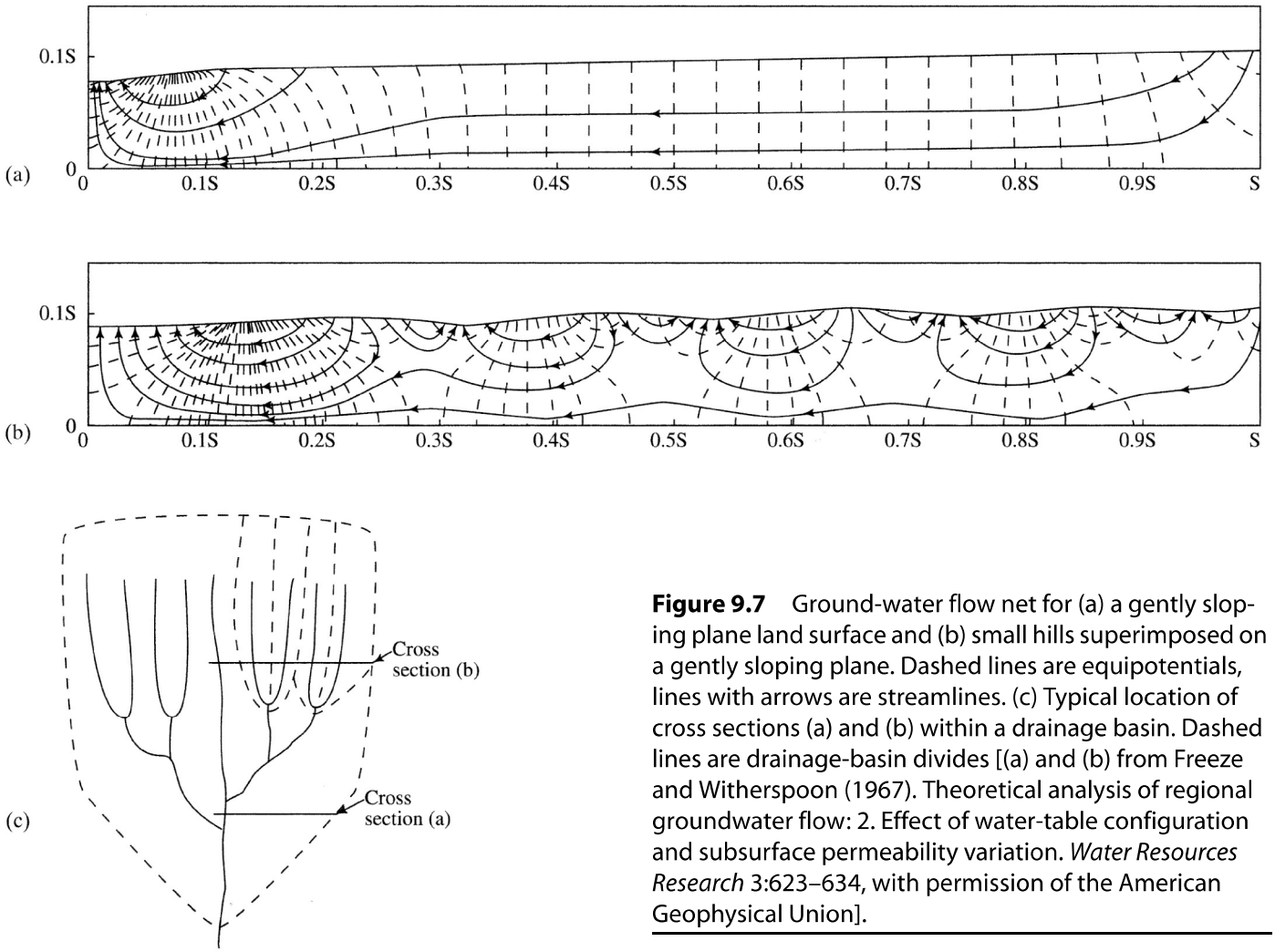

Figure 9.7 Ground-water flow net for (a) a gently sloping plane land surface and (b) small hills superimposed on a gently sloping plane. Dashed lines are equipotentials, lines with arrows are streamlines. (c) Typical location of cross sections (a) and (b) within a drainage basin. Dashed lines are drainage-basin divides [(a) and (b) from Freeze and Witherspoon (1967). Theoretical analysis of regional groundwater flow: 2. Effect of water-table configuration and subsurface permeability variation. *Water Resources Research* 3:623–634, with permission of the American Geophysical Union].

the distance from the main valley to the divide, and the more pronounced the relief, the deeper the local systems extend; regional systems are favored where the impermeable layer is deep relative to that distance. (These relations are examined further in section 9.2.5.)

Thus, as noted by Freeze and Cherry (1979), topography alone can create complex ground-water flow patterns. In general, uplands are recharge areas and lowlands are discharge areas; hinge lines are usually closer to the valleys than to the divides and discharge areas typically constitute less than 30% of a given drainage basin.

9.2.4 Effects of Geology

The most important geologic factors controlling the directions and relative rates of ground-water movement are:

1. **Lithology**: The mineral composition, grain-size distribution, and grain-shape characteristics of rocks and unconsolidated geologic materials that control the hydraulic conductivity distribution.
2. **Stratigraphy**: The geometrical relations among the various formations which, except for intrusive igneous or highly metamorphosed rocks, are typically layered.
3. **Structure**: The general arrangement and relative positions of formations, especially as modified by deformational processes such as folding, faulting, and jointing (formation of cracks) and intrusion of igneous rocks.

As noted by Freeze and Cherry (1979), an understanding of the lithology, stratigraphy, and structure of a region usually leads directly to an understanding of the distribution of aquifers and

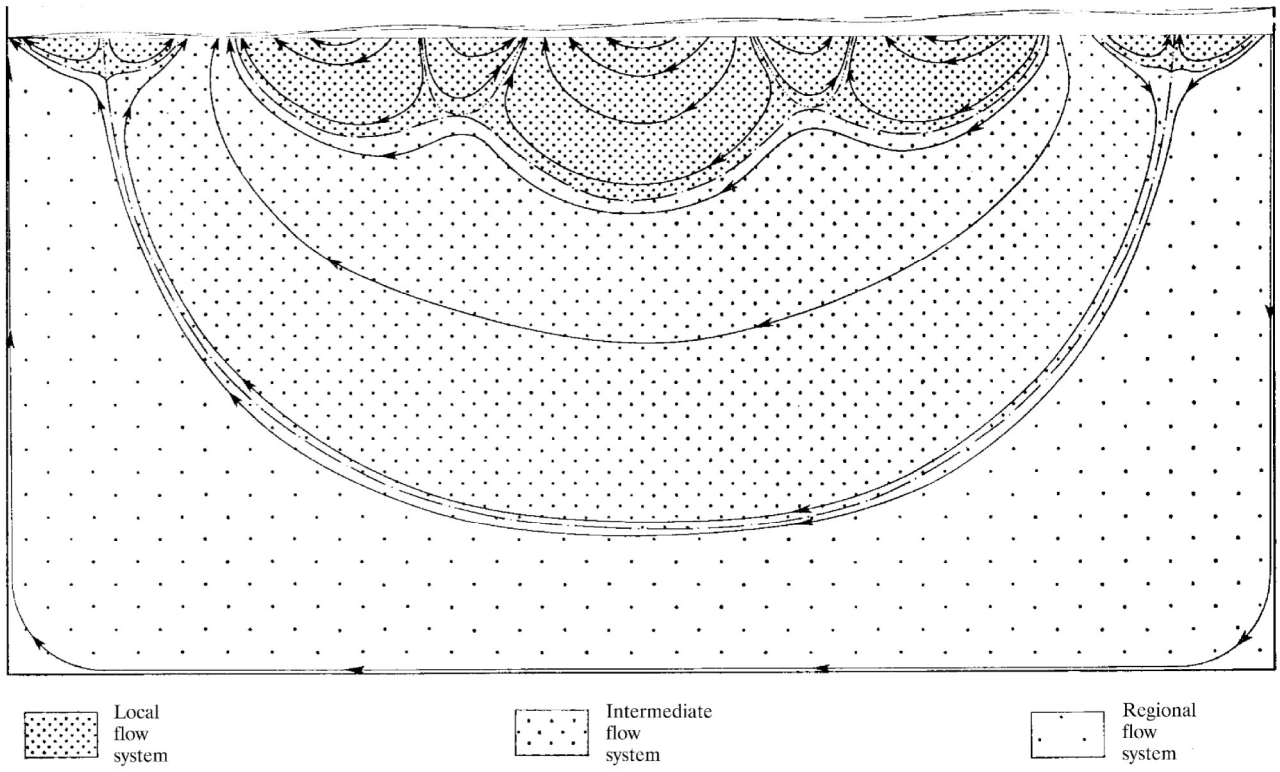

Figure 9.8. Local, intermediate, and regional ground-water flow systems [Tóth (1963). A theoretical analysis of groundwater flow in small drainage basins. *Journal of Geophysical Research* 68:4795–4812, with permission of the American Geophysical Union].

confining beds, and hence to a qualitative understanding of at least the major characteristics of ground-water movement. Complete understanding of the role of ground water in a region's hydrology must be based on detailed geologic mapping, subsurface exploration, and modeling.

Figure 7.9 shows the ranges of saturated hydraulic conductivity and table 9.1 gives some typical values of porosity, specific yield, and specific retention for various geologic materials. Figure 9.9 shows the distribution of the principal types of aquifers in the conterminous United States. More detailed information about regional ground-water geology and the ground-water characteristics of various types of geologic materials can be found in McGuinness (1963), Freeze and Cherry (1979), US Geological Survey (1985), and Fetter (2001).

Geologic conditions display infinite variability, so we can only suggest the types and magnitudes of geologic effects on ground-water flow patterns by examining a few idealized situations. In these depictions, variations in geology are represented by differences in the relative magnitudes of saturated hydraulic conductivity.

Figure 9.10 on p. 403 shows the effects of a buried layer with hydraulic conductivity 100 times greater than the overlying layer on the flow net for a sloping-plane topography. Comparing this net with figure 9.7a, where the flow is essentially horizontal, the flow in the upper layer now has a strong vertical component and the hinge line moves upslope.

The effect of a buried high-conductivity layer in a region of hilly topography can be seen by comparing figure 9.11 with figure 9.7b. In figure 9.11 on p. 403, the buried layer changes the local flow systems near the divide to intermediate systems, reduces the flow intensities in the remaining local systems, and increases the intensity and extent of the discharge area in the main valley.

Figure 9.12 on p. 404 shows the effect of a basal lens of high-conductivity material in the upper portion of a system with flat topography. The flow net is much altered from that in figure 9.7a, with a discharge zone in mid-basin.

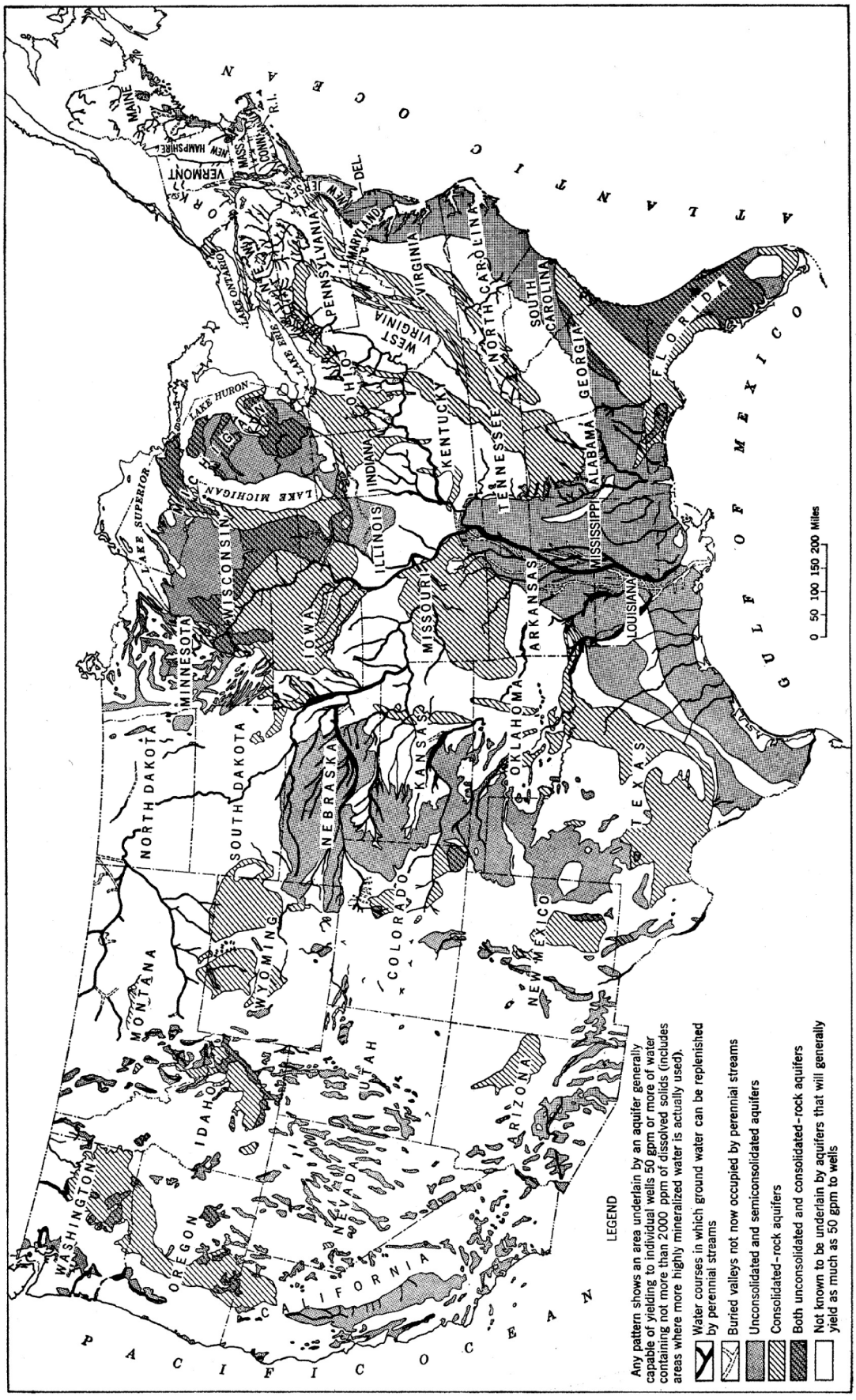

Figure 9.9 Major aquifers of the conterminous United States [McGuinness (1963)].

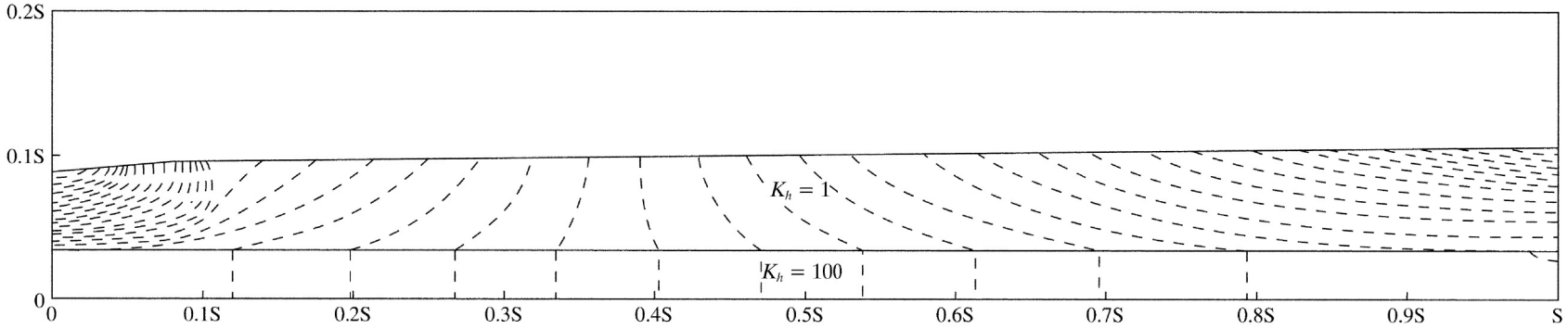

Figure 9.10 Equipotentials for topography of figure 9.7a, but with a buried layer with hydraulic conductivity 100 times greater than that of the overlying material [Freeze and Witherspoon (1967). Theoretical analysis of regional groundwater flow: 2. Effect of water-table configuration and subsurface permeability variation. *Water Resources Research* 3:623–634, with permission of the American Geophysical Union].

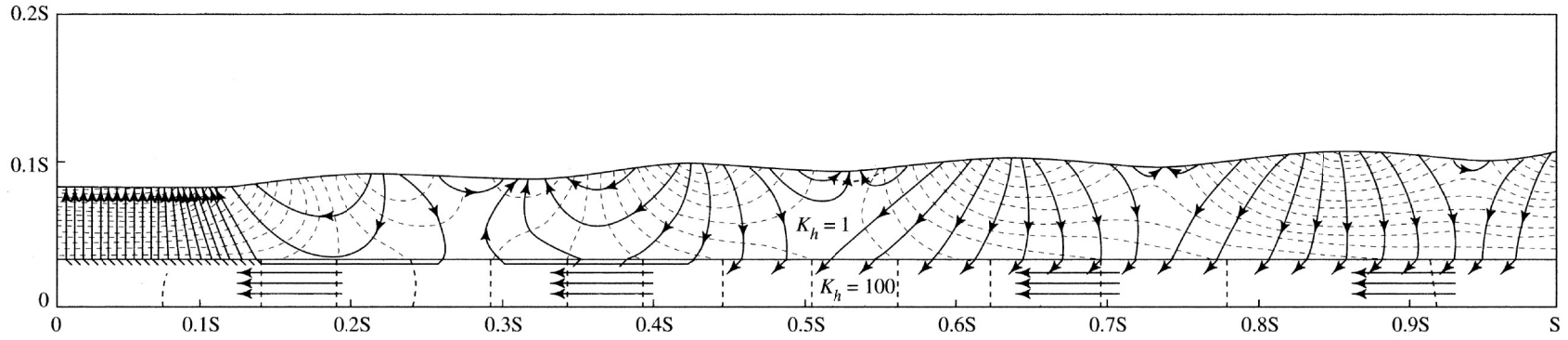

Figure 9.11 Flow net for hilly topography of figure 9.7b, but with a buried layer with hydraulic conductivity 100 times greater than that of the overlying material. Dashed lines are equipotentials, arrows are streamlines [Freeze and Witherspoon (1967). Theoretical analysis of regional groundwater flow: 2. Effect of water-table configuration and subsurface permeability variation. *Water Resources Research* 3:623–634, with permission of the American Geophysical Union].

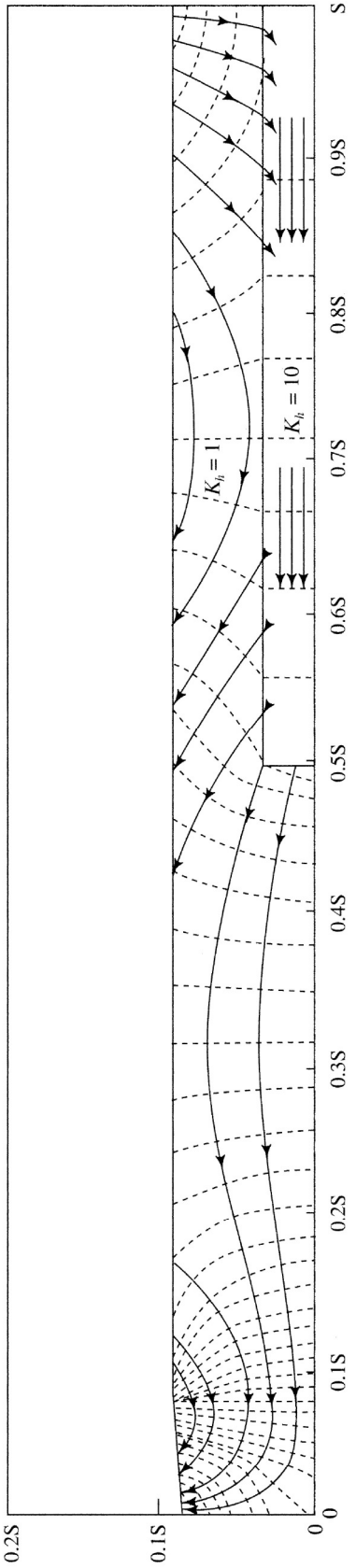

Figure 9.13 is a cross section of an actual flow system in glacial deposits in Saskatchewan, Canada, that illustrates the complexity of flow patterns that can exist in nature. Note that recharge occurs over almost the entire section, and that Notukeu Creek is a site of recharge, not discharge. Discharge occurs only to Wiwa Creek, but there is also flow beneath that stream and the northern upland to some other regional discharge site to the northeast.

Freeze and Witherspoon (1967) presented flow nets for combinations of idealized topography and geology other than those shown here. All these examples show clearly that variations in geology, which might not be apparent without detailed subsurface exploration, can produce a wide range of possible flow-net configurations consistent with a given water-table configuration. Thus information about subsurface geologic conditions and hydraulic head is necessary for formulating an accurate picture of regional ground-water flow.

9.2.5 Synthesis: Effects of Topography, Geology, and Climate

9.2.5.1 Hydrologic Landscapes

Winter (2001) introduced the concept of **hydrologic landscape** as a framework for synthesis and analysis of the interactions between topography, geology, and climate. This concept is based on the idea that a simple landform—an upland adjacent to a lowland separated by an intervening steeper slope (figure 9.14 on p. 406)—along with its geology and climate, is the basic building block of all hydrologic landscapes. Winter (2001) called this feature a **fundamental hydrologic landscape unit** (**FHLU**).

The central hydrologic feature of an FHLU is a simple ground-water flow cell from the upland to the lowland, involving the movement of water between the atmosphere (precipitation and evapotranspiration), surface water (controlled by the slopes and permeability of the unit's surfaces), and ground water (controlled by the hydraulic characteristics of the unit's geologic framework). Thus in a given context,

Figure 9.12 Flow nets for topography of figure 9.7a, but with a buried lens with hydraulic conductivity 10 times greater than that of the overlying material in different positions [Freeze and Witherspoon (1967). Theoretical analysis of regional groundwater flow: 2. Effect of water-table configuration and subsurface permeability variation. *Water Resources Research* 3:623–634, with permission of the American Geophysical Union].

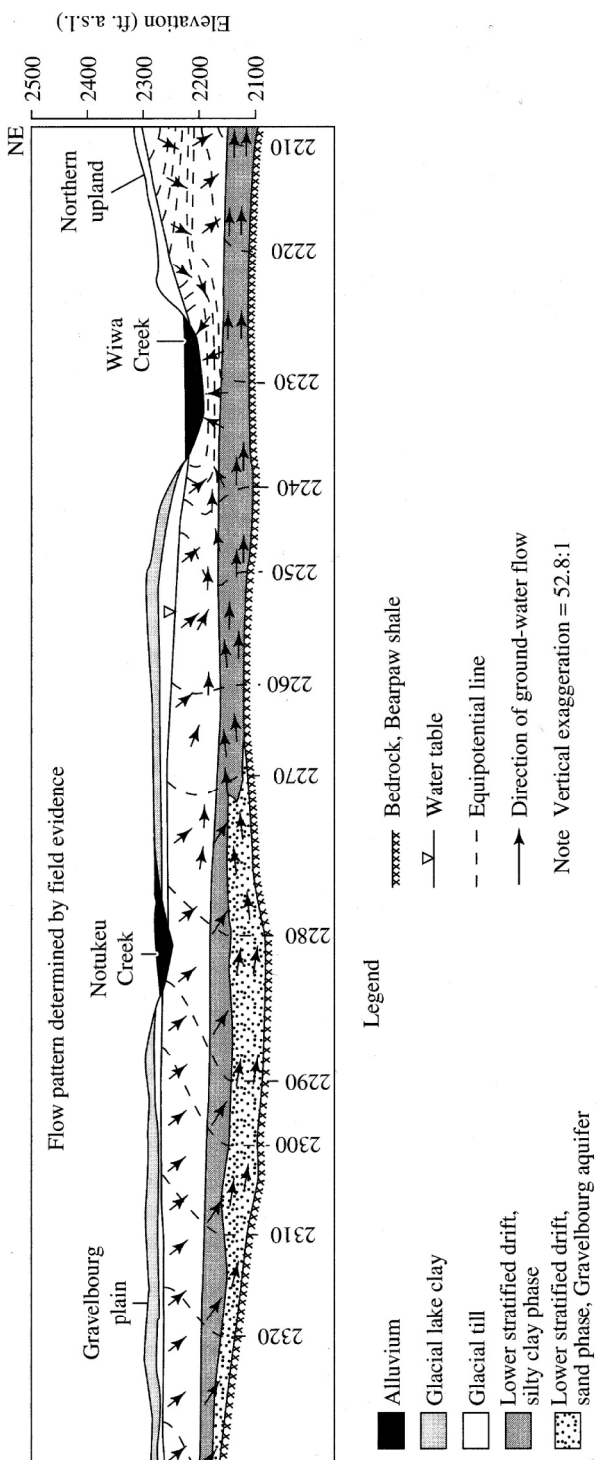

Figure 9.13 Geologic cross section and ground-water flow pattern in glacial deposits in the Wiwa Creek drainage basin, Saskatchewan, Canada, as determined from field measurements [Freeze and Witherspoon (1968). Theoretical analysis of regional groundwater flow: 3. Quantitative interpretations. *Water Resources Research* 4:581–590, with permission of the American Geophysical Union].

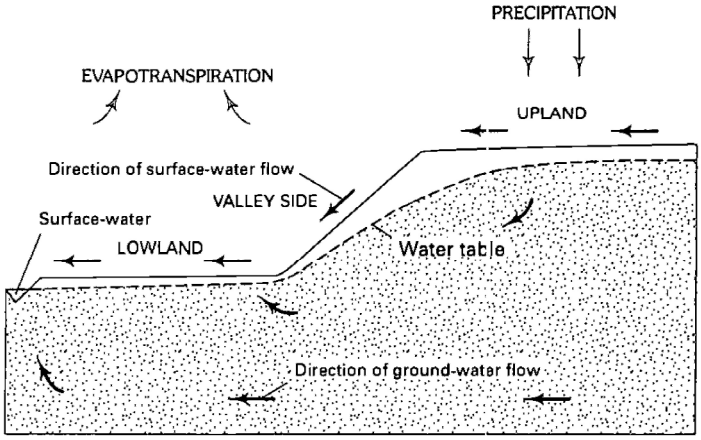

Figure 9.14 The fundamental hydrologic landscape unit (FHLU) consists of an upland adjacent to a lowland separated by an intervening steeper slope, along with its geology and climate [reproduced from Winter (2001). The concept of hydrologic landscapes. *Journal of the American Water Resources Association* 37(2):335–349, with permission of Wiley].

the characterization of the FHLU would involve a description of climate; the surface slopes and areas of the upland, lowland, and intervening steeper slopes; and the hydraulic properties of the geologic units.

Figure 9.15 shows six general FHLU types that occur commonly in various parts of the world. In all these systems

- The water table is a subdued replica of the topography; and
- Downward components of ground-water flow occur at downward breaks-in-slope of the water table, and upward components at upward breaks-in-slope.

In some settings, this may result in wetlands in the area of lower slope; wetlands may also occur where the water table intersects the lower part of the steeper land-surface slope.

The FHLU concept provides useful generalizations about the nature of ground-water–surface-water interactions in various physiographic, geologic, and climatic settings. It also provides a basis for subdivision of a region of any scale into areas likely to have similar surface-runoff and/or ground-water flow fields for hydrologic analysis and hypothesis testing.

> The hypotheses can then be tested by study of a particular area, or they can be the foundation for plans of study, design, and evaluation of data networks, syntheses of existing information, enhancing transfer value of information from well studied to unstudied sites, or comparisons of research results from a wide variety of small research sites. (Winter 2001, p. 341)

9.2.5.2 Water-Table Ratio

A recent quantitative approach to regional ground-water analysis (Gleeson et al. 2011) combines the influences of topography, geology, and climate into a dimensionless **water-table ratio** (***WTR***):

$$WTR \equiv \frac{R \cdot X^2}{8 \cdot K_h \cdot H \cdot Z}, \qquad \textbf{(9.16)}$$

where R is average recharge rate [L T^{-1}], X is average horizontal distance between streams [L], K_h is hydraulic conductivity [L T^{-1}], H is average vertical extent of the aquifer flow system [L], and Z is maximum watershed relief [L] (figure 9.16 on p. 408). Where $WTR > 1$, the water table is **topography-controlled**: the water table is relatively shallow and closely associated with topography. Where $WTR < 1$, the water table is **recharge-controlled**: the water table is deep and largely unrelated to topography.

Using available databases for values of R (0 to 2.2 m/yr), K_h (0 to 4,000 m/yr), and Z (0 to 4,000 m), Gleeson et al. (2011) calculated WTR for watersheds of ~100 km^2 area in the contiguous United States (H and X were assumed to be essentially constant because all the watersheds were of similar size). These values varied over ~11 orders of magnitude, largely because of the variability of K_h, so values of log(WTR) were mapped. Although there was very little correlation among the R, K_h, and Z values, there was strong regional coherence in log(WTR) values. They found that areas with topography-controlled water tables [log(WTR) > 0] occur in humid (high-recharge) regions with subdued topography, low hydraulic conductivity, and shallow and less variable water-table depths; local rather than regional ground-water flow is typical of these areas (e.g., in the Northeast). Conversely, recharge-controlled water tables [log(WTR) < 0] occur in arid re-

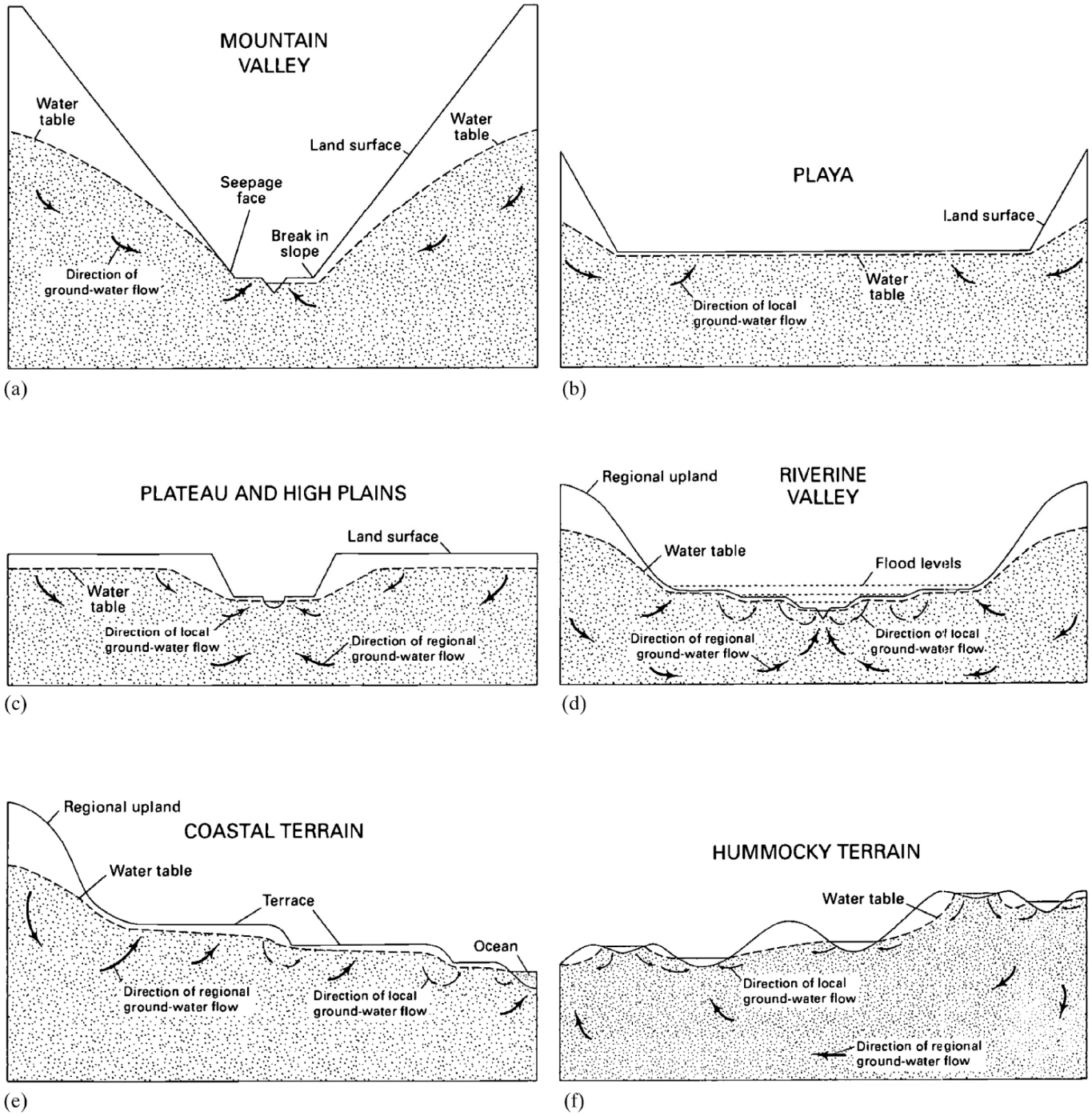

Figure 9.15 Generalized hydrologic landscapes: (a) narrow uplands and lowlands separated by a large, steep valley side (mountainous terrain); (b) large, broad lowland separated from narrow uplands by steeper valley sides (playas and basins of interior drainage); (c) small, narrow lowlands separated from large, broad uplands by steeper valley side (plateaus and high plains); (d) small FHLUs nested within a larger fundamental hydrologic landscape unit (large riverine valley with terraces); (e) small FHLUs superimposed on a larger fundamental hydrologic landscape unit (coastal plain with terraces and scarps); (f) small FHLUs superimposed at random on larger, fundamental hydrologic landscape units (hummocky glacial and dune terrain) [reproduced from Winter (2001). The concept of hydrologic landscapes. *Journal of the American Water Resources Association* 37(2):335–349, with permission of Wiley].

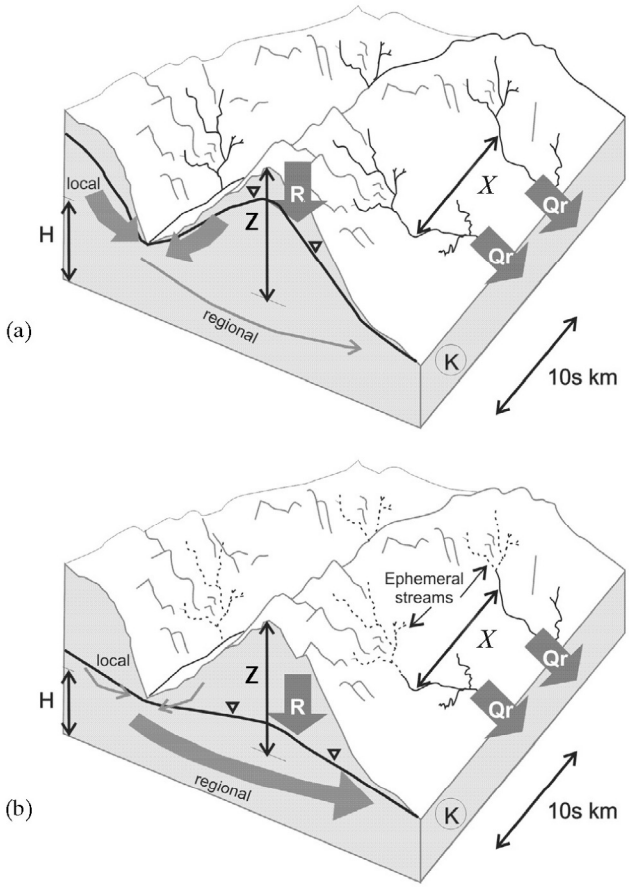

Figure 9.16 Regional water-table types classified by Gleeson et al. (2011). The arrow thickness represents the relative magnitude of regional ground-water flow. (a) Topography-controlled. (b) Recharge-controlled. The water-table depth is generally deeper and more variable in recharge-controlled water tables [Gleeson et al. (2011). Classifying the water table at regional to continental scales. *Geophysical Research Letters* 38, with permission of the American Geophysical Union].

gions with mountainous topography and high hydraulic conductivity; water tables are deep, and regional rather than local flow systems dominate (e.g., in the Southwest and Rocky Mountains).

Gleeson et al. (2011) concluded that differentiating water-table types on the basis of *WTR* provides a basis for conceptualizing regional ground-water flow systems, understanding the relation between ground water and surface water, and understanding the coupling of land-surface processes (precipitation, snowmelt, and evapotranspiration) to ground-water circulation. Thus in many respects, *WTR* is a quantification of Winter's (2001) hydrologic landscape approach.

9.3 Ground-Water–Surface-Water Relations

9.3.1 Ground Water and Streams

Streams range in size from rills to brooks to rivers, and there are no strict quantitative boundaries to the application of these terms. The channel geometry, bank and bed materials, and flow characteristics of a given stream as identified by a single name (e.g., Beaver Brook, Mekong River) usually change significantly along its length. Thus for purposes of describing and understanding natural streams we focus on the **stream reach**, which is a stream segment with fairly uniform size and shape, water-surface slope, channel materials, and relation to ground-water inflows and outflows. The length of a reach depends on the scale and purposes of a study. The volumetric flow rate (volume per unit time) within a channel is the **discharge** or **streamflow** [$L^3\ T^{-1}$]; this quantity varies along a stream and with time at a given location.

Here we examine the types of relations that can exist between stream reaches and ground water, define some useful terms, and introduce a simple but useful quantitative model of the relation between recharge, ground-water flow, and streamflow. Approaches to quantifying ground-water contributions to streamflow are discussed in section 9.5.3.

9.3.1.1 Event Flow and Base Flow

Water that enters streams promptly in response to individual water-input events (rain and/or snowmelt) is called **event flow**, **direct flow**, **storm flow**, or **quick flow**. This is distinguished from **base flow**, which is water that enters from persistent, slowly varying (long-residence-time) sources and maintains streamflow between water-input events. Stream reaches that receive large proportions of their flow as base flow tend to have relatively low temporal flow variability, and hence provide a more reliable source of water for various water-resource purposes (water supply, waste-water dilution, navigation, hydropower generation, etc.).

It is usually assumed that most, if not all, base flow is supplied by ground-water discharge, as depicted in figures 9.5–9.7 and 9.10–9.12. However, base flow can also come from lakes or wetlands, or even from the slow drainage of relatively thin soils on upland hillslopes (Hewlett and Hibbert 1963). Conversely, ground water can also contribute to quick flow; these aspects of ground-water–surface-water relations are examined in chapter 10.

9.3.1.2 Stream Types

A stream reach that occurs in a discharge area and receives ground-water flow is called a **gaining** (or **effluent**) **reach**; its discharge increases downstream. The surface of gaining reaches is generally very slightly below the out-cropping of the water table, with a thin **seepage face** between the two surfaces (figure 9.17a).

A **losing** (or **influent**) **reach** is one in which discharge decreases downstream; such a reach typically occurs in a recharge zone and may either be connected to (figure 9.17b) or "perched" above (figure 9.17c) the general ground-water flow. A **flow-through reach** is one that simultaneously receives and loses ground water (figure 9.17d).

Relations between ground water and streams are highly dynamic, especially in humid regions. During wet seasons, when recharge exceeds evapotranspiration, the water table rises and intersects stream channels widely over the watershed, converting dry, losing reaches to gaining and making the watershed more responsive to water-input events (section 10.4). In seasons when precipitation is less or evapotranspiration greater, the water table recedes and upstream gaining reaches become losing. A stream reach that contains flow all year is **perennial**; one with flow only during wet seasons is **intermittent**; one with flow only in response to a water-input event is **ephemeral**. Perennial and intermittent reaches are usually sustained by ground-water flow between water-input events (gaining), while ephemeral reaches are usually losing.

9.3.1.3 Hyporheic Flow

Hyporheic flow is the exchange of stream water and ground water that occurs in the stream bed. The

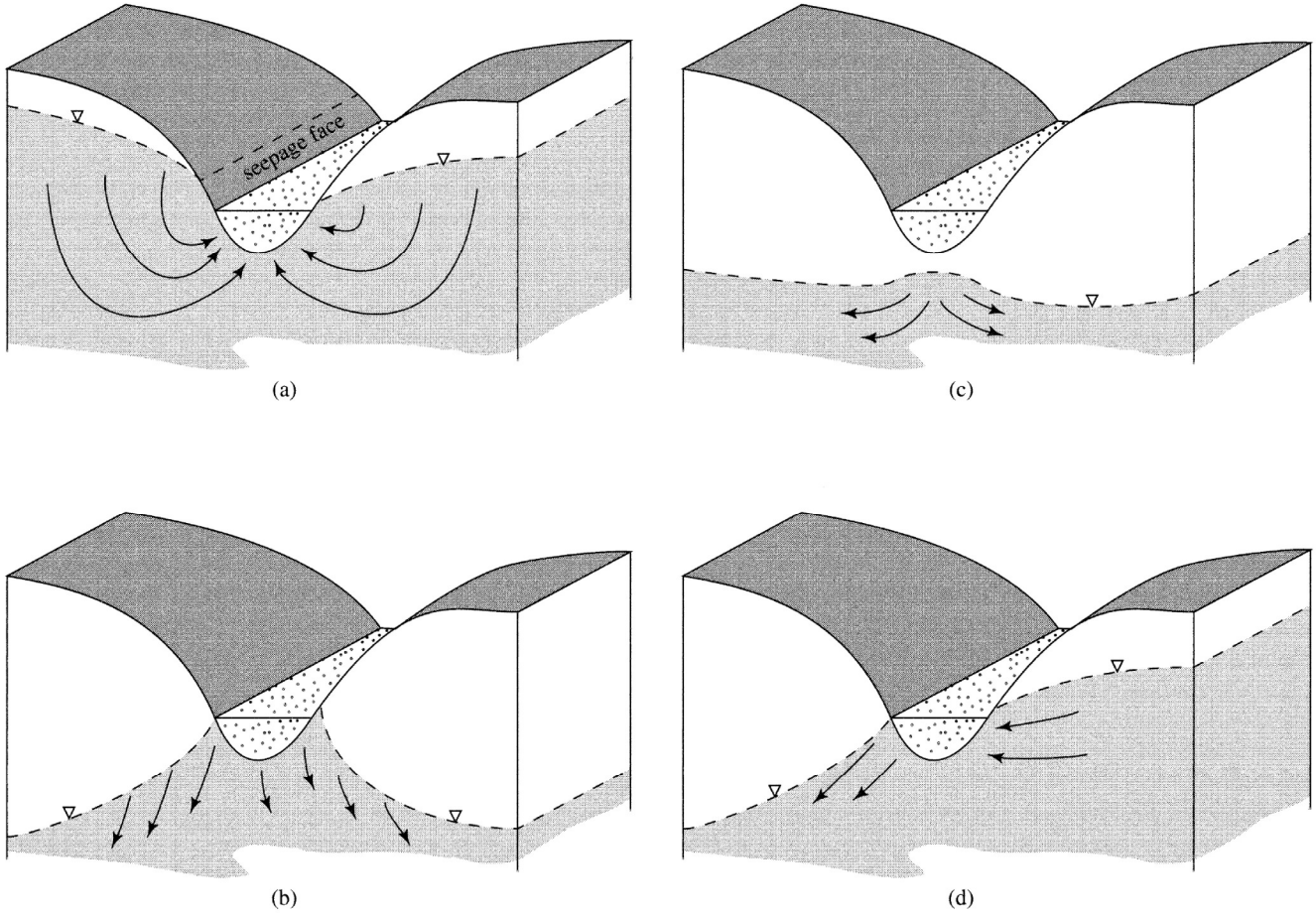

Figure 9.17 Stream-aquifer relations. (a) Gaining stream receiving water from local, intermediate, or regional ground-water flow; (b) losing stream connected to water table; (c) losing stream perched above water table; (d) flow-through stream.

hyporheic zone can extend laterally from the stream up to hundreds of meters under the floodplain (e.g., Jones et al. 2007), and vertically several meters into the stream bed (Tonina and Buffington 2011). Buried paleochannels can create high-conductivity zones that conduct hyporheic flow away from and back toward the active channel (e.g., Kasahara and Wondzell 2003). The importance of the hyporheic zone to water quality and aquatic organisms, including fish spawning, is increasingly being recognized (e.g., Hakenkamp et al. 1993).

Hyporheic flow is produced by variations in bed topography that create pressure-head differences: Flow enters the bed in zones of high pressure, and reenters the channel in zones of low pressure. Based on flume experiments and modeling, Tonina and Buffington (2011) found that the depth of the hyporheic zone was about 0.3 times the streamwise spacing of the bedforms, and that the characteristics of hyporheic exchange vary with stream discharge, bedform amplitude, and depth of alluvium, as summarized in table 9.2. The depth of alluvium is the primary control on the character of hyporheic flow when an impermeable sublayer is present at a depth less than 0.3 times the bedform spacing. Stream discharge controls the pressure distribution at the sediment interface and bedform amplitude influences pressure distribution and the area of bed available for exchange.

9.3.1.4 Bank Storage

The lateral exchange of water between the channel and banks is commonly significant during high flows, and is termed **bank storage**. When an event flow enters a gaining reach, a flood wave forms and travels downstream (section 10.5). As the leading edge of the wave passes, the stream-water level rises above the water table in the bank, reversing the head gradient and inducing flow from the stream into the bank (figure 9.18b). After the peak of the wave passes, the stream level declines and a streamward gradient is once again established (figure 9.18c). Now the wedge of stream-water storage created by the rapid rise drains in both directions, but ultimately all returns to the stream.

By temporarily removing water from the channel, bank storage reduces the magnitude and delays the peak of the flood wave that would otherwise have occurred in response to the water-input event (figure 9.19). The importance of this natural flood-control process varies depending on the channel configuration and material, the extent of the permeable banks, and the rate of rise, magnitude, and duration of the flood wave. Approaches to quantitative modeling of bank storage have been developed by Rorabaugh (1964), Pinder and Sauer (1971), Moench et al. (1974), Hunt (1990), and Whiting and Pomeranets (1997).

9.3.1.5 The Dupuit Approximation

In gaining streams, which are typical of humid regions, streamflow consists largely of drainage from unconfined aquifers (figures 9.6 and 9.17a). Flow in unconfined aquifers is inherently difficult to characterize because the position of the upper flow boundary (the water table) changes with time. However,

Table 9.2 Relations between Hyporheic-Flow Characteristics and Stream Discharge, Bedform Amplitude, and Depth of Alluvium.

Characteristic	Stream Discharge (Q)	Bedform Amplitude (Z_{BF})	Depth of Alluvium[a] (Z_A)
Average depth of hyporheic zone (Z_{HZ})	$Z_{HZ}\downarrow$ as $Q\uparrow$ when bedforms partially submerged. $Z_{HZ}\uparrow$ as $Q\uparrow$ when bedforms fully submerged.	$Z_{HZ}\downarrow$ as $Z_{BF}\downarrow$	$Z_{HZ}\downarrow$ as $Z_A\downarrow$
Average residence time in hyporheic zone (T_{HZ})	$T_{HZ}\downarrow$ as $Q\uparrow$	$T_{HZ}\downarrow$ as $Z_{BF}\downarrow$ when bedforms partially submerged.	$T_{HZ}\downarrow$ as $Z_A\downarrow$
Average downward hyporheic flux, (Q_{HZ})	$Q_{HZ}\uparrow$ as $Q\uparrow$	$Q_{HZ}\uparrow$ as $Z_{BF}\uparrow$	$Q_{HZ}\downarrow$ as $Z_A\downarrow$

$\uparrow$ = increases

$\downarrow$ = decreases

[a]When $Z_A > Z_{HZ}$, Z_A does not affect hyporheic-flow characteristics.

Source: Adapted from Tonina and Buffington (2011).

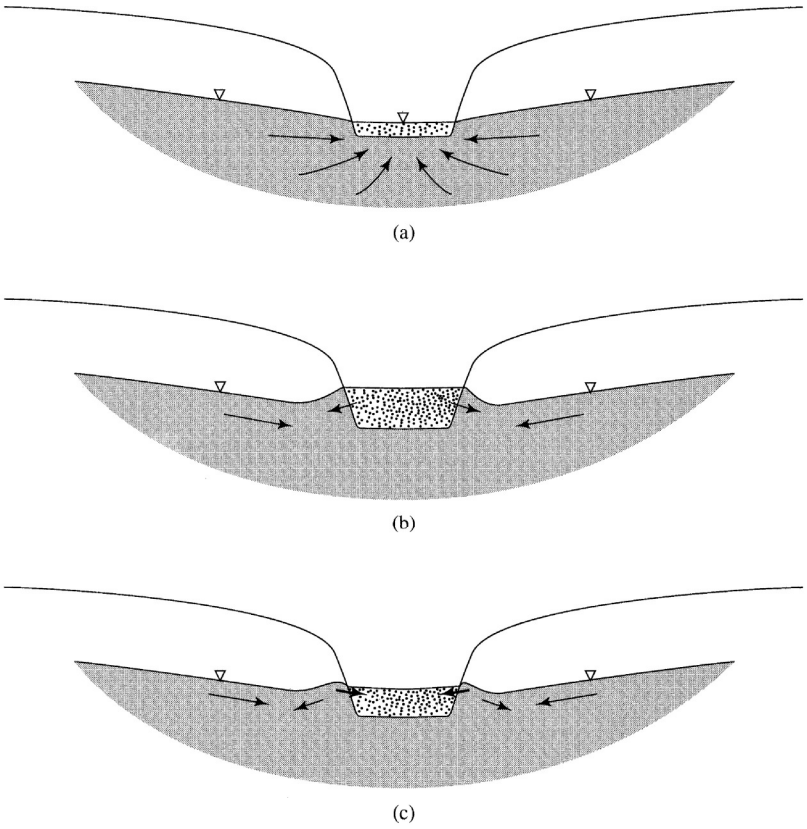

Figure 9.18 The bank-storage process. In (a) the stream is receiving base flow only. In (b) a flood peak is passing, and flow is induced into the banks. In (c) the peak has passed and the bank-storage wedge is draining.

useful approximate analytical solutions to many unconfined flow problems can be developed using assumptions formulated by the French engineer A. J. E. J. Dupuit in 1863. The **Dupuit equations** are derived in box 9.3 (figure 9.20), and are applied to a simplified steady-state model of an aquifer draining to streams in box 9.4 (figure 9.21 on p. 413).

Equation (9B4.9) gives significant insight into the water-balance relations between ground-water and surface-water flows: It shows that average ground-water discharge to streams depends only on the average rate of recharge from infiltration, which is essentially climatically determined, and the stream spacing. The hydraulic conductivity determines the configuration of the water table required to transmit the recharge to streams [equation (9B4.5)], but not the flow rate.

Note that q_{GW} in equation (9B4.9) is the ground-water contribution to streamflow *per unit length of stream* from one-half of the drainage basin above the cross section. Thus for a drainage basin,

$$q_{GW} = \frac{Q_{GW}}{2 \cdot L}, \qquad \textbf{(9.17)}$$

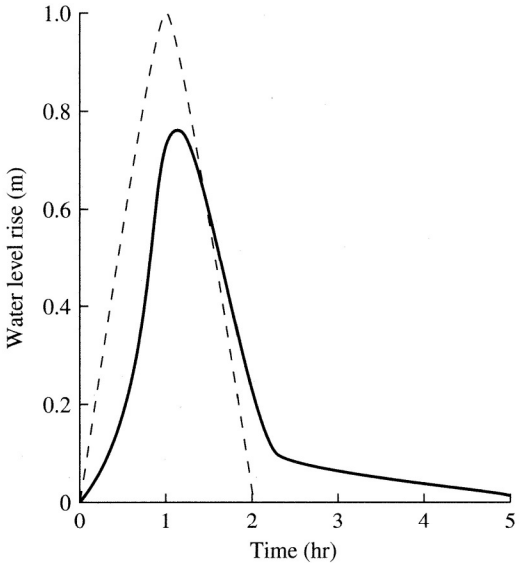

Figure 9.19 Flood-control effect of bank storage. The dashed line shows the magnitude of a hypothetical flood wave in the absence of bank storage; the solid line shows the peak reduction and delay due to bank storage for conditions modeled by Hunt (1990). Bank storage is filling/draining when the dashed hydrograph is above/below the solid-line hydrograph.

Box 9.3 Dupuit Approximation for Unconfined Flow

The Dupuit formulation follows the reasoning used in deriving the general equation for ground-water flow in box 7.3, but with the following simplifying assumptions (see figure 9.20): (1) the control volume extends from a horizontal impermeable base in the *x*-*y* plane up to the water table; (2) at any point in the *x*-*y* plane the total head, *h*, is constant in the vertical (*z*-) direction so that the vertical flow rate $q_z = 0$; and (3) the head gradients are assumed equal to the slope of the water table. These assumptions do not introduce significant errors for water-table slopes < 0.18 (Smith and Wheatcraft 1992).

Under these conditions, the mass inflow, M_{in}, (through faces 1, 2, and 3) during time period d*t* is

$$M_{in} = \rho \cdot q_x \cdot h \cdot dy \cdot dt + \rho \cdot q_y \cdot h \cdot dx \cdot dt + \rho \cdot R_I \cdot dx \cdot dy \cdot dt, \quad \textbf{(9B3.1)}$$

where R_I is the net rate of recharge from infiltration per unit area [L T^{-1}] and q_x and q_y are the Darcy velocities [L T^{-1}] in the *x*- and *y*-directions, respectively. Since both *q* and *h* may change in the *x*- and *y*-directions, the outflow (through faces 3 and 4 only, since face 6 is impermeable) in d*t*, M_{out}, is

$$M_{out} = \rho \cdot \left[q_x \cdot h + \frac{\partial (q_x \cdot h)}{\partial x} \cdot dx \right] \cdot dy \cdot dt + \rho \cdot \left[q_y \cdot h + \frac{\partial \left(q_y \cdot h\right)}{\partial y} \cdot dy \right] \cdot dx \cdot dt. \quad \textbf{(9B3.2)}$$

The change in storage during d*t* is

$$\rho \cdot S_y \cdot \frac{\partial h}{\partial t} \cdot dx \cdot dy \cdot dt, \quad \textbf{(9B3.3)}$$

where S_y is the aquifer specific yield. Thus

$$M_{in} - M_{out} = R_I - \frac{\partial (q_x \cdot h)}{\partial x} - \frac{\partial \left(q_y \cdot h\right)}{\partial y} = S_y \cdot \frac{\partial h}{\partial t}. \quad \textbf{(9B3.4)}$$

Replacing q_x and q_y with the flow rates given by Darcy's law then yields

$$R_I - \frac{\partial}{\partial x}\left(-K_{hx} \cdot \frac{\partial h}{\partial x} \cdot h \right) - \frac{\partial}{\partial y}\left(-K_{hy} \cdot \frac{\partial h}{\partial y} \cdot h \right) = S_y \cdot \frac{\partial h}{\partial t}. \quad \textbf{(9B3.5)}$$

If the aquifer is homogeneous and isotropic ($K_{hx} = K_{hy} = K_h$), this is further simplified to

$$\frac{R_I}{K_h} + \frac{\partial}{\partial x}\left(h \cdot \frac{\partial h}{\partial x} \right) + \frac{\partial}{\partial y}\left(h \cdot \frac{\partial h}{\partial y} \right) = \frac{S_y}{K_h} \cdot \frac{\partial h}{\partial t}. \quad \textbf{(9B3.6)}$$

Now we can make use of the mathematical identities

$$h \cdot \frac{\partial h}{\partial x} = \frac{1}{2} \cdot \frac{\partial \left(h^2\right)}{\partial x}; \quad h \cdot \frac{\partial h}{\partial y} = \frac{1}{2} \cdot \frac{\partial \left(h^2\right)}{\partial y} \quad \textbf{(9B3.7)}$$

to rewrite equation (9B3.6) as

$$\frac{2 \cdot R_I}{K_h} + \frac{\partial^2 \left(h^2\right)}{\partial x^2} + \frac{\partial^2 \left(h^2\right)}{\partial y^2} = \frac{2 \cdot S_Y}{K_h} \cdot \frac{\partial h}{\partial t}, \quad \textbf{(9B3.8)}$$

which is the Dupuit equation for time-varying flow in a homogeneous isotropic aquifer. For steady flow in a homogeneous isotropic aquifer, equation (9B3.8) becomes

$$\frac{2 \cdot R_I}{K_h} + \frac{\partial^2 \left(h^2\right)}{\partial x^2} + \frac{\partial^2 \left(h^2\right)}{\partial y^2} = 0. \quad \textbf{(9B3.9)}$$

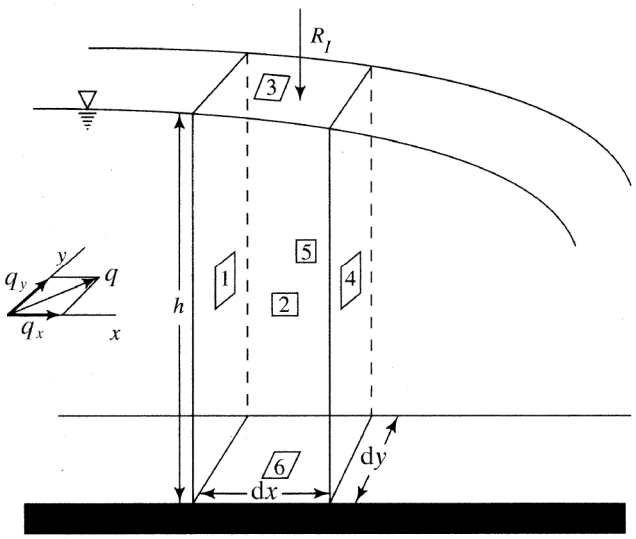

Figure 9.20 Definition diagram for derivation of the Dupuit equation (box 9.3).

Box 9.4 Dupuit Approximation for Steady-State Unconfined Aquifer Drainage to Streams

Figure 9.21 is a simplified version of figure 9.6, in which the land surface between streams is horizontal and the streams are **fully penetrating**, i.e., they extend downward to the basal impermeable layer. We consider long-term average (i.e., steady-state) conditions, and to make the development more general we show an asymmetrical situation, with $h_0 \neq h_X$. Since flow is in the x-direction only, equation (9B3.9) becomes

$$\frac{\partial^2\left(h^2\right)}{\partial x^2} = 0. \qquad \textbf{(9B4.1)}$$

Separating variables and integrating twice yields

$$h^2 = -\frac{R_I}{K_h}\cdot x^2 + C_1 \cdot x + C_2. \qquad \textbf{(9B4.2)}$$

The constants of integration, C_1 and C_2, are evaluated by noting that

$$h = h_0 \text{ at } x = 0 \qquad \textbf{(9B4.3)}$$

and

$$h = h_X \text{ at } x = X, \qquad \textbf{(9B4.4)}$$

so that

$$h^2 = -\frac{R_I}{K_h}\cdot x^2 + \left(\frac{h_X^2 - h_0^2}{X} + \frac{R_I \cdot X}{K_h}\right)\cdot x + h_0^2. \qquad \textbf{(9B4.5)}$$

Equation (9B4.5) states that the water table in this situation is a curved surface whose shape is determined by the stream spacing (X), the hydraulic conductivity (K_h), the recharge rate (R_I), and the stream elevations h_0 and h_X. By manipulation of this relation, we can show that the maximum water-table elevation (i.e., the groundwater divide), h_{max}, occurs at $x = X_d$, where

$$X_d = \left[\frac{X}{2} - \frac{K_h \cdot \left(h_0^2 - h_X^2\right)}{2 \cdot R_I \cdot X}\right] \qquad \textbf{(9B4.6)}$$

and has a value

$$h_{max} = \left[h_0^2 - \frac{\left(h_0^2 - h_X^2\right)\cdot X_d}{X} - \frac{R_I \cdot (X - X_d)\cdot X_d}{K_h}\right]^{1/2}. \qquad \textbf{(9B4.7)}$$

Note that for $h_0 = h_X$ the configuration becomes symmetrical, analogous to figure 9.6. Under these conditions, the discharge to the streams (per unit stream length), q_{GW}, is

$$q_{GW} = q_{GW\,0} = q_{GW\,X} = -K_h \cdot h_X \cdot \left.\frac{dh}{dx}\right|_X. \qquad \textbf{(9B4.8)}$$

Evaluating dh/dx from equation (9B4.5) and substituting into equation (9B4.8) then leads to

$$q_{GW} = \frac{R_I \cdot X}{2}. \qquad \textbf{(9B4.9)}$$

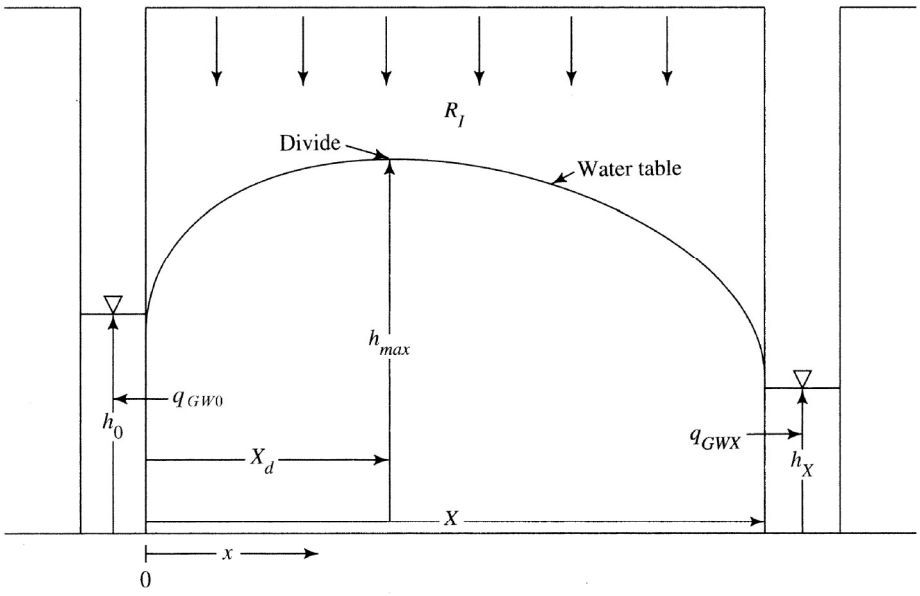

Figure 9.21 Definition sketch for Dupuit flow to streams (box 9.4). Under the Dupuit assumptions (box 9.3), equipotential lines are vertical and streamlines are horizontal, in contrast to figure 9.6.

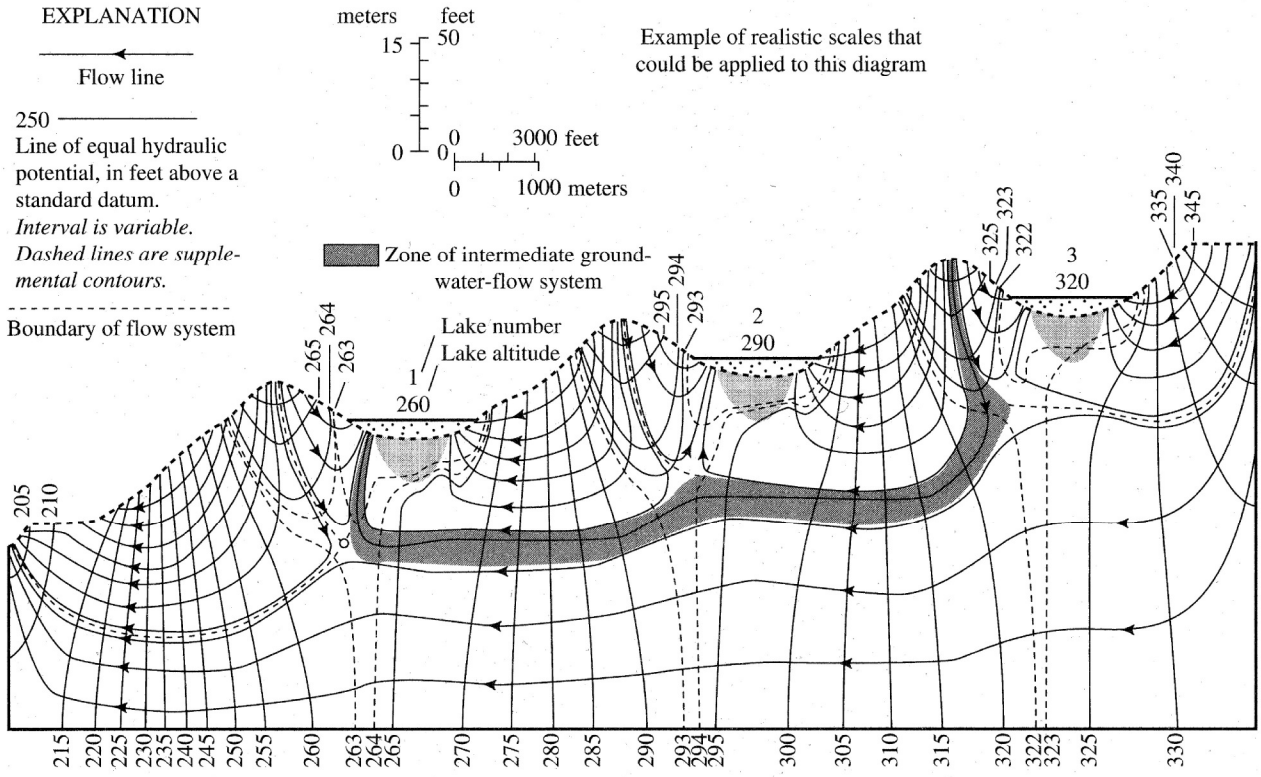

Figure 9.22 Hypothetical ground-water–lake relations. (a) Flow net for a system of three lakes above a main stream. With a homogeneous aquifer there are local, intermediate, and regional flow systems and the lakes are zones of discharge for local systems [Winter (1976)].

where Q_{GW} is the ground-water contribution to streamflow from the drainage basin above the cross section and L is the length of the main stream above the cross section (perpendicular to the cross section). An important implication of equation (9B4.9) is that one can estimate recharge from infiltration as

$$R_I = \frac{Q_{GW}}{X \cdot L}. \qquad \textbf{(9.18)}$$

Methods for evaluating Q_{GW} are discussed in section 9.5.3.

9.3.2 Ground Water and Lakes and Wetlands

Lakes have the same range of relations to ground water as shown for streams in figure 9.17. Like gaining streams, perennial lakes usually occur in discharge zones, although some are flow-through systems. Seasonal lakes can be local sources of recharge, like losing streams. In gaining and flow-through situations, the lake surface is at the water-table elevation.

Most fresh-water wetlands are on the borders of streams or lakes, or are former lakes that have been largely or wholly filled with mineral and organic soil and vegetation in various proportions. Thus they are hydrologically similar to lakes, and the discussion here can also be applied to bogs, swamps, and marshes. Dooge (1975) and LaBaugh (1986) provide useful reviews of wetland hydrology and Doss (1993), Hunt et al. (1996), and Rosenberry and Winter (1997) describe field investigations.

As with regional flow systems, much of our understanding of ground-water–lake interactions is based on mathematical simulations of idealized situations (McBride and Pfannkuch 1975; Winter 1976, 1978, 1983; Cheng and Anderson 1994), supplemented increasingly by field studies (e.g., Crowe and Schwartz 1985; Cherkauer and Zager 1989; Shaw and Prepas 1990; Winter 1999; Winter et al. 2003). Figure 9.22 shows examples of some of the complex ground-water–lake interactions that can exist in a simple topographic setting as revealed by modeling studies. In figure 9.22a the subsurface has uniform

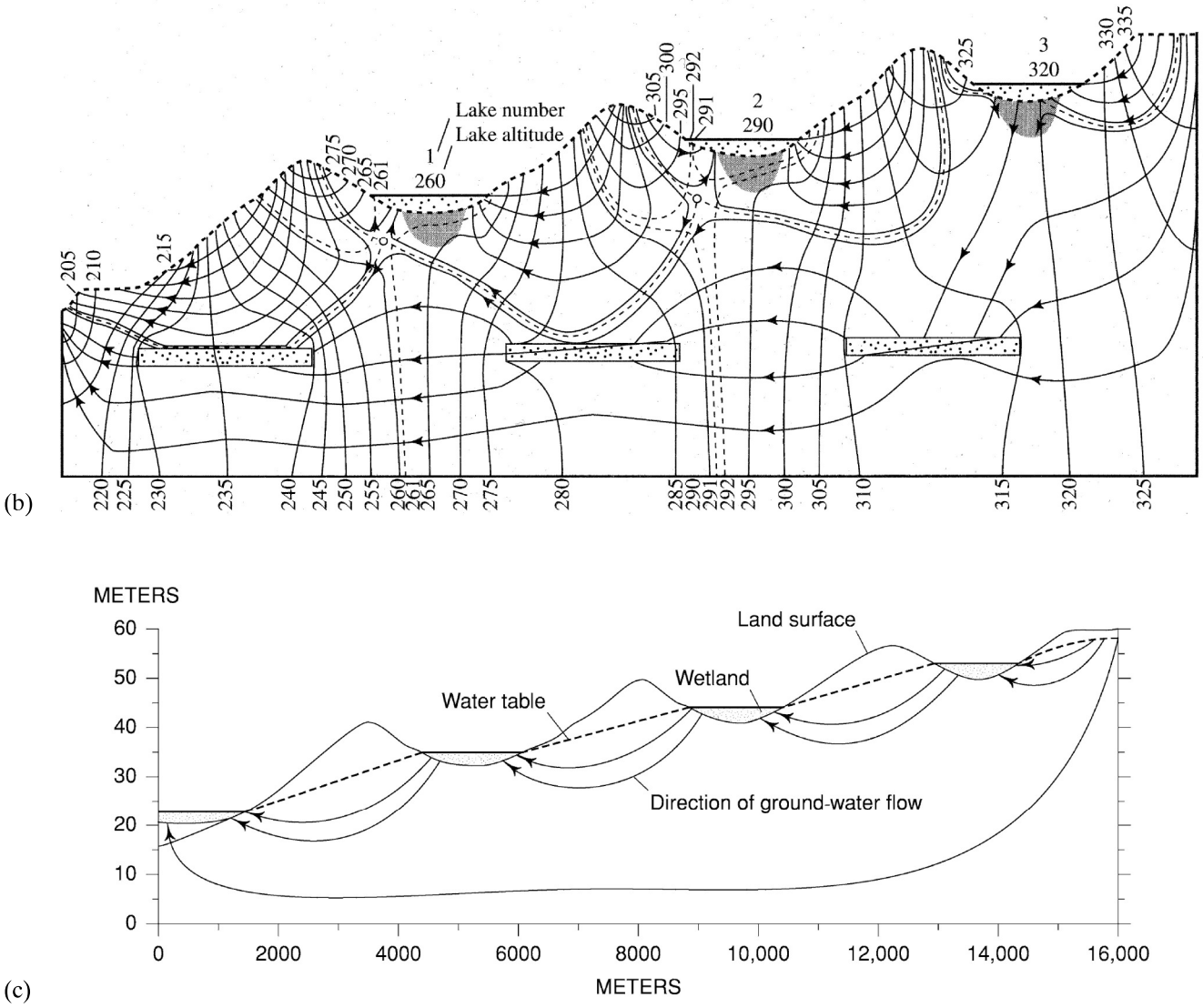

Figure 9.22 *(continued)* (b) Same as (a), but with three high-conductivity lenses at depth. Now the intermediate system disappears and the highest lake receives discharge near its edge and contributes recharge in its center [Winter (1976)]. (c) Ground-water flow systems where water table highs do not underlie topographic highs. The surface water bodies are flow-through with respect to ground water [reproduced from Winter et al. (2003), Where does the ground water in small watersheds come from? *Ground Water* 41(7):989–1000, with permission from Wiley].

and isotropic hydraulic conductivity and the water table slopes toward the three lakes from all sides. Here the lakes are in the discharge zones of local flow systems; there is a regional flow system at depth, and an intermediate system that discharges into the lowest lake. Figure 9.22b shows a situation topographically identical to figure 9.22a, but here discontinuous lenses of high hydraulic conductivity at depth change the flow net so that the highest lake contributes recharge through its bottom while receiving discharge around its perimeter. Flow-through lakes tend to occur where water tables do not rise under topographic highs (figure 9.22c).

Modeling and field studies have also shown that, even where the surrounding geologic materials are homogeneous, ground-water inflow to lakes is concentrated in the littoral zone whether or not there are relatively impermeable sediments present in the deeper part of the lake. However, high-conductivity zones in the lake bed can be loci of local

concentration of inflows (springs), or zones of outflow (recharge), depending on the regional ground-water configuration (Cherkauer and Nader 1989; Winter 1999).

In some situations, lakes can be recharge sites exclusively, at least at certain seasons. Meyboom (1966) showed that, in southern Saskatchewan, Canada, spring snowmelt runoff accumulates in small depressions (prairie potholes) that are above the recharge zone of a regional flow system. The subsequent leaking of these small ponds produces localized ground-water mounds representing recharge to this system. This local ground-water flow pattern reverses in the summer, when trees growing around the edges of the potholes extract ground water and thereby make the potholes sites of discharge for temporary local flow systems.

Studies by Winter (1983), Sacks et al. (1992), and Anderson and Cheng (1993) also showed significant seasonal changes in local ground-water flow systems adjacent to lakes. Winter et al. (2003) reviewed field studies of ground-water–lake interactions and noted that surface-water and ground-water watersheds of lakes commonly do not coincide. It is often difficult to determine the extents of subsurface contributing areas because of the lack of detailed subsurface information, the coexistence of ground-water circulations of local to regional scales, and often the effects of seasonal variability on system boundaries. They found that lakes and wetlands in small watersheds at the lower end of extensive ground-water flow systems may receive subsurface inflow from shallow flow systems that extend far beyond their surface watershed, and may also receive ground-water inflow from deeper regional flow systems.

The above review makes it clear that the hydrologic setting of lakes and wetlands may be complex and very difficult to determine without detailed subsurface information, perhaps over an extensive area. This makes it difficult to quantify the most basic hydrologic characterization—the water-balance equation relating inflows, outflows, and storage changes.

9.3.3 Ground Water and the Ocean

Figure 9.23 depicts the relations between fresh and salt ground water in a simple coastal aquifer. The Ghyben–Herzberg relation (box 9.5 on pp. 418–419) indicates that the salt/fresh interface lies at a depth below sea level equal to 40 times the height of the water table above sea level, and the water-table elevation decreases to zero at the coast. Equation (9B5.6) gives the depth of the interface as a function of distance from the coast.

In real situations the position of the interface differs somewhat from the static equilibrium given by the Ghyben–Herzberg relation because the aquifer receives recharge from infiltration, and water-balance considerations dictate that the average net recharge rate must be balanced by an equal average discharge to the ocean. This discharge occurs through an outflow face that extends seaward from the coast, the width of which is given by equation (9B5.9). The average discharge, q_{GW}, per unit length of coastline is given by

$$q_{GW} = R \cdot X, \qquad \textbf{(9.19)}$$

where R is the net recharge rate [L T^{-1}] and X is the distance inland to the ground-water divide. Equation (9B5.10) gives the depth of the interface when the outflow face is accounted for.

As the example in box 9.5 shows, the width of the outflow face is usually small compared to the scale of the flow system, and the Ghyben–Herzberg relation gives a useful approximation, except very near the coast, in many situations.

9.4 Ground Water in the Regional Water Balance

In this section we apply the basic water-balance equation (section 1.8.1) to the ground water of a region. The main purposes of the analysis are to (1) define the ground-water balance components and (2) show how the ground-water balance relates to the overall regional water balance. Section 9.5 then describes approaches to quantifying the various components.

The surface extent of the control volume for the water-balance equation can be defined arbitrarily—it could be a political division, an aquifer, or a topographically defined watershed. The lower boundary of the control volume is usually defined as the "depth at which ground-water flow is negligible"; if the geology is known, this can be more precisely specified.

Choosing a watershed as a control volume has one important advantage: It is usually possible to measure at least one of the balance components, surface-water outflow (streamflow), accurately. However,

> researchers studying small watersheds need to be aware that ground water flow divides do not underlie surface divides in many settings. Only if a surface watershed of a research site is at the highest ridge

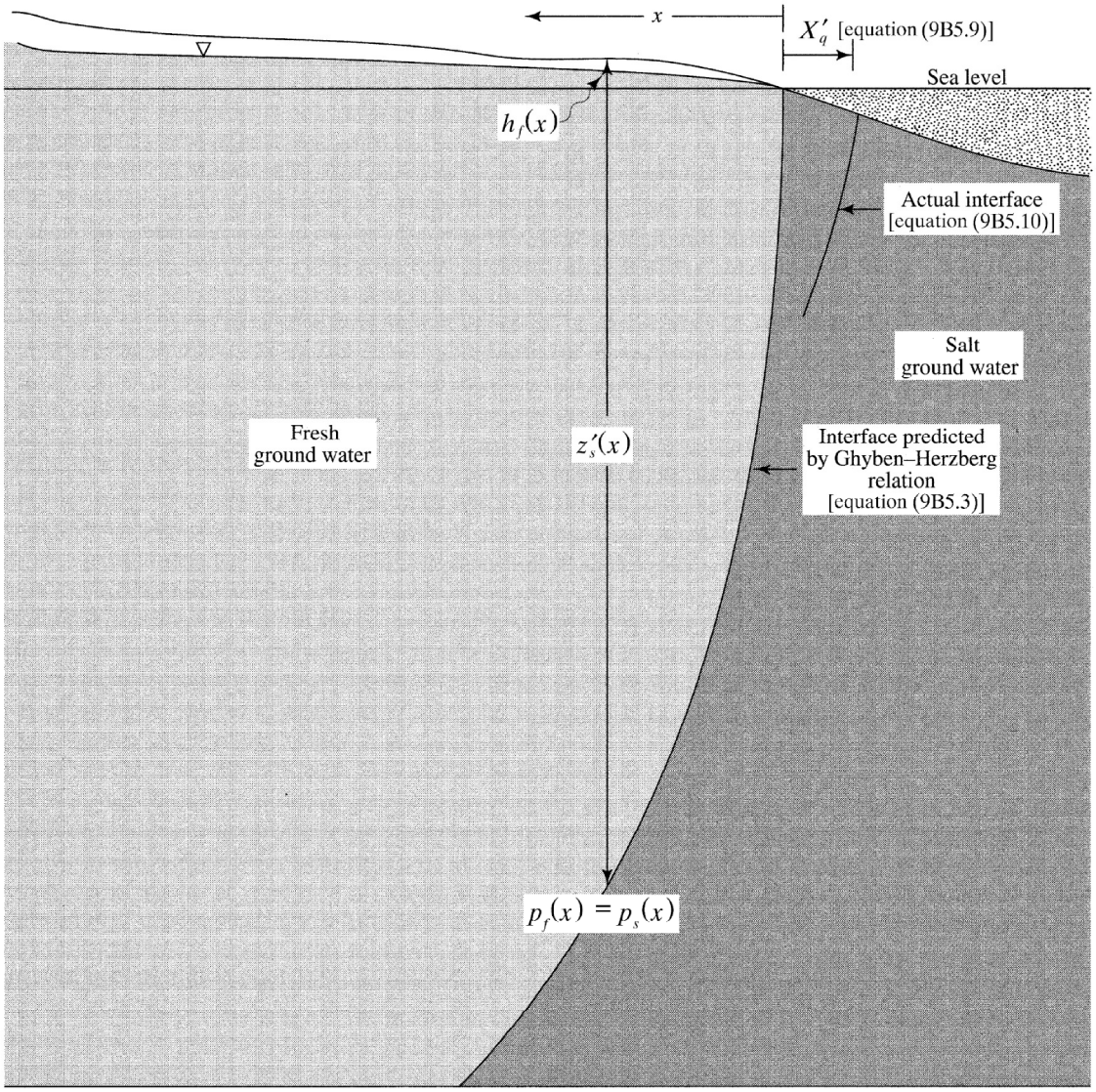

Figure 9.23 Definition sketch for deriving the Ghyben–Herzberg relation (box 9.5). The salt-water–fresh-water interface position predicted by this hydrostatic relation differs somewhat from the actual position near the coast due to the dynamics of the flow, which produces an outflow face of width X_q', which can be estimated via equation (8B5.8).

away from major hydrologic sinks such as regional rivers, can one be sure that ground water is not moving into the area from distant sources. For most other watersheds, ground water can move into watersheds either because ground water divides are not present beneath the surface divides or because ground water moves into the area from deeper flow systems. Ground water divides move in response to changing recharge conditions, which in turn is related to the dynamics of climate and precipitation. (Winter et al. 2003, pp. 998–999)

An example of a situation where ground-water and surface-water divides do not coincide is shown in figure 9.24 on p. 419.

Thus, although the water-balance equations are straightforward, recall from section 1.11.2 that measurement errors, which are inevitable, are propagated through calculations and can lead to large uncertainty in final estimates. For regional water balances, these errors are likely to result from (1) insufficient knowledge of the system boundaries and (2) failure to fully account for regional variability.

Box 9.5 The Fresh/Salt Ground-Water Interface in Coastal Aquifers

Ghyben–Herzberg Relation

Figure 9.23 shows the interface between fresh and salt ground water in a homogeneous unconfined aquifer at a coastline. If we assume that this interface is a static sharp boundary, the hydrostatic pressure on the fresh-water side of the fresh/salt interface, $p_f(x)$, is

$$p_f(x) = \gamma_f \cdot [h_f(x) + z_s'(x)], \qquad \textbf{(9B5.1)}$$

where x is distance inland from the coast, γ_f is the weight density of fresh water, $h_f(x)$ is the elevation above sea level of the water table, and $z_s'(x)$ is the distance below sea level of the interface. The hydrostatic pressure on the sea-water side of the interface, $p_s(x)$, is

$$p_s(x) = \gamma_s \cdot z_s'(x), \qquad \textbf{(9B5.2)}$$

where γ_s is the weight density of sea water.

At hydrostatic equilibrium $p_f(x) = p_s(x)$, so equating equations (9B5.1) and (9B5.2) and solving for $z_s'(x)$ yields

$$z_s'(x) = \Gamma \cdot h_f(x), \qquad \textbf{(9B5.3)}$$

where

$$\Gamma \equiv \frac{\gamma_f}{\gamma_s - \gamma_f} = \frac{9{,}800\ \text{N/m}^3}{10{,}045\ \text{N/m}^3 - 9{,}800\ \text{N/m}^3} = 40. \qquad \textbf{(9B5.4)}$$

Thus

$$z_s'(x) = 40 \cdot h_f(x); \qquad \textbf{(9B5.5)}$$

i.e., at any distance inland, x, the depth below sea level to the salt/fresh interface is 40 times the height above sea level of the water table. This analysis of the fresh/salt ground-water interface was formulated over 100 years ago, and is known as the **Ghyben–Herzberg relation**.

Todd (1953) used the Ghyben–Herzberg assumptions along with the Dupuit equation (box 9.4) to give the depth to the interface as a function of the ground-water discharge and the hydraulic conductivity of the aquifer:

$$z_s'(x) = \left(\frac{2 \cdot \Gamma \cdot q_{GW} \cdot x}{K_h} \right)^{1/2}, \qquad \textbf{(9B5.6)}$$

where q_{GW} is the ground-water discharge to the ocean per unit length of coastline [$L^2\ T^{-1}$] and K_h is hydraulic conductivity. Equating (9B5.3) and (9B5.6) gives relations for the height of the water table as a function of distance from the coast, discharge, and conductivity:

$$h_f(x) = \left(\frac{2 \cdot q_{GW} \cdot x}{\Gamma \cdot K_h} \right)^{1/2}. \qquad \textbf{(9B5.7)}$$

Ground-Water Outflow to Ocean

Analogously to equation (9.17), q_{GW} is the product of the average recharge rate, R [$L\ T^{-1}$], and the distance from the ground-water flow divide to the coast, X [L]:

$$q_{GW} = R \cdot X. \qquad \textbf{(9B5.8)}$$

The Ghyben–Herzberg analysis does not provide for a sub-sea zone in which this discharge must occur. To account for this, Glover (1964) developed a simple model that gives the seaward extent of the **outflow face**, X_q', as

$$X_q' = \frac{\Gamma \cdot q_{GW}}{2 \cdot K_h} = 20 \cdot \frac{q_{GW}}{K_h}. \qquad \textbf{(9B5.9)}$$

To account for this, an additional term is included in equation (9B5.6) giving the depth to the salt/fresh interface:

$$z_s'(x') = \left(\frac{2 \cdot \Gamma \cdot q_{GW} \cdot x'}{K_h} + \frac{\Gamma^2 \cdot q_{GW}^2}{K_h^2} \right)^{1/2}, 0 \le x', \qquad \textbf{(9B5.10)}$$

where x' is the distance seaward from the coast. The relative importance of this additional term increases toward the coast, and at the coast ($x' = 0$) the interface depth is

$$z_s(0) = \frac{\Gamma \cdot q_{GW}}{K_h}. \qquad \textbf{(9B5.11)}$$

Example

Here we use the relations derived above to calculate aspects of the ground-water discharge to the Atlantic Ocean from the southern part of Long Island, New York. The region is underlain by relatively homogeneous glacial sands and gravels about 120 m thick overlying coastal-plain sedimentary rocks, which are relatively impermeable. The distance from the central ground-water divide to the south coast is about 16 km. The average annual recharge is about 0.57 m/yr, the hydraulic conductivity of the aquifer is about 50 m/day = 18,250 m/yr. Thus using equation (9B5.8), the discharge to the ocean is

$$q_{GW} = 0.57\ \text{m/yr} \times 16{,}000\ \text{m} = 9{,}120\ \text{m}^2\text{/yr per m of coastline.}$$

Our analysis will not be valid for points landward of where the fresh/salt interface depth equals the aquifer thickness; to calculate that distance, X^*, we rearrange equation (9B5.6) and find the distance corresponding to the aquifer thickness:

$$X^* = \frac{K_h \cdot z_s(X^*)^2}{2 \cdot \Gamma \cdot q_{GW}} = \frac{(18{,}250\ \text{m/yr}) \times (120\ \text{m})^2}{2 \times 40 \times (9{,}120\ \text{m}^2\text{/yr})} = 360\ \text{m};$$

Table 9B5.1 compares the depths to the interface at increasing distances from the coast computed via equations (9B5.7) and (9B5.10) for $x \leq X^*$.

The width of the outflow face, X_q', extending seaward from the south coast is found from equation (9B5.9):

$$X_q' = \frac{40 \times 9{,}120 \text{ m}^2/\text{yr}}{2 \times 18{,}250 \text{ m/yr}} = 9.99 \text{ m}.$$

Table 9B5.1

Distance, x (m)	Equation (9B5.7)		Equation (9B5.9)	
	Interface Depth, z_s' (m)	Water-Table Height, h_f (m)	Interface Depth, z_s' (m)	Water-Table Height, h_f (m)
0	0	0.0	20	0.5
10	20	0.5	40	1.0
20	28	0.7	48	1.2
50	45	1.1	65	1.6
100	63	1.6	83	2.1
200	89	2.2	109	2.7
250	100	2.5	120	3.0
300	110	2.7	120	—
360	120	3.0	120	—

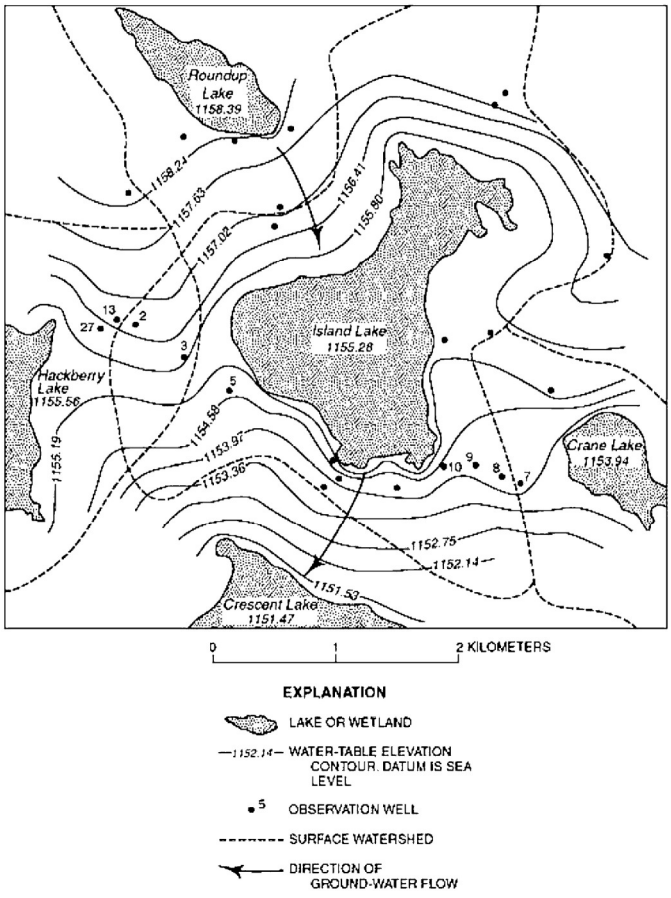

Figure 9.24 Island Lake area in Nebraska showing surface-water bodies, surface watersheds, contours of the water table (m), and direction of ground-water flow on October 28, 1982. Note ground-water flow across surface-water divides [reproduced from Winter et al. (2003), Where does the ground water in small watersheds come from? *Ground Water* 41(7):989–1000, with permission from Wiley].

Under natural (i.e., no pumping or artificial water imports or exports) conditions,[2] the regional water balance can be written as

$$P + G_{in} = Q + ET + G_{out} \qquad \textbf{(9.20)}$$

where P is precipitation, Q is stream outflow, ET is evapotranspiration, G_{in} is water entering as ground water, G_{out} is water leaving as ground water, and all quantities are long-term average values (i.e., storage changes are assumed zero) (figure 9.25). Note that the terms in these water-balance relations can be expressed as volumes [L^3] or volumes per unit area [L] during a specific time period, or as average rates [$L^3\ T^{-1}$] or [$L\ T^{-1}$].

Under the same conditions, the long-term average water balance for the aggregated ground-water reservoir in the basin is

$$R_I + R_{SW} + G_{in} = CR + Q_{GW} + G_{out} \qquad \textbf{(9.21)}$$

where R_I is recharge from infiltration, R_{SW} is recharge from surface-water bodies, CR is the move-

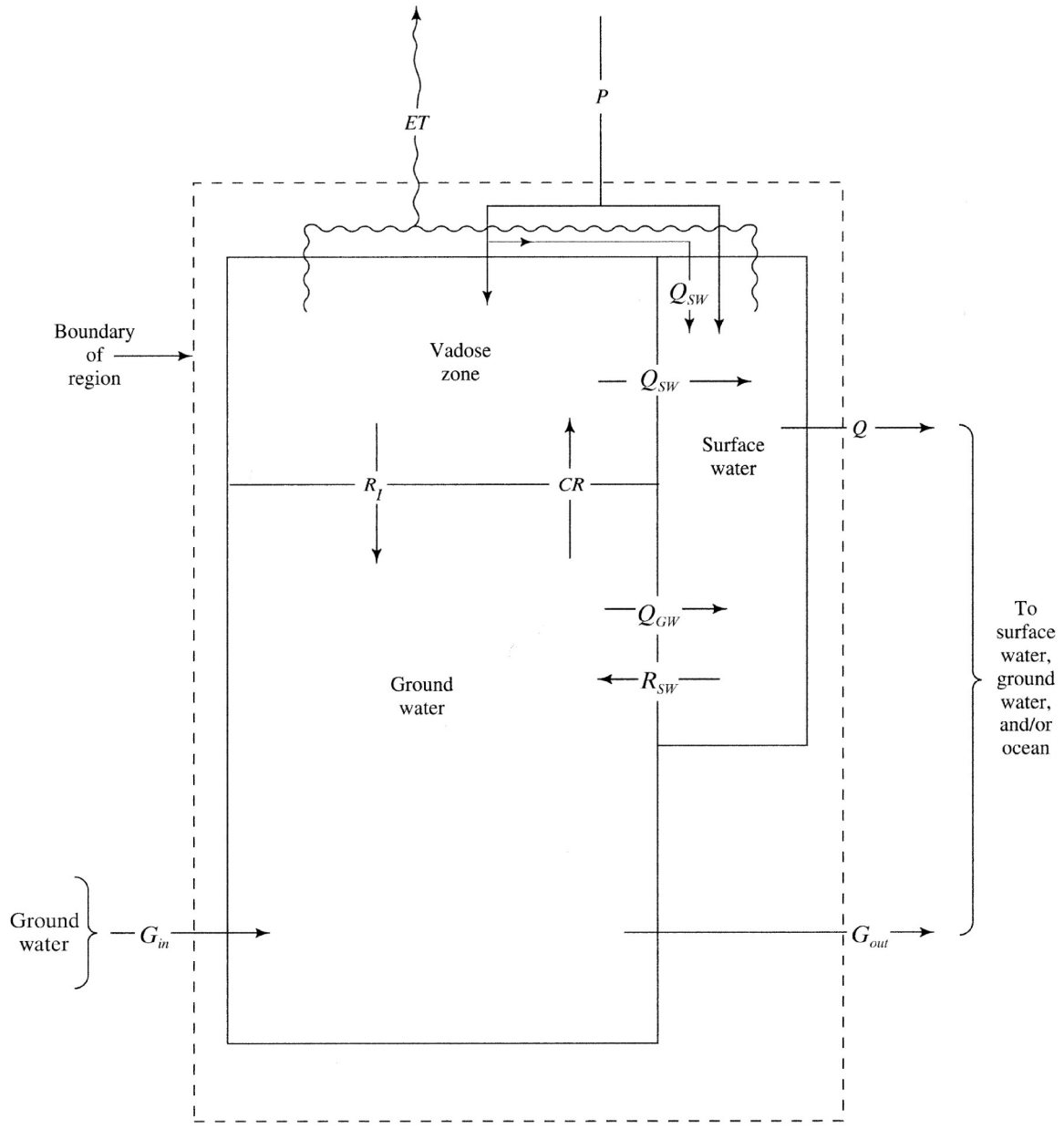

Figure 9.25 Schematic water balance for a drainage basin.

ment of water from ground water into the capillary fringe (capillary rise),[3] and Q_{GW} is the ground-water contribution to streamflow. We can then define **net recharge**, R, as

$$R \equiv R_I + R_{SW} - CR. \qquad \textbf{(9.22)}$$

Equations (9.20)–(9.22) can be combined to give

$$P - Q - ET = R_I + R_{SW} - CR - Q_{GW} = R - Q_{GW} \qquad \textbf{(9.23a)}$$

or

$$P - Q_{SW} - ET = R_I + R_{SW} - CR = R, \qquad \textbf{(9.23b)}$$

where Q_{SW} is the non-ground-water contribution to streamflow.

Box 9.6 provides an example of a very simple "first-cut" approach to estimating the ground-water balance, in which standard network hydroclimatological data and general knowledge of basin geology and water-table configurations are used to estimate various ground-water balance terms. In general, this approach has severe limitations, usually because of incomplete knowledge of ground-water divides. These are probably fairly well known in this case, but even if we also make the assumptions that long-term average values of P, Q, and ET are well known, we can at best use equation (9.20) to estimate ($G_{out} - G_{in}$), and equations (9.21) and (9.22) to estimate ($R_I + R_{SW} - CR - Q_{GW}$) = ($R - Q_{GW}$).

Thus even under ideal conditions where standard network data provides good estimates of P, ET, and Q, firm knowledge of a basin's water balance usually requires independently evaluating at least some of the terms in equation (9.21). Approaches to obtaining quantitative estimates of these terms are described in the following section.

Box 9.6 Ground-Water-Balance Example

Cohen et al. (1968) developed a water balance for the aquifer described in the example in box 9.5 based on standard network meteorologic and hydrologic data collected over the period 1940–1965. Long-term average water-balance data are given in table 9B6.1. P estimates were based on data collected at five stations and Q estimates on records at five gauging stations. ET was estimated based on average monthly temperatures via the Thornthwaite approach (see chapter 6). Estimates of CR (here assumed equal to direct evapotranspiration from ground water), Q_{GW}, R_{SW}, and G_{in} were based on hydrologic judgment and the configuration of the water table.

Table 9B6.1

Quantity	Value (mm/yr)	Source
P	1,120	m
ET	541	em, eh
Q	249	m
CR	10	eh
Q_{GW}	224	eq
R_{SW}	0	eh
G_{in}	0	eh

m ≡ measured
em ≡ estimated from meteorological measurements
eh ≡ estimated based on water-table configuration
eq ≡ estimated via base-flow analysis (section 9.5.3.6)

Estimates of G_{out}, R_I, and R are found by substitution of the appropriate values from table 9B6.1 into the appropriate water-balance equations, as shown in table 9B6.2.

Table 9B6.2

Quantity	Equation	Value (mm/yr)
G_{out}	9.16	328
R_I	9.17	561
R	9.18	551

Note that G_{out} here represents direct ground-water flow to the ocean plus outflow across the drainage-basin boundaries; these were estimated by Cohen et al. (1968) as 237 mm/yr and 91 mm/yr, respectively.

The aquifer has an average thickness of 60 m. From table 9.1, the specific yield of unconsolidated sand and gravel $S_y \approx 0.30$. Thus the average residence time of ground water is estimated via equation (9.14) as

$$T_R = \frac{60\text{ m} \times 0.30}{0.551\text{ m/yr}} \approx 33\text{ yr}.$$

9.5 Evaluation of Ground-Water Balance Components

This section reviews approaches to quantitative evaluation of the components of the ground-water balance [equation (9.21), figure 9.25] in a given location from field measurements. Most of these approaches are based on application of basic water-balance concepts and/or Darcy's law, in some cases employing various water-quality constituents as tracers and/or remotely sensed observations. A still useful and historically interesting review of early (1686–1931) approaches to estimating ground-water components was compiled by Meinzer (1932). Smerdon et al. (2009) described a modern comprehensive approach that integrates a range of tools, including ground-water modeling, to assess the ground-water budget in a mountain watershed.

9.5.1 Recharge from Infiltration, R_I

Infiltrated water can carry contaminants from agriculture, industries, and waste-disposal sites to the ground-water reservoir, so quantification of R_I has important implications for the study of water quality as well as quantity.

As noted, the water-table configurations in the regional ground-water flows depicted in figures 9.5 to 9.7 and 9.10 to 9.12 were specified as boundary conditions to illustrate typical flow configurations, and these conditions determined the locations of recharge and discharge zones. Since recharge from infiltration is the principal source of water to unconfined aquifers and is the ultimate source of most streamflow, it is of interest to explore further the natural factors that determine the regional distribution of recharge and discharge.

Direct measurement of recharge requires elaborate instrumentation and is feasible only in a research setting. In one of the few such studies, Wu et al. (1996) installed lysimeters consisting of 60-cm diameter soil-filled cylinders in which the water table was kept at depths ranging from 1.5 to 5 m. At the shallowest depth almost every water-input event caused a separate recharge event that was reflected in a rise, peak, and decline of the water table; but at 5 m individual events were not identifiable and there was a single annual peak. At intermediate depths, individual recharge events were associated with input events separated by a "critical" time interval that increased with depth. The relationship between recharge, precipitation (P), and evapotranspiration (ET) for individual events were

$$\text{1.5-m depth: } R_I = 0.87 \cdot (P - 5.25) \quad \textbf{(9.24a)}$$

$$\text{4.5-m depth: } R_I = 0.87 \cdot (P - ET - 27.4) \quad \textbf{(9.24b)}$$

where all quantities are in cm.

In nature the depth of the water table at a given location is determined by feedbacks among precipitation, infiltration, runoff, and evapotranspiration at that location along with the regional flow, which integrates those quantities throughout the drainage basin under the influence of topography and geology. On average, the water table is at an equilibrium depth such that the net recharge (i.e., percolation minus capillary rise to supply evapotranspiration) from above is just balanced by the net ground-water flow away from (recharge areas) or toward (discharge areas) the water table. When the water table is above this depth, losses to evapotranspiration exceed recharge and a discharge zone exists; when below this depth, recharge exceeds evapotranspiration and a recharge zone exists.

Levine and Salvucci (1999) quantitatively modeled these relations and showed how water-table depth is related to net recharge for various soil types. They found that net recharge increases and evapotranspiration and surface runoff generally decrease as water-table depth increases (figure 9.26). Figure 9.27 on p. 424 shows regional ground-water flow and recharge and discharge zones modeled using these more realistic relationships in climatic, topographic, and geologic conditions similar to those assumed in figure 9.7b. Note that local, intermediate, and regional circulations occur in both, but that discharge zones are more concentrated in figure 9.27. Salama et al. (1994) showed that aerial photographs and satellite imagery can be used to map regional recharge and discharge areas.

Because of the difficulty in direct measurement of recharge, hydrologists have attempted to evaluate R_I by applying various combinations of water-balance concepts, applications of Darcy's law, soil-physics principles, mathematical systems models, and water-quality measurements. The major methodological approaches are briefly described here, following in part the review of Van Tonder and Kirchner (1990). Most of these methods require elaborate and careful data collection, and Sophocleous and Perry (1984) provide a useful overview of considerations in selecting instrumentation for recharge studies.

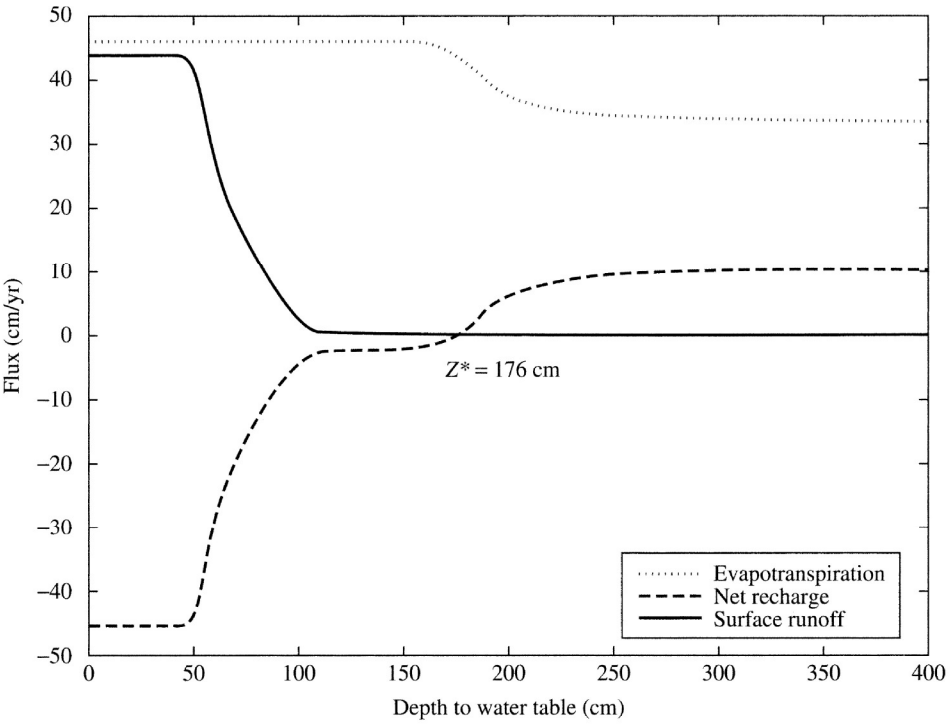

Figure 9.26 Variations of evapotranspiration, net recharge, and surface runoff as a function of water-table depth for a silt-loam soil [Levine and Salvucci (1999). Equilibrium analysis of groundwater-vadose zone interactions and the resulting spatial distribution of hydrologic fluxes across a Canadian prairie. *Water Resources Research* 35:1369–1383, with permission of the American Geophysical Union].

9.5.1.1 Soil-Water Balance Method

The water balance for the root zone of a soil for a time period Δt can be written as

$$R_I = P - ET - Q_{SW} - R_{SW} + CR + \Delta S, \quad \textbf{(9.25)}$$

where Q_{SW} represents surface outflow, ΔS is the change in soil-water storage during Δt, and the other symbols are as defined for equation (9.20) and (9.21). Equation (9.25) is usually applied to a small plot where P and Q_{SW} are directly measured, ET is determined by measuring meteorological parameters and applying one of the approaches discussed in chapter 6, R_{SW} and CR are assumed negligible, and ΔS is calculated from measurements of water content at several depths using one of the approaches discussed in section 7.2.1.2. Rushton and Ward (1979) found that Δt should not exceed 1 day to minimize propagation of measurement errors. Steenhuis et al. (1985) used equation (9.25), assuming that all terms except P and ET were negligible, and estimated regional R_I on Long Island, New York, as simply

$$R_I = P - ET, \quad \textbf{(9.26)}$$

where P was measured and ET was calculated from detailed energy-balance measurements at the site (section 6.8.3).

As noted, the major concerns in applying various forms of the water-balance equation are (1) making measurements with sufficient precision such that errors in the final computations are within acceptable limits and (2) acquiring sufficient measurements to characterize the regional situation. Finch (1998) found that recharge estimates are highly sensitive to soil characteristics, and Rushton and Ward (1979) concluded that uncertainties of ±15% should be expected with this approach.

In spite of these caveats, the basic method—with varying approaches to modeling ET and soil-water storage—has been successful in estimating R_I in a small coastal-plain drainage basin in Maryland (Rasmussen and Andreasen 1959), chalk and sandstone aquifers of England (Wellings 1984; Ragab et al. 1997) and France (Thiery 1988), glacial deposits on Long Island, New York (Steenhuis et al. 1985; Steenhuis and Van Der Molen 1986), and Sweden (Johansson 1987), and in a large drainage basin in Australia (Chiew and McMahon 1990).

9.5.1.2 Analysis of Well Hydrographs

Well hydrographs are observations of water levels in monitoring wells plotted against time. To evaluate recharge, the hydrographs are combined with hyetographs showing the timing and amount of water input

(figure 9.28). Recharge is reflected in the rise of the hydrograph following a water-input event, after which drainage to surface-water bodies is reflected in a gradual decline. There are several approaches to estimating recharge from well hydrographs; most of these assume that unconfined aquifers can be modeled as linear reservoirs (box 9.7; figure 9.29, both on p. 426), which is often approximately true (Brutsaert and Lopez 1998).

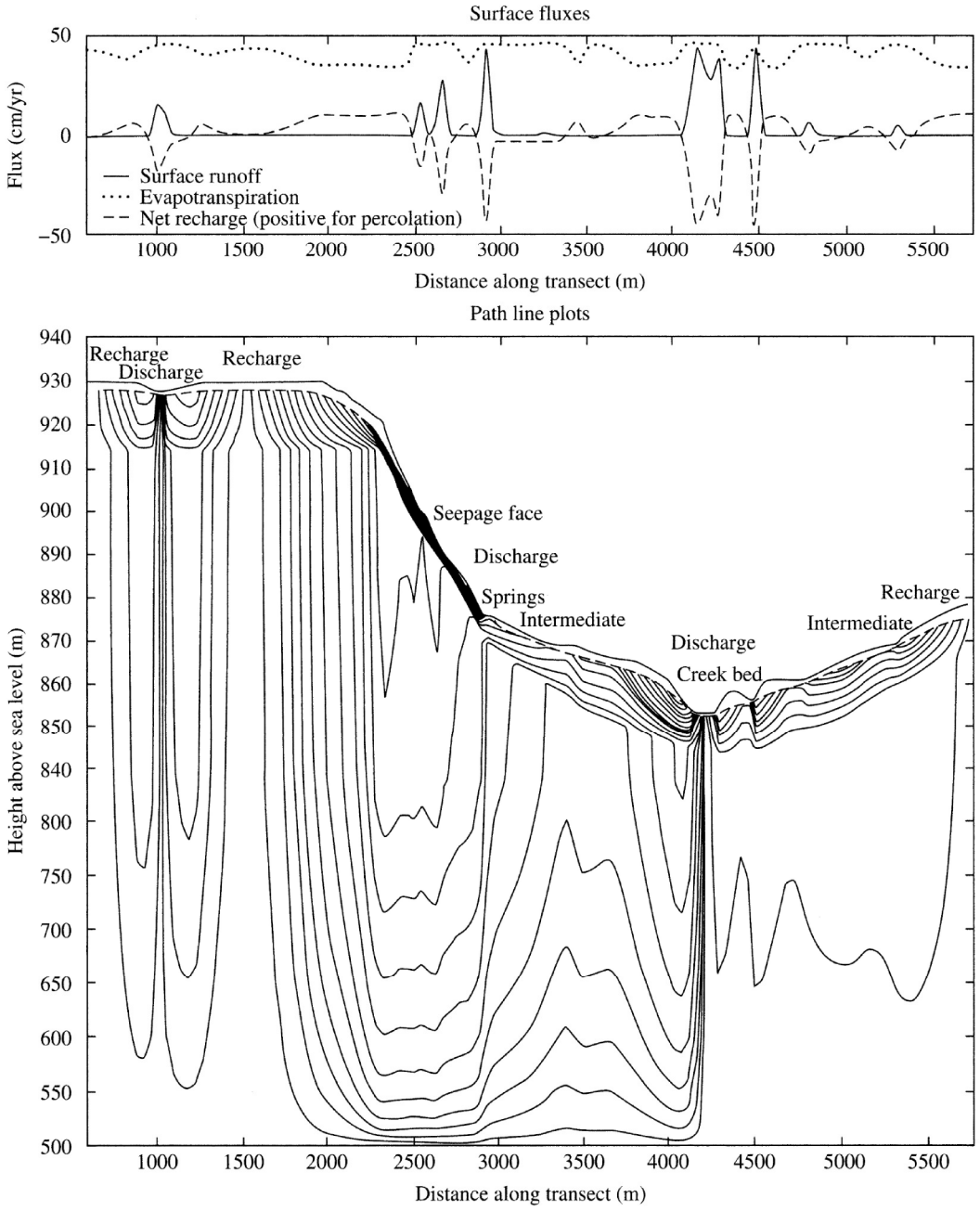

Figure 9.27 Recharge areas, discharge areas, and streamlines for a cross section of a drainage basin in Alberta, Canada, as determined by coupling recharge estimated via unsaturated flow modeling with a ground-water flow model. Note that the discharge areas are more concentrated than predicted from ground-water flow modeling with imposed water-table configuration (compare figure 9.7) [Levine and Salvucci (1999). Equilibrium analysis of groundwater-vadose zone interactions and the resulting spatial distribution of hydrologic fluxes across a Canadian prairie. *Water Resources Research* 35:1369–1383, with permission of the American Geophysical Union].

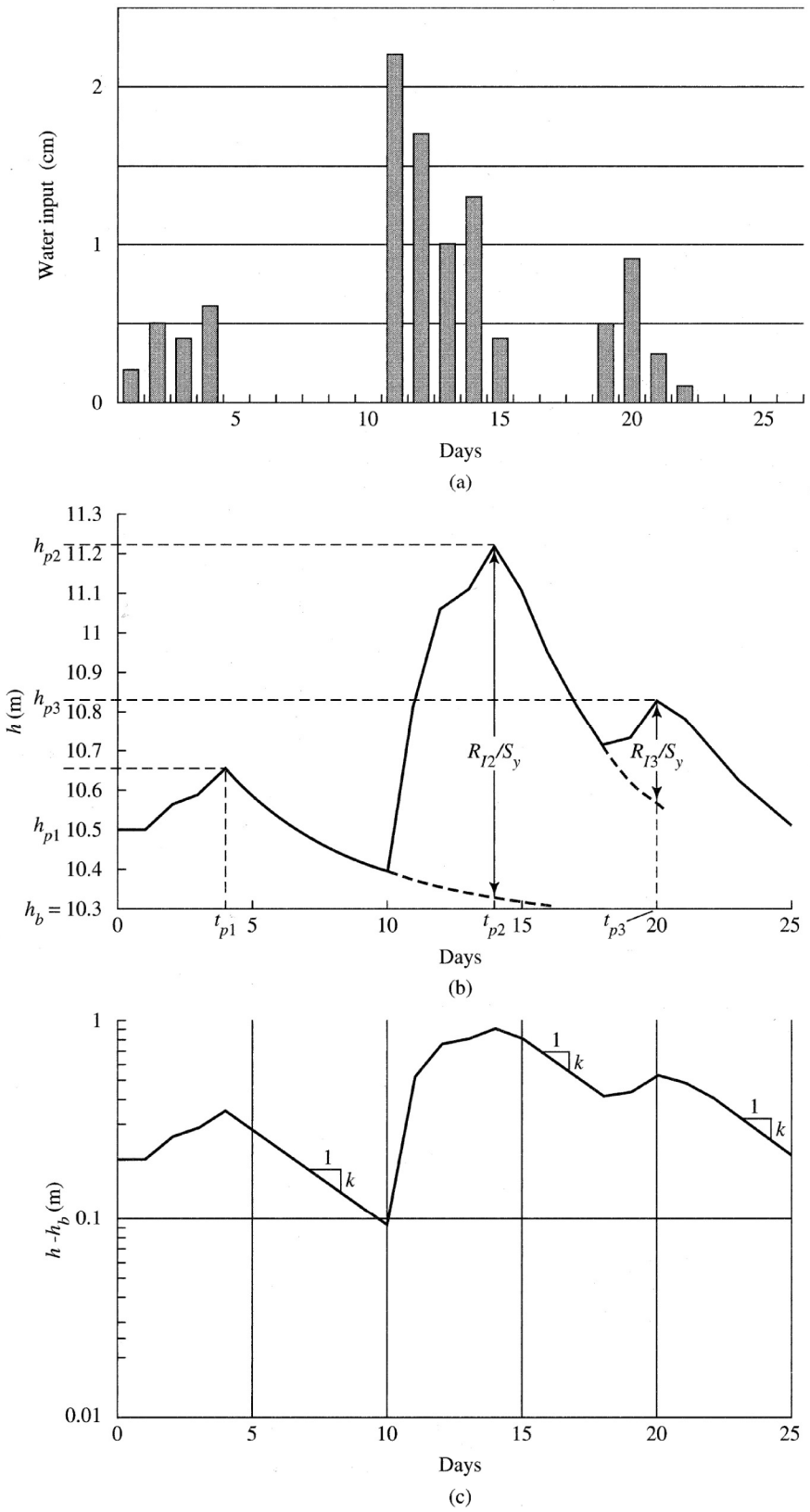

Figure 9.28 Typical plot for estimation of recharge via well-hydrograph analysis. (a) Rainfall hyetograph. (b) Well hydrograph plotted on arithmetic scale. Dashed lines are the extensions of hydrograph recessions (assumed exponential decay). R_{I2} and R_{I3} are recharge from storm events 2 and 3, respectively, estimated as the vertical distance between the extended recession and the hydrograph peak times the specific yield [see equation (9.29)]. (c) Well hydrograph plotted on logarithmic scale.

Box 9.7 Drainage of a Linear-Reservoir Aquifer

Figure 9.29 shows an idealized unconfined aquifer of area A and specific yield S_y receiving recharge from infiltration, R_I [L T^{-1}], and discharging to a stream at a rate Q_{GW} [L^3 T^{-1}]. Assuming constant density, the conservation-of-mass equation for a time period dt for this situation is

$$A \cdot R_I \cdot \mathrm{d}t - Q_{GW} \cdot \mathrm{d}t = A \cdot S_y \cdot \mathrm{d}h. \qquad \textbf{(9B7.1)}$$

Defining $q_{GW} \equiv Q_{GW}/A$, this becomes

$$R_I - q_{GW} = S_y \cdot \frac{\mathrm{d}h}{\mathrm{d}t}. \qquad \textbf{(9B7.2)}$$

If the aquifer behaves as a linear reservoir, outflow rate is proportional to storage [see equation (1.24)],

$$q_{GW} = k \cdot S_y \cdot (h - h_b), \qquad \textbf{(9B7.3)}$$

where h_b is a level below which no discharge occurs and k [T^{-1}] is the inverse of the residence time [equation (9.14)] of the aquifer. With equation (9B7.3), (9B7.2) becomes

$$R_I - k \cdot S_y \cdot (h - h_b) = S_y \cdot \frac{\mathrm{d}h}{\mathrm{d}t}. \qquad \textbf{(9B7.4)}$$

If there is no recharge or capillary rise and the aquifer is draining, $R_I = 0$ and equation (9B7.4) can be written as

$$-k \cdot \mathrm{d}t = \frac{\mathrm{d}h}{h - h_b}. \qquad \textbf{(9B7.5)}$$

Integrating (9B7.5) yields

$$-k \cdot t = \ln(h - h_b) + C, \qquad \textbf{(9B7.6)}$$

and evaluating the constant of integration, C, from the initial condition $h = h_0$ when $t = 0$ leads to

$$h = h_b + (h_0 - h_b) \cdot \exp(-k \cdot t). \qquad \textbf{(9B7.7)}$$

Equation (9B7.7) shows that drainage of a linear aquifer follows an exponential decay asymptotic to h_b with decay constant k. Substituting equation (9B7.7) into equation (9B7.3) yields

$$q_{GW} = k \cdot S_y \cdot h_0 \cdot \exp(-k \cdot t), \qquad \textbf{(9B7.8)}$$

and we see that a linear aquifer produces ground-water outflow that also follows an exponential decay with the same decay constant. For well-hydrograph analysis, k is usually evaluated empirically as the slope of the hydrograph when plotted on a semilogarithmic graph.

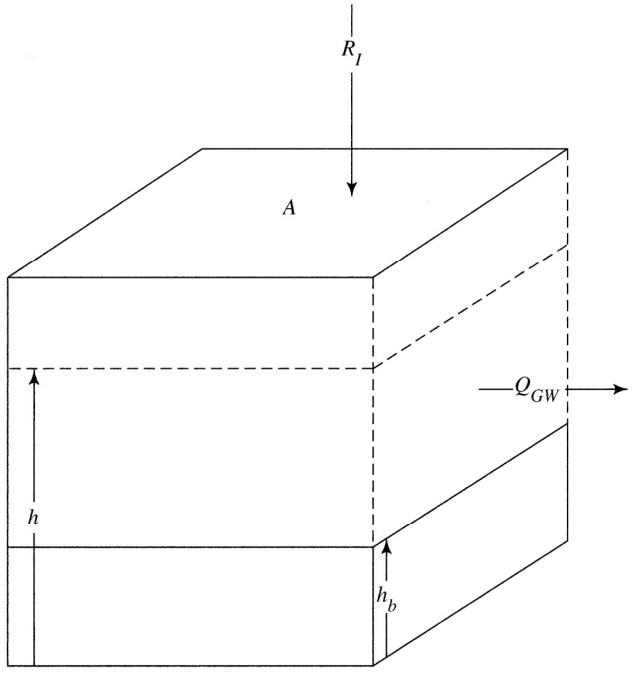

Figure 9.29 Definition diagram for analysis of drainage of a horizontal aquifer (box 9.7).

If recharge from streams and capillary rise are negligible, the ground-water balance equation, accounting for storage changes, is

$$R_I = Q_{GW} + \Delta S, \qquad \textbf{(9.27)}$$

where ΔS now denotes the change in storage in the aquifer. If the aquifer behaves as a linear reservoir, the analysis in box 9.7 shows that equation (9.27) becomes

$$R_I = k \cdot S_y \cdot (h - h_b) + S_y \cdot \frac{\mathrm{d}h}{\mathrm{d}t}, \qquad \textbf{(9.28)}$$

where R_I has units of [L T^{-1}], h is the water level in the aquifer, and h_b is the level at which Q_{GW} becomes negligible. As shown in figure 9.28, the parameter k is evaluated as the slope of the straight line that best defines the hydrograph recessions when plotted on a semilogarithmic graph, and h_b can be evaluated as the level to which the recessions become asymptotic during extended periods of no recharge. The seasonal variation of R_I can then be estimated by observing water-table elevations in monitoring wells and using equation (9.28). Figure 9.30 is an example of this approach as applied to a glacial aquifer in Sweden.

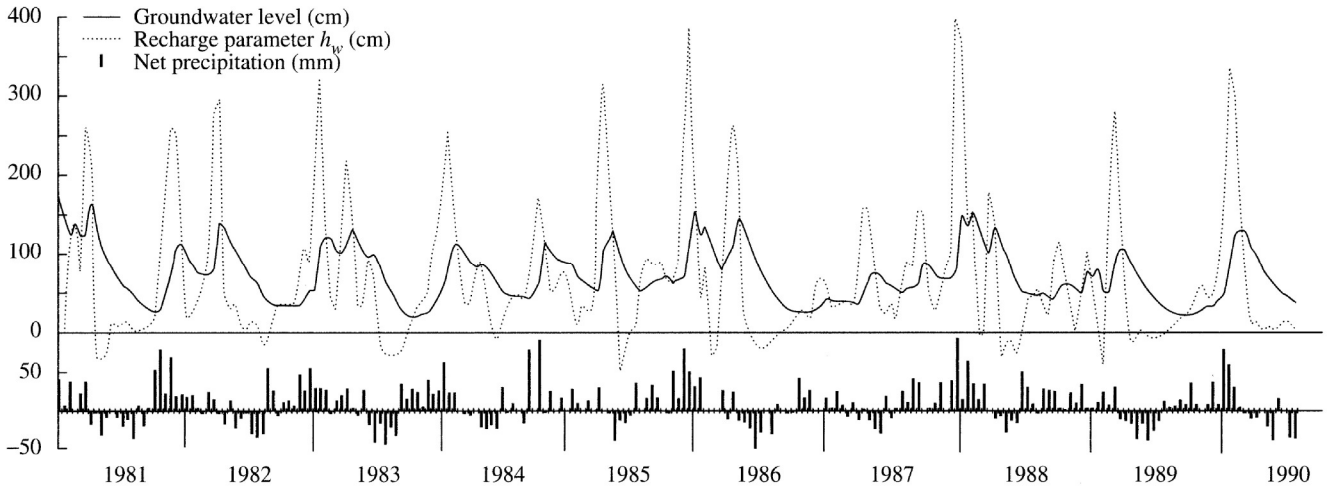

Figure 9.30 Hyetograph (histogram), well hydrograph (solid line), and recharge as estimated via equation (9.28) (dashed line) in Sweden over a 10-yr period [reproduced from Olin and Svensson (1992), Evaluation of geological and recharge parameters for an aquifer in southern Sweden, *Nordic Hydrology* 23:305–314, with permission from the copyright holders, IWA Publishing].

Another approach to well-hydrograph analysis applies the linear-reservoir model in a somewhat different way. Again, assuming an exponential recession and referring to figure 9.28, recharge for event i, $R_{I,i}$ [L], becomes

$$R_{I,i} = \{h_{p,i} - h_{p,i-1} \cdot \exp[-k \cdot (t_{p,i} - t_{p,i-1})]\} \cdot S_y, \qquad \textbf{(9.29)}$$

where $h_{p,i}$ and $h_{p,i-1}$ are the peak water levels associated with events i and $i-1$, respectively; $t_{p,i}$ and $t_{p,i-1}$ are the times of occurrence of the successive peak water levels; and S_y is the specific yield. Rasmussen and Andreasen (1959) obtained reasonable results with this method in Maryland, with a constant S_y determined via successive approximations as the value most consistent with weekly water-balance data.

A third approach to estimating recharge from well hydrographs applies a simplified water-balance equation to the entire aquifer of area A:

$$R_I = S_y \cdot \Delta h_+ \cdot A - (G_{in} - G_{out}), \qquad \textbf{(9.30)}$$

where Δh_+ is the spatial average increase in aquifer water level in response to a water-input event and G_{in} and G_{out} are the ground-water inflows and outflows, respectively, to the aquifer. Van Tonder and Kirchner (1990) suggested estimating the G terms by approximating Darcy's law as

$$G = T \cdot L \cdot \frac{i_1 + i_2}{2}, \qquad \textbf{(9.31)}$$

where G is the appropriate flow rate, T is the transmissivity [equation (9.11)] for the inflow or outflow boundary, L is the width of the boundary, and i_1 and i_2 are the hydraulic gradients at the boundary at the beginning and end of the observation period, respectively. Van Tonder and Kirchner (1990) found that this method was the only one to give reliable estimates of recharge in clastic sedimentary rock aquifers in South Africa. Das Gupta and Paudyal (1988) showed how an approximate analytical solution of the one-dimensional ground-water flow equation could be used to account for the G terms when equation (9.31) is applied to an aquifer.

Although the studies cited above have claimed success in estimating recharge from well-hydrograph analysis, the approach is subject to two sources of potentially large uncertainty:

1. **Difficulty of determining the appropriate areal value of specific yield**: A characteristic value of S_y for the aquifer material is often assumed, but this can range widely (table 9.1). Furthermore, the specific yield cannot in general be assumed constant in the near-surface zones of aquifers. This is especially true if the water table is within a few meters of the surface, where water contents are a function of depth due to the complex interplay of infiltration, percolation, and capillary rise. In general, the equilibrium water-content profile varies with the water-table elevation (figure 8.8), so a

given water-table rise represents different amounts of recharge depending on the elevation range covered. Another cause of inconstancy in S_y is related to the wetting/drying hysteresis in soils (figure 7.17): In a wetting soil, air bubbles are typically trapped in the pores, so that S_y for a rising water table is generally less than S_y for a falling water table. Sophocleous and Perry (1985) showed that recharge estimates based on the assumption of a constant S_y can be seriously in error.

2. **Uncertainty that an increase in water level actually represents an increment of recharge**: Increases in water-table elevation unrelated to recharge may occur due to: (a) fluctuations in atmospheric pressure due to the expansion and contraction of air trapped beneath the water table; (b) thermal effects, including freezing and thawing; and (c) pressurization of the capillary fringe. This latter phenomenon is especially likely to occur where the capillary fringe extends up to the soil surface; infiltrating water can then cause an almost instantaneous rise of the water table to the surface with virtually no change in ground-water storage (Novakowski and Gillham 1988; this is discussed further in section 10.4.3.2).

9.5.1.3 Direct Application of Darcy's Law

This approach requires (1) careful determination of the $K_h(\theta)$–θ and $\psi(\theta)$–θ relations for the soil of interest (table 7.4), and (2) periodic measurement of the vertical water-content gradient in the unsaturated zone of that soil. Recharge is then computed as the flux across the base of the root zone, $q_{z'}$, as given by Darcy's law for vertical unsaturated flow:

$$R_I = q_{z'} = K_h(\theta) - K_h(\theta) \cdot \frac{\partial \psi(\theta)}{\partial z'}. \qquad \textbf{(9.32)}$$

Sophocleous and Perry (1985) and Stephens and Knowlton (1986) obtained reasonable recharge estimates using this approach in humid and semiarid environments, respectively. Steenhuis et al. (1985) also successfully applied this method in a humid region, using biweekly observations of soil-water content at depths of 90 and 120 cm in a sandy loam soil. They found that the hydraulic gradient across the soil layer varied linearly with time following a rainstorm, and the hydraulic conductivity varied linearly with the square root of time. Thus the average rate of recharge between two observation times t_1 and t_2 was calculated from a modified version of Darcy's law for unsaturated flow:

$$R_I = -\left[K_h(\theta_{t1}) \cdot K_h(\theta_{t2})\right]^{1/2} \cdot \left(\frac{1}{2}\right) \cdot \left[\left(\frac{dh}{dz}\right)_{t1} + \left(\frac{dh}{dz}\right)_{t2}\right] \cdot (t_2 - t_1), \qquad \textbf{(9.33)}$$

where h is the hydraulic head [$= \psi(\theta) + z$)] and the subscripts indicate the time of measurement.

A variation on this method involves ignoring the capillary-force gradient in the one-dimensional form of Darcy's law and estimating recharge as a function of water content:

$$R_I = K_h(\theta). \qquad \textbf{(9.34)}$$

Stephens and Knowlton (1986) found good agreement between results obtained with equation (9.34) and those using the more complete version of Darcy's law.

Principal limitations of this approach are the spatial variability of soils in a typical drainage basin, the difficulty in establishing precise $K_h(\theta)$–θ relations for a given soil, and the possibility that recharge can occur via macropores or fissures in which flow is not well modeled by Darcy's law (Van Tonder and Kirchner 1990).

9.5.1.4 Inverse Application of Ground-Water Flow Equation

The general equation for steady-state ground-water flow [equation (7.18)] can be incorporated into a model that accounts for an assumed regional distribution of recharge. The inverse application of such a model involves finding the values of recharge by calibration: The values of recharge in the model are changed until the computed head distribution corresponds to the values observed in piezometers in the region.

A number of studies have shown that useful estimates of recharge can be obtained via the inverse method, including those of Smith and Wikramaratna (1981), Wikramaratna and Reeve (1984), Chiew et al. (1992), Boonstra and Bhutta (1996), and Levine and Salvucci (1999).

However, the inherent problem of the inverse approach is the nonuniqueness of solutions: There may be many distributions of recharge that give head distributions that match the field observations within the uncertainty of those observations. The problem is exacerbated by the difficulties in obtaining a precise picture of the distribution of hydraulic conductivities.

9.5.1.5 Impulse-Response Analysis

The objective of impulse-response analysis is to determine recharge from the relation between water inputs (the impulse) and water-table rises (the response) using the principles of the mathematical analysis of time series. Given a series of daily observations of water level in an observation well and water input, the level on a given day, h_i, is assumed to depend on the previous day's level and the previous days' water inputs as

$$h_i = a_0 + a_1 \cdot h_{i-1} + b_0 \cdot W_i + b_1 \cdot W_{i-1} + \ldots + b_n \cdot W_{i-n}, \quad \textbf{(9.35)}$$

where *a*s and *b*s are constants, the *W*s are water inputs (rain plus snowmelt), the subscripts are day counters, and n is the maximum number of days required for water to percolate to the water table.

The values of the constants in equation (9.35) are found by mathematical techniques that minimize the differences between estimated and observed h_i values over some period of observation of the particular wells of interest. Viswanathan (1984) showed that the average fraction of water input that becomes recharge is given by

$$\frac{R_I}{W} = S_y \cdot \sum_{j=0}^{n} b_j, \quad \textbf{(9.36)}$$

so that the method can be used to estimate long-term average recharge from long-term average water input (= average precipitation). Note, though, that this relation is also based on the uncertain assumption of a constant specific yield.

9.5.1.6 Methods Based on Water Quality

Under some circumstances, recharge rates can be estimated from the concentrations of certain chemicals and stable and radioactive isotopes that function as natural tracers of water movement.

9.5.1.6.1 Chemical Tracers

A chemical tracer suitable for estimating recharge must be: (1) present in measurable amounts in precipitation or, if deposited in solid form from the atmosphere, highly soluble; (2) not taken up or released in the vadose zone; and (3) not taken up or released by vegetation. For a column of the vadose zone in which no horizontal flow occurs above a water table, the balance for such a tracer is

$$C_w \cdot W = C_{GW} \cdot R_I, \quad \textbf{(9.37)}$$

where W is water input, C_w is the concentration of the tracer in the water input as it infiltrates, C_{GW} is the concentration in ground water at the water table, and all terms represent long-term averages. Recharge can thus be directly calculated if all other terms are determined from observations.

One candidate tracer is the chloride ion (Cl^{-1}), which is commonly present in precipitation, is not used by plants, and is not commonly involved in soil-chemical reactions. Recharge has been estimated from Cl^{-1} concentrations in Colorado (Claassen et al. 1986), Australia (Thorburn et al. 1991; Walker et al. 1991), and Niger (Bromley et al. 1997). Detailed aspects of using Cl^{-1} to estimate recharge were discussed by Allison et al. (1984) and Taniguchi and Sharma (1990).

Chlorofluorocarbons (CFCs) are chemically stable man-made compounds that have been accumulating in the atmosphere since their introduction as propellants and refrigerants in the 1930s. Detectable concentrations of CFCs are present in ground water that fell as precipitation since 1945, and their concentration can be used to compute recharge rates. Busenberg and Plummer (1992) and Dunkle et al. (1993) discuss the methodology in detail. However, due to the effects of CFCs on stratospheric ozone, their manufacture ceased by international agreement in the 1990s, so their future use as tracers is infeasible.

9.5.1.6.2 Stable Isotopes

A small fraction of water molecules contain the heavy oxygen isotope ^{18}O, or the heavy hydrogen isotope ^{2}H (deuterium) (see appendix B). The concentrations of these isotopes in precipitation tend to vary seasonally at a given location, but they are not affected by soil-chemical reactions or by plant uptake. Thus comparisons of concentrations in ground water with those in precipitation at various times of the year can provide qualitative information on the seasonality of recharge.

It is usually difficult to use stable isotopes for quantitative estimates of R_I without additional information or assumptions about the percolation mechanism, i.e., whether a piston-like wetting front occurs, whether macropores are important, or whether isotopic equilibration takes place between percolating and immobile water. Darling and Bath (1988) cited several studies in which ^{18}O and ^{2}H were used to obtain information about the seasonality and rate of recharge.

9.5.1.6.3 Radioactive Isotopes

Atmospheric testing of nuclear weapons in the 1950s and 1960s increased concentrations of tritium (^{3}H) in precipitation by orders of magnitude above

its natural levels. In subsequent decades, ^{3}H proved very useful for recharge studies, as it is part of the water molecule and its concentration is not affected by chemical reactions (e.g., Larson et al. 1987 and studies cited therein). However, atmospheric nuclear testing has been banned since the 1960s, and ^{3}H concentrations have decreased to the point where it is no longer usable as a tracer.

9.5.2 Recharge from Surface Water, R_{SW}

Although there are few published studies in which R_{SW} has been estimated, we can outline the principal approaches that can be applied to evaluation of this quantity.

9.5.2.1 Ground-Water Balance Computation

In arid regions, average evapotranspiration is nearly equal to average precipitation, so most infiltrating water evaporates and most recharge is from losing streams (figure 9.17b and c) rather than infiltration. For example, Osterkamp et al. (1994) applied water-balance computations along with streamflow measurements (see below) and ground-water modeling techniques to a 20,000-km^2 river basin in Nevada and California to estimate that only 1.6% of basin precipitation became recharge and that 90% of recharge was from streams.

9.5.2.2 Direct Measurement of Ground-Water Potential or Flux

The gradient of ground-water flow out of (or into) a stream can be measured by comparing (1) the water level of the stream with the head measured in a piezometer inserted into the subjacent bed or (2) the levels in two piezometers inserted to different distances below the bed (figure 9.31). If the gradient is directed downward, the ground-water flux out of the stream can be calculated directly via Darcy's law using measured or estimated hydraulic conductivities. However, there is likely to be considerable spatial and temporal variability in local values (and even direction) of gradients as well as conductivities, so such measured values must be extrapolated with caution. Winter et al. (1988) give details on the construction of piezometers used for this purpose.

Workman and Serrano (1999) combined measurements of near-stream water levels with a simple ground-water flow model to estimate that 65% of the recharge to alluvial aquifers in Ohio came from overbank flow due to floods, and hence was highly sporadic.

9.5.2.3 Direct Measurement of Streamflow Increments

The difference between stream discharge at the upstream and downstream limits of a stream reach

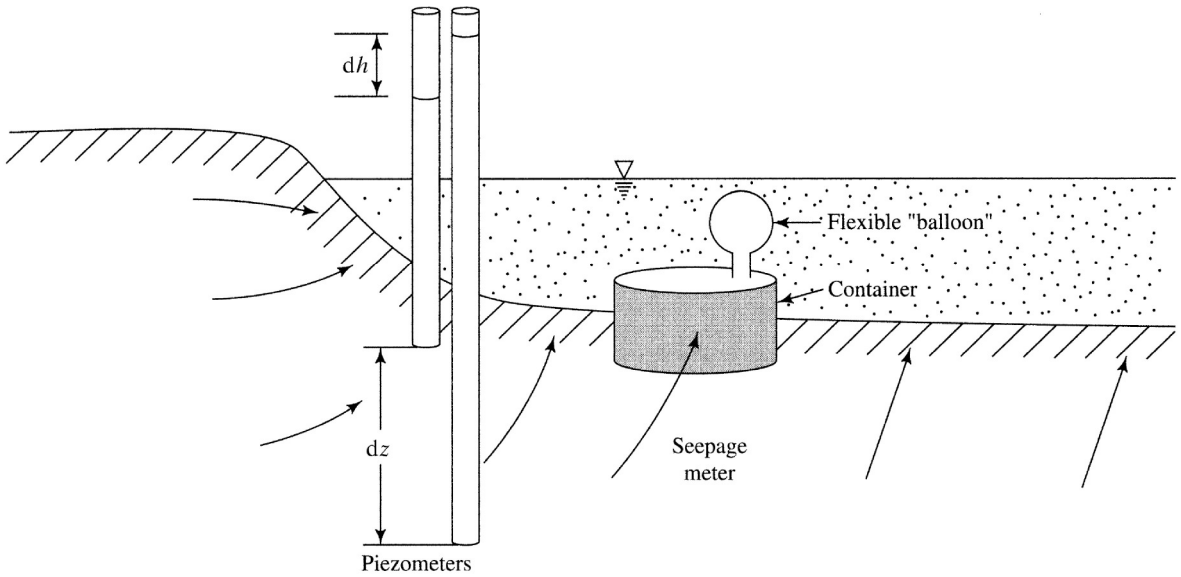

Figure 9.31 Sketch showing installation of piezometers and seepage meter to measure ground-water flux to a stream. Arrows indicate flow direction. d*h* is the head difference and d*z* is the elevation difference between the two piezometers; vertical flow is calculated via Darcy's law. Water flowing into the container of the seepage meter is collected in the flexible "balloon."

that receives no overland or tributary flow can be attributed to ground-water inflow or outflow. Techniques for measuring streamflow are discussed in appendix E; typically "velocity-area" methods, in which flow depth and average flow velocity are measured at a number of points across the stream width, are most applicable since they do not require fixed installations.

The accuracy of an estimate of R_{SW} or Q_{GW} using this approach depends on the precision of the streamflow measurements (see appendix E) and is increased by maximizing the difference between the upstream and downstream discharges (i.e., by making the measurement reach as long as possible while not including inflow from tributaries). Here again one must be aware that rates and directions of ground-water–surface-water exchange may be highly variable in space and time.

9.5.2.4 Water-Temperature Measurements

Stream temperatures are temporally highly variable due to daily and seasonal cycles. Where streams are losing water to subjacent ground water, this variability becomes progressively damped with distance below the stream bed. The outflow flux can be evaluated by measuring temperature fluctuations a short distance below the channel bottom, measuring the thermal properties of the bed sediment, and applying basic heat-flow relations (Silliman et al. 1995). Analytical methods that are commonly used in this approach are limited by uncertainties in the effective thermal properties of the sediments at the ground-water–surface-water interface.

McCallum et al. (2012) developed a new analytical method that utilizes both the amplitude ratio and phase shift of pairs of temperature measurements at the interface to estimate the magnitude and direction of the Darcy velocity. They applied the method to a stream reach in Australia, and were able to accurately measure ground-water–surface-water exchanges in both directions (bank storage).

9.5.3 Ground-Water Contribution to Streamflow, Q_{GW}

9.5.3.1 Application of Dupuit Approximation

As described in boxes 9.3 and 9.4, steady flow in horizontal unconfined aquifers draining to streams can often be usefully described by the Dupuit approximation. If significant water is not being pumped from such aquifers (section 9.6.2.2), and if capillary rise is negligible, these equations state that $Q_{GW} = R_I$ on a long-term average, per unit area basis [equation (9.18)]. Thus under these conditions, the techniques described above for estimating R_I also provide information about Q_{GW}. Note, however, that the Dupuit formulation assumes fully penetrating streams, which seldom occur in nature, and that application of equation (9.18) assumes that the recharge area coincides with the surface watershed.

9.5.3.2 Flow Nets

Principles of graphical flow-net construction are developed in most ground-water texts (e.g., Freeze and Cherry 1979; Fetter 2001) and are discussed in detail by Cedergren (1989). If enough information on the spatial distribution of hydraulic conductivities and average water-table elevations is available, one can develop a numerical or graphical solution to equation (9.15) and sketch one or more flow nets that represent the major ground-water flow features of the basin along various stream reaches. Referring to figure 9.32, the discharge per unit length of stream Δq_{GW} into a stream for each streamtube can then be calculated as

$$\Delta q_{GW} = K_h \cdot \Delta h, \qquad \textbf{(9.38)}$$

where K_h is the appropriate conductivity and Δh is the head difference between the stream and the next up-gradient equipotential line; the total discharge per unit stream length for a reach, q_{GW}, is given by

$$q_{GW} = n \cdot \Delta q_{GW}, \qquad \textbf{(9.39)}$$

where n is the number of streamtubes discharging to the stream. The total flow into the stream for the reach, Q_{GW}, is then found as

$$Q_{GW} = L \cdot q_{GW}, \qquad \textbf{(9.40)}$$

where L is the length of the reach.

Flow nets constructed in the horizontal plane can also be used to estimate ground-water inflow to streams. In practice, however, it is usually difficult to obtain enough information about subsurface geology and conductivities to warrant computations based on a flow net, and there are only a few published studies that have used this approach (Freeze 1968; Freeze and Witherspoon 1968; Ophori and Tóth 1990).

9.5.3.3 Direct Measurement of Ground-Water Potential or Flux

As for R_{SW}, Q_{GW} can be evaluated by measuring the heads in adjacent piezometers in the stream bed or banks or comparing the stream water level with the sub-bed hydraulic head (Winter et al. 1988) and

using those values along with information about conductivities to calculate the ground-water flux into the stream via Darcy's law.

Direct local measurement of Q_{GW} can be made using seepage meters, which are devices that capture water flowing upward into a portion of a water body over some time period (figure 9.31). The flux into the container is simply the volume collected divided by the time period. Lee (1977) described the construction and use of seepage meters.

As noted earlier, the main concern in using piezometer or seepage meter measurements is whether the sampling is spatially and temporally representative. Piezometer observations in stream beds in relatively homogeneous glacial deposits on Long Island, New York, were consistent with mathematical simulations (Prince et al. 1989). However, Lee and Hynes (1978) found very large spatial variability of ground-water input to a small stream in Ontario, Canada, and concluded that determination of average rates of ground-water input to streams from point measurements of seepage flux was not generally possible.

9.5.3.4 Direct Measurement of Streamflow Increments

As described for evaluating R_{SW}, the difference between streamflow measured via velocity-area stream gauging (appendix E) at the upstream and downstream ends of a stream reach in which no tributaries enter provides a direct measurement of Q_{GW}. For gaining streams, the longer the distance between measurement cross sections, the lower the absolute error in the difference in the measured flow rates. However, the applicability of this approach is limited because of the frequent occurrence of tributaries, which must also be gauged. Cey et al. (1998) found

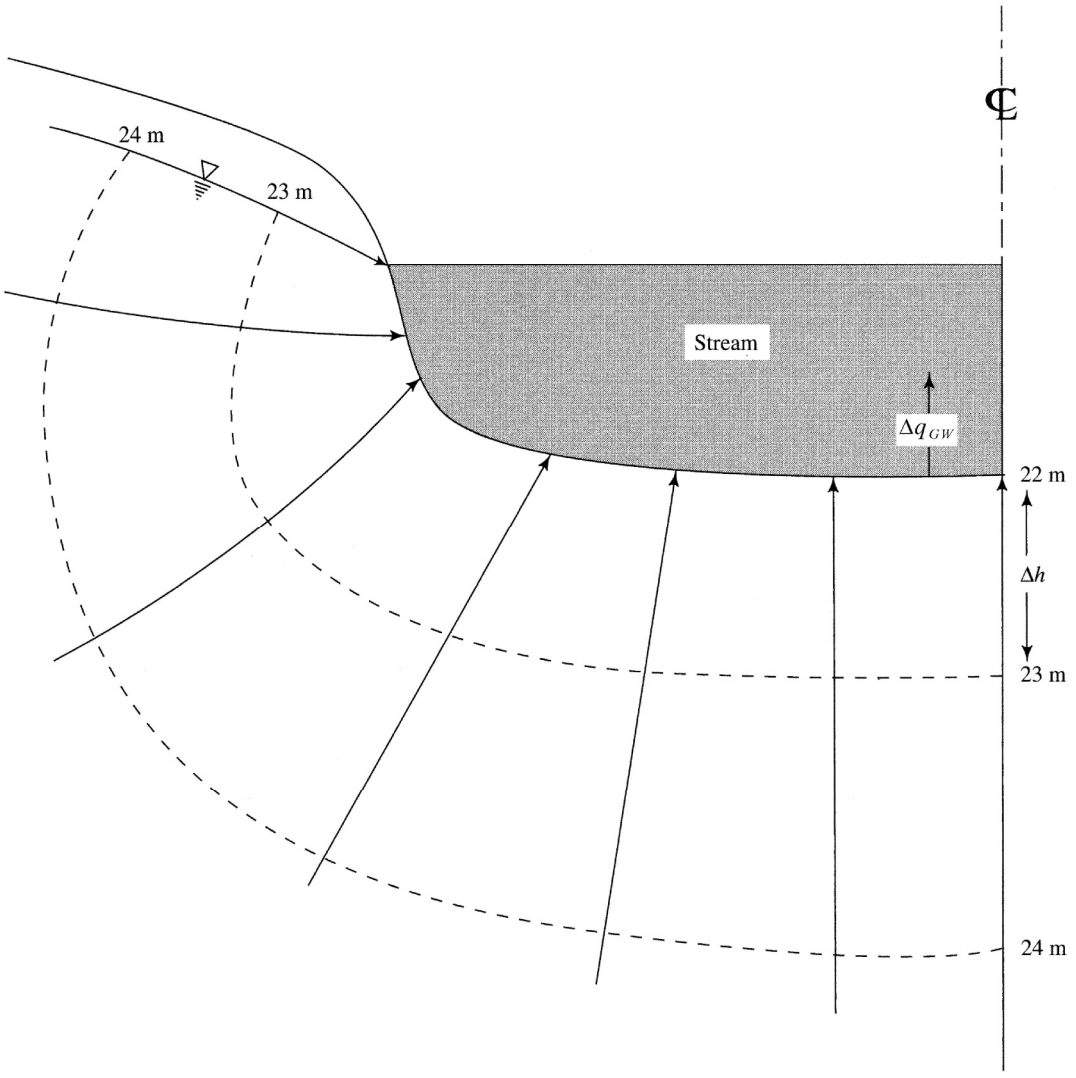

Figure 9.32
Flow net in the vicinity of a stream receiving ground water; defining terms in equations (9.38)–(9.40).

that this approach gave the most reliable results in their study of a small Canadian stream.

9.5.3.5 Methods Based on Water Quality

If streamflow, Q, at any instant is assumed to be a mixture of water from two sources, e.g., (1) surface water, Q_{SW}, and (2) ground water, Q_{GW}, each of which has a characteristic concentration of some chemical or isotope, C_{SW} and C_{GW}, then

$$Q = Q_{SW} + Q_{GW} \quad \textbf{(9.41)}$$

and

$$C \cdot Q = C_{SW} \cdot Q_{SW} + C_{GW} \cdot Q_{GW}, \quad \textbf{(9.42)}$$

where C is the concentration in the streamflow. If Q and C are measured and C_{SW} and C_{GW} determined from sampling the respective sources in the watershed, Q_{GW} can be found by combining equations (9.41) and (9.42):

$$Q_{GW} = Q \cdot \left(\frac{C - C_{SW}}{C_{GW} - C_{SW}} \right). \quad \textbf{(9.43)}$$

Use of equation (9.43) assumes that there are only two sources of streamflow, that each source has a constant concentration of tracer, and that these concentrations are significantly different. To relax some of these constraints, Pilgrim et al. (1979) showed how the relation could be modified when the concentration of one of the components is a function of time since the beginning of the event, and Swistock et al. (1989) derived a version of equation (9.43) for use when there are three runoff components.

Equation (9.43) has been used with apparent success in several studies, using as tracers various anions and cations (e.g., Newbury et al. 1969; Pinder and Jones 1969), stable isotopes ^{18}O and ^{2}H (e.g., Sklash and Farvolden 1979; Space et al. 1991), and the radioactive gas radon (^{222}Rn) (e.g., Ellins et al. 1990). Figure 9.33 shows the estimated ground-water contribution to streamflow in a case where the sulfate ion (SO_4^{-2}) was used as the tracer in equation (9.43). This approach is discussed further in section 10.3.

9.5.3.6 Base-Flow Analysis

9.5.3.6.1 Definitions

In figure 9.34 on p. 435, **streamflow hydrographs** show the typical response of a stream to an isolated water-input event: There is a relatively rapid flow increase (the **hydrograph rise**) to a **peak**, which usually occurs at or soon after the input ceases, followed by a more gradual decline (the **hydrograph recession**). If the recession continues long enough before the next event, at some point recession flow equals *base flow*. As discussed in section 9.3.1.1,

Base flow is the portion of streamflow that is presumed to have entered the watershed in previous events and is derived from persistent, slowly varying sources.

Base flow is usually assumed to be from aquifers that drain to the stream network within the stream's watershed, i.e., Q_{GW} (e.g., Wolock 2003), and the attempt to identify ground-water contributions to streamflow by analysis of stream hydrographs, usually called **base-flow analysis**, **base-flow separation**, or **recession analysis**, has a long history (Hall 1968; Tallaksen 1995) and remains a common practice (Chapman 1999; Santhi et al. 2008). However, it is important to recognize that

- The concept of base flow has no scientific basis; and
- The actual source of base flow is seldom known, and may include the drainage of surface water (lakes, reservoirs, wetlands), the slow drainage of soils (e.g., Hewlett and Hibbert 1963; Dingman 1970), late-melting snow, regional ground-water flow that originated outside the watershed, or anthropogenic stream inputs.

Here we introduce some theoretical links between recession flow and ground-water inflows to streams, and some more arbitrary methods that have been used to separate base flow from event flow.

9.5.3.6.2 Recession Flow and Aquifer Drainage

If flow (Q_R) during the recession represents drainage from watershed storage—some of which is water that entered in the current event and some in past events—and declines as storage decreases, we can infer that

$$Q_R = f(S), \quad \textbf{(9.44)}$$

where S is the volume of water in storage and f is a positive function (i.e., flow decreases as storage decreases). The form of this function is assumed to be determined largely by watershed characteristics (e.g., size, geology, slope, etc.) [see equation (1.23)], but can only be inferred empirically. The function is often assumed to be a power law:

$$Q_R = k \cdot S^b; \quad \textbf{(9.45)}$$

if $b = 1$, this leads to

$$Q_R = Q_{R0} \cdot \exp[-k \cdot (t - t_0)] \qquad \textbf{(9.46)}$$

(the linear reservoir of box 9.7); if $b > 1$,

$$Q_R = Q_{R0} \cdot [1 + d \cdot (t - t_0)]^{b/(1-b)}, \qquad \textbf{(9.47)}$$

where k, b, and d are constants, t is time, and Q_{R0} is the flow rate at the selected initial time t_0. Values of the constants are found empirically by choosing t_0 (the time of peak flow or later) and finding values of b and d that give a line that best fits the subsequent recession.

In fact, because total watershed storage S cannot actually be determined, flow-storage relations are best inferred from relations between concurrent values of the rate of change of flow and flow during recessions, which can also commonly be approximated as power-law relations:

$$-\frac{dQ_R}{dt} = a \cdot Q_R^b, \qquad \textbf{(9.48)}$$

where a and b are characteristic of a given watershed that can be estimated by plotting dQ_R/dt versus Q_R on logarithmic graph paper and determining a and b from the slope and intercept of the line that best fits the plot (Brutsaert and Nieber 1977). [This approach was used in the analysis of section 1.12; see equation (1.48).] Note that although equations (9.46)–(9.48) may give the form of the recession hydrograph, they provide no information about the actual source of the water.

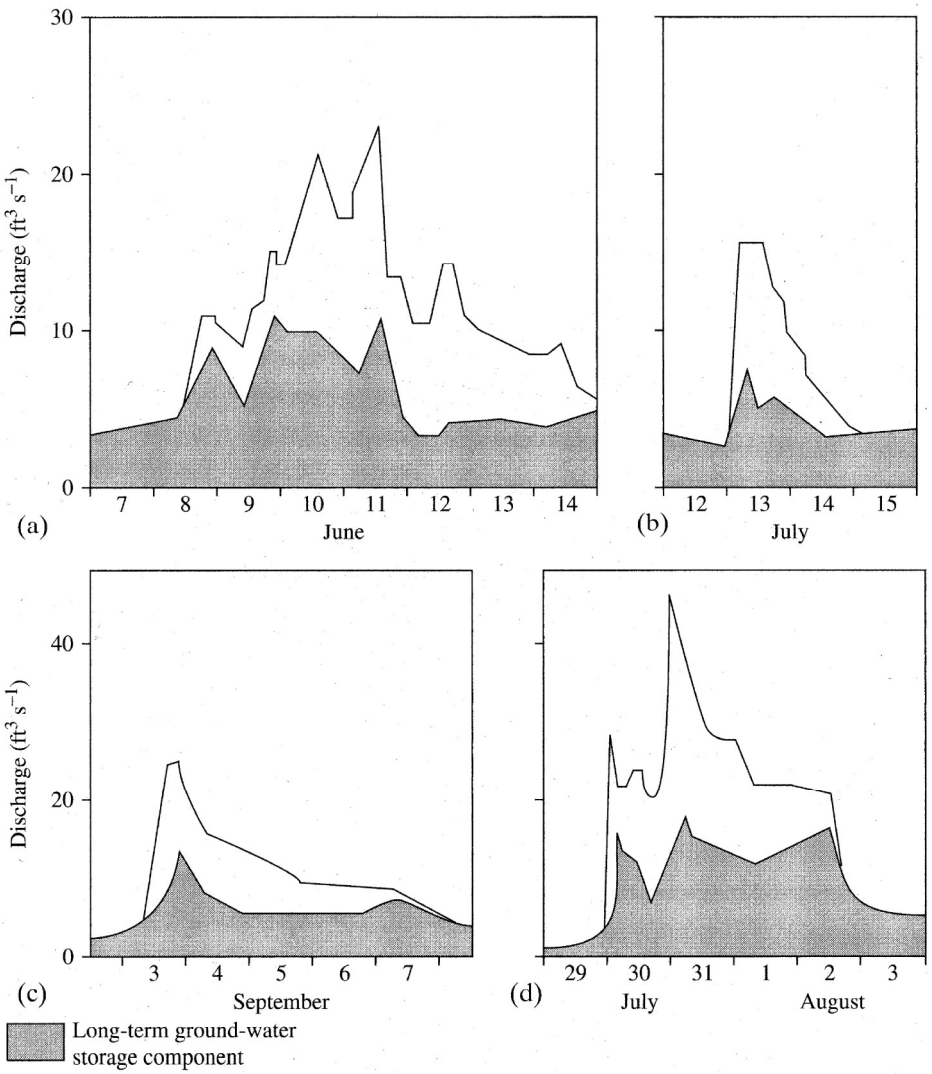

Figure 9.33 Total streamflow and streamflow attributed to ground-water base flow for four runoff events in Wilson Creek, Manitoba, as estimated using equation (9.43) with SO_4^{-2} as a tracer [reproduced from Newbury et al. (1969), Groundwater-streamflow systems in Wilson Creek Experimental Watershed, Manitoba, *Canadian Journal of Earth Sciences* 6:613–623, © Canadian Science Publishing or its licensors].

As shown by Brutsaert (1992, 1994), drainage from a horizontal aquifer under the Dupuit assumptions (box 9.3) can be approximated as an exponential decay with the parameters related to aquifer properties as

$$q_{GW} = \frac{h_0^2 \cdot K_h}{X} \cdot \exp\left(\frac{1.23 \cdot K_h \cdot h_0}{X^2 \cdot S_y} \cdot t\right), \quad \textbf{(9.49)}$$

where q_{GW} is ground-water flow per unit stream length and the other symbols are as in boxes 9.3 and 9.4. If recession flow is drainage from quasi-horizontal watershed aquifers, this provides a theoretical basis for the exponential-decay recession [equation (9.46)] and a possible basis for estimating recession flow on the basis of aquifer properties (or vice versa, if some of the properties are known). These possibilities are explored further by Harman et al. (2009).

9.5.3.6.3 Arbitrary Base-Flow Separation Methods

In practice, base-flow separation is assumed to represent Q_{GW}, and base-flow separation is usually

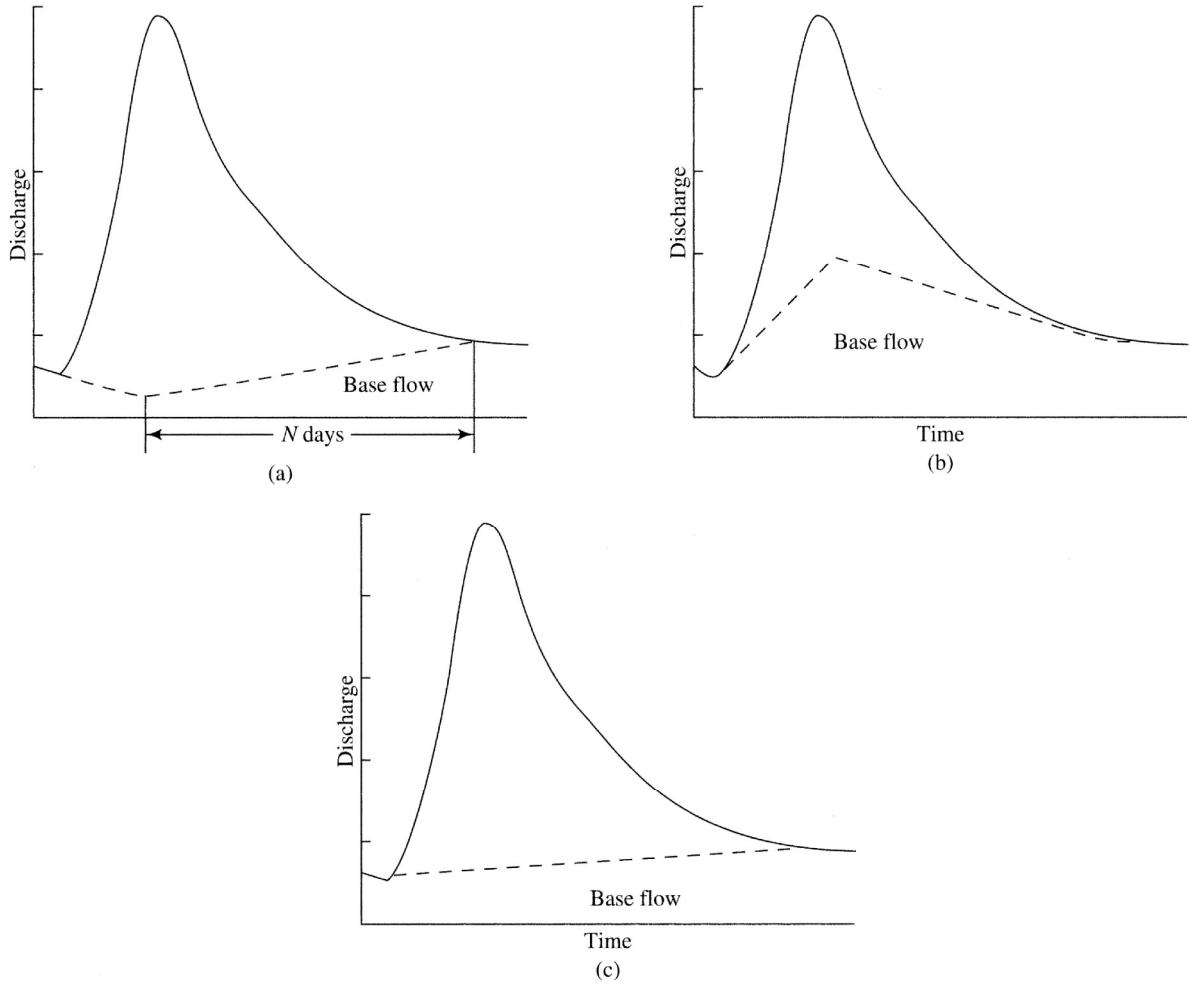

Figure 9.34 Methods of graphical base-flow separation. (a) The preevent flow trend is projected until the time of peak, after which the base-flow hydrograph is connected by a straight line that intersects the total-flow hydrograph N days after the peak, where N (days) = $0.82 \cdot A^{0.2}$, and A is drainage area in km^2. (b) The hydrograph is plotted on semi-logarithmic paper (log[$Q(t)$] versus t). A straight line is fitted to the end of the hydrograph recession on this graph and projected backward in time under the peak. This projected line is transferred onto arithmetic graph paper and a smooth line is sketched connecting it to the end of the preceding recession. (c) From the point of initial hydrograph rise, a line that slopes upward at a rate of 0.0014 m^3/s $\cdot$ A km^2 per hour is drawn and extended until it intercepts the hydrograph (A < 50 km^2) [Dunne and Leopold (1978)].

done by plotting the measured stream hydrograph and constructing by arbitrary methods a line coincident with or below the hydrograph that is designated the base flow. Construction of the line requires answers to the following questions: (1) How does base flow behave while the stream is responding to water input? and (2) At what point does base flow become equal to total flow?

The theoretical analyses just described may provide plausible guidance in answering these questions. However, because no information as to the true sources of stream flow is usually available, many purely arbitrary approaches to separation have been proposed. In fact, base-flow separation has been called "one of the most desperate analysis techniques in use in hydrology" (Hewlett and Hibbert, 1967, p. 276).

Three arbitrary separation methods that have been used on relatively small watersheds are described in figure 9.34; others are described by Nathan and McMahon (1990), Tallaksen (1995), Arnold and Allen (1999), and Chapman (1999). One of the most widely used methods for larger watersheds was developed by the Institute of Hydrology (UK) (now the Centre for Ecology and Hydrology); this is described in box 9.8 and illustrated in figure 9.35. This method is usually used to calculate the **base-flow index** (***BFI***), defined as

$$BFI \equiv \frac{\sum_{i=1}^{N} Q_{Bi}}{\sum_{i=1}^{N} Q_i}, \qquad \textbf{(9.50)}$$

where Q_{Bi} are daily base-flow values determined by the method, and Q_i are average daily streamflows. Similar computations of the relative magnitude of base flow can be based on other separation methods.

In a region of generally similar geology, larger watersheds tend to have more storage and a higher proportion of base flow. A watershed containing very permeable soils or low slopes typically has a high proportion of base flow (e.g., $BFI > 0.95$), while one with high slopes underlain by impermeable material has a low proportion ($BFI < 0.2$). If relations between *BFI* and watershed properties can be established, they may provide a basis for inferring stream behavior in watersheds where flow measurements have not been made. Kling and Nachtnebel (2009) presented a simple method for the regional estimation of runoff-separation parameters for the monthly water-balance model using the *BFI* and catchment characteristics, and Santhi et al. (2008) mapped *BFI* values for the United States and related them to hydrologic landscape regions and watershed properties such as relief and percentage of sand.

Note that the total volume of base flow varies greatly depending on the separation method used. This illustrates the crucial point: If a consistent method is applied, base-flow separation can be a useful tool for comparing the relative contributions of ground water to streamflow in different watersheds. However,

All base-flow separation methods are based on assumptions and require arbitrary decisions; thus, by themselves they cannot be used to identify the actual ground-water component of streamflow (Freeze 1972a; Anderson and Burt 1980).

The topic of base-flow separation is also important for the study of event flow, and is examined further in section 10.2.2.

9.5.4 Capillary Rise, CR

Capillary rise is induced by extraction of water from the unsaturated zone and capillary fringe by evapotranspiration, and by migration of water to a freezing front. Capillary rise is usually considered to be a minor to negligible component of the water budget in humid regions, but may be a significant proportion of evapotranspiration in semiarid and arid areas. Net capillary rise may be difficult to estimate as a separate component, and it is often tacitly included as part of basin evapotranspiration, as done here.

One approach to estimating capillary rise is to identify those portions of the drainage basin where the water table is close enough to the surface that plants can obtain water from the capillary fringe or the saturated zone below. The presence of wetland vegetation and plants that are known **phreatophytes** can be used in this identification. One can then assume that evapotranspiration from these areas will always be at the potential rate, and use one of the methods described in chapter 6 to estimate PET. Nichols (1993, 1994) applied such methods in estimating *CR* in the western United States.

In areas where plants are extracting water from the capillary fringe, the water table may show a diurnal fluctuation (figure 9.36 on p. 438). Johansson (1986) showed that transpiration could produce such

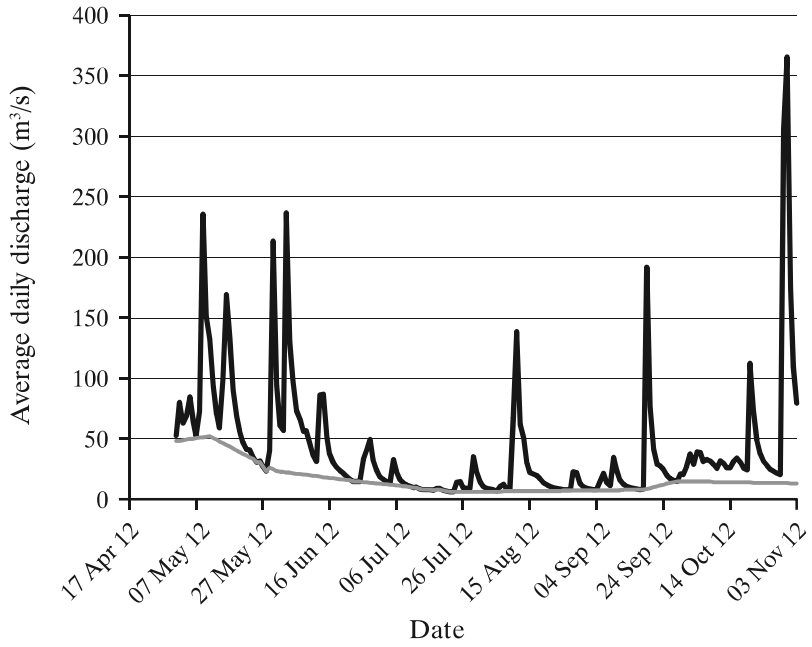

Figure 9.35 Measured discharge and base flow as calculated by the Institute of Hydrology base-flow separation method (box 9.8) for the Pemigewasset River at Plymouth, New Hampshire, for 17 April 2012 to 3 November 2012.

Box 9.8 Institute of Hydrology Base-Flow Separation Method

This base-flow separation method was developed by the Institute of Hydrology (1980) and is implemented via a computer program or in a spreadsheet. The initial data required are a time series of mean *daily* streamflow rates. The method is not appropriate for small "flashy" streams in which hydrograph rises take place over hours rather than days.

To access such data for stream gauges in the United States, go to the National Water Information System website (http://waterdata.usgs.gov) and follow these steps:

1. Select "Surface Water."
2. Select "Daily Data."
3. Under "Site Identifier," enter site (stream) name.
4. Under "Water Level/Flow Parameters," select "Streamflow ft^3/s."
5. Scroll down to "Choose Output Format" and select an appropriate format, then go to "Retrieve USGS Surface-Water Daily Data for Selected Sites" and enter the first date and last date of the time period of interest.
6. Scroll down and select "Tab-separated data" and "Save to file" to save the data in a spreadsheet.
7. In the spreadsheet, convert flows from ft^3/s to m^3/s by dividing by 35.31.

Given a sequence of N mean daily flows Q_1, Q_2, …, Q_N, the basic procedure is to determine the minima of nonoverlapping consecutive 5-day periods and identify "turning points" in the sequence of minima. The turning points, which are separated by varying numbers of days, are then connected by straight lines that define the ordinate of the daily base-flow hydrograph, Q_{BF1}, Q_{BF2}, …, Q_{BFN}, with the constraint that $Q_{BFi} \leq Q_i$. The detailed steps in the procedure are:

1. Divide the daily flows into nonoverlapping blocks of 5 days.
2. Determine the minimum value for each block, designate these Q_{m1}, Q_{m2}, etc.
3. For each group of three successive minima (Q_{m1},Q_{m2},Q_{m3}), (Q_{m2},Q_{m3},Q_{m4}), (Q_{m3},Q_{m4},Q_{m5}), etc., determine whether the central value is < 0.9 times both outer values. If this is true for day i, $Q_{BFi} = Q_{mj}$; i.e., the central value is an ordinate of the base-flow hydrograph, designated Q_{BFi}. These will be separated by varying numbers of days.
4. Linearly interpolate between successive Q_{BFi} values to determine the potential base-flow ordinates for the intervening days.
5. If any Q_{BFi} value determined in step 4 is greater than the actual flow, Q_i, set $Q_{BFi} = Q_i$.

An example is shown in figure 9.35.

Aksoy et al. (2009) developed a modification of the Institute of Hydrology method that removes sharp peaks and troughs in the base-flow line via digital filtering and smoothing.

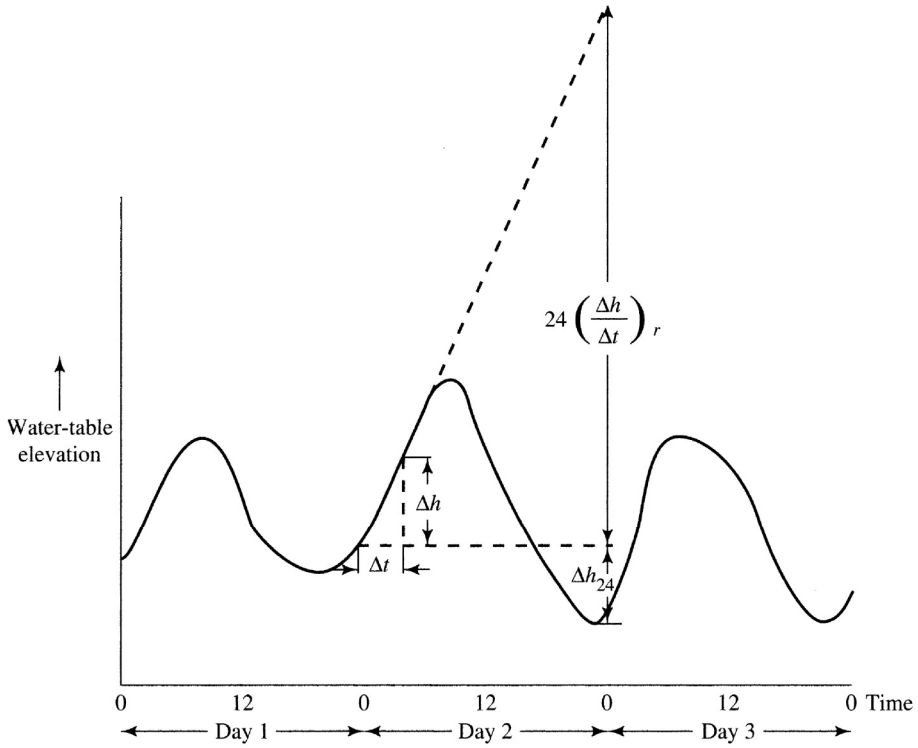

Figure 9.36 Estimation of evapotranspiration from the capillary fringe (capillary rise) using diurnal water-table fluctuations [equation (9.51)] [adapted from Freeze and Cherry (1979)].

fluctuations even with water tables at depths of 2 m or more. White (1932) suggested that evapotranspiration could be estimated from such diurnal water-table fluctuations as

$$ET = \left[24 \cdot \left(\frac{\Delta h}{\Delta t}\right)_r + \Delta h_{24}\right] \cdot S_y, \qquad \textbf{(9.51)}$$

where ET is the daily evapotranspiration [L], $(\Delta h/\Delta t)_r$ is the rate of rise of the water table during the period midnight to 4:00 AM, and Δh_{24} is the net fall in water level over the 24-hr period. This method was successfully used by Meyboom (as cited in Freeze and Cherry 1979), who suggested that the appropriate value of S_y used in equation (9.51) is one-half the conventional value.

Daniel (1976) developed a method for estimating evaporative extractions of ground water based on theoretical aquifer-drainage relations, and applied it successfully in Alabama.

9.5.5 Deep Seepage, G_{in} and G_{out}

In the context of the water-balance relations developed earlier [equations (9.21)–(9.23)], **deep seepage** refers to the ground-water inflow and outflow terms G_{in} and G_{out}, respectively. The magnitudes of these terms are very difficult to determine, and they are often assumed to be negligible or to cancel (i.e., $G_{out} = G_{in}$). However, the earlier discussion of regional ground-water flow suggests that it is often unwise to cavalierly adopt such assumptions.

9.5.5.1 Piezometer Measurements and Flow Nets

Installation of piezometers and observation wells at strategic locations gives the most definitive information about the magnitude of deep seepage. This information is most effectively used in combination with flow-net construction, as by Freeze and Witherspoon (1968). Winter et al. (1989) and Winter et al. (2003) combined piezometer observations with hydroclimatologic observations to develop information on the magnitude of deep seepage in smaller watersheds in many regions (see section 9.3.2), and found that it is often significant.

9.5.5.2 Water-Balance Analyses

9.5.5.2.1 Watershed Segments

Figure 9.37 shows a hypothetical drainage basin in which the main stream is gauged at N successive downstream locations. Starting at each of these locations, topographic divides can be delineated that define N subbasin segments, numbered $i = 1, 2, \ldots, N$ from upstream to downstream. If we assume that there is no flow across the main basin divides, and

that ground water as well as surface water moves only in the down-basin direction, the long-term average water balance for the *i*th segment is

$$Q_i = (P_i - ET_i) \cdot A_i + G_{i-1} - G_i + Q_{i-1}, \quad \textbf{(9.52)}$$

where Q is stream outflow [$L^3\ T^{-1}$], P and ET are areal average precipitation and evapotranspiration rates, respectively [$L\ T^{-1}$], A is the area of the segment [L^2], and G is ground-water outflow rate [$L^3\ T^{-1}$].

If we assume that all the quantities in equation (9.52) can be determined with reasonable precision except the G terms, there are N equations of the form of (9.52) with $N + 1$ unknowns (including G_0). However, if G_0 as well as $Q_0 = 0$ as assumed, there are actually only N unknowns, and the ground-water outflow for the *i*th segment can be found as

$$G_i = (P_i - ET_i) \cdot A_i + G_{i-1} + Q_{i-1} - Q_i. \quad \textbf{(9.53)}$$

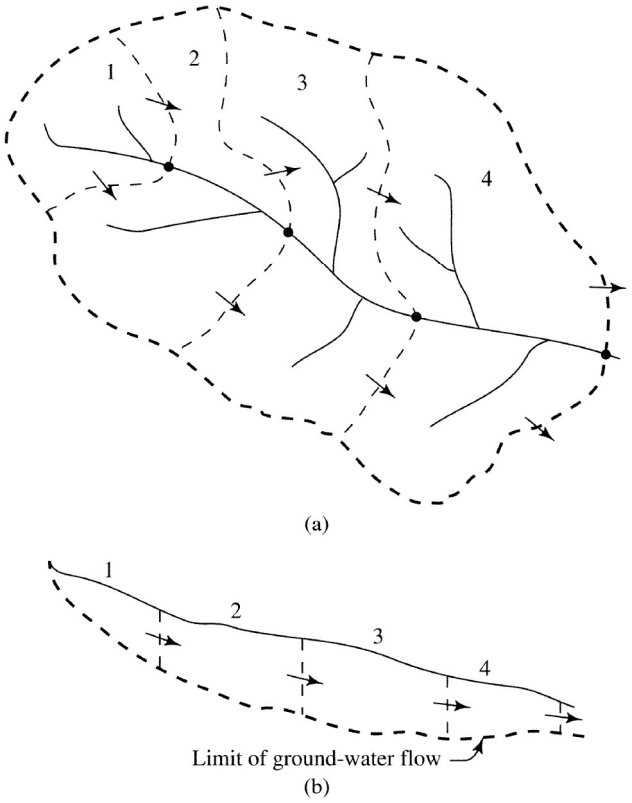

Figure 9.37 Schematic diagram defining terms for derivation of water-balance estimates of deep seepage [equations (9.52)–(9.53)]. Arrows indicate general direction of ground-water flow, dots are gauging stations. (a) Plan view of basin showing segments. (b) Longitudinal cross section.

Box 9.9 gives an example application of equation (9.53). However, as with all water-balance approaches, the uncertainty in all the "known" terms is hidden in the terms found by subtraction.

9.5.5.2.2 Water Balance as a Function of Basin Elevation

As discussed in section 4.1.5, average precipitation (P) is a strong function of elevation in many regions. Since average evapotranspiration (ET) is strongly related to average air temperature, which decreases with elevation, ET usually decreases with elevation. Dingman (1981) developed relations for estimating P and ET as functions of elevation in northern New England and then compared values of $P - Q$ with ET, where Q is measured average streamflow for small watersheds that each span a limited range of elevation. The results are shown in figure 9.38 on p. 441: The presence of ground-water outflow is indicated for watersheds in which $(P - Q) > ET$. The data suggest that many higher-elevation watersheds in northern New England have deep-seepage outflows on the order of 100 mm/yr.

9.5.5.2.3 Regional Water Balance

Schaller and Fan (2009) presented a quantitative survey of ground-water inflows and outflows based on a simple water-balance analysis for some 1,555 watersheds over the contiguous United States. Watershed surplus (recharge, R) was calculated at a resolution of ~10 km as

$$R = P - ET, \quad \textbf{(9.54)}$$

where P was determined from gridded observations, and ET from a 50-year simulation using a hydrologic model. The recharge was partitioned into streamflow, Q, and ground-water outflow, G_{out}:

$$R = Q + G_{out}, \quad \textbf{(9.55a)}$$

i.e., G_{out} was calculated as

$$G_{out} = R - Q = P - ET - Q, \quad \textbf{(9.55b)}$$

where Q was measured at gauging stations selected to minimize the effects of reservoir operations, ground-water extraction, and other artificial influences. The ratio Q/R (the fraction of recharge that leaves the watershed as streamflow) was used to characterize this partition: If $Q/R > 1$, the observed river flow includes ground-water inflow from other watersheds, and the basin is a ground-water importer; if $Q/R < 1$, the watershed is a ground-water exporter.

The results are shown in figure 9.39 on p. 442. Values of Q/R ranged from < 0.1 (> 90% of recharge exits as ground-water outflow, G_{out}) to > 2 (> 50% of the streamflow is imported ground water, G_{in}). Half (49.6%) of the watersheds examined are ground-water exporters and half are importers. As would be expected, Q/R values greater or less than 1 were more frequent in arid regions (P < 500 mm/yr; figure 9.39b); they are more common in watersheds with recharge-controlled water tables as indicated by the water-table ratio (WTR) described in section 9.2.5.2. There is a tendency of the Q/R ratio to be closer to 1 with increasing watershed area (figure 9.39c), consistent with regional ground-water flow dynamics. There is no clear relation between Q/R and elevation (figure 9.38d). However, the watersheds studied were

Box 9.9 Example Calculation of G_{in} and G_{out} from Watershed-Segment Water Balances

Table 9B9.1 gives areas and long-term average values of precipitation, evapotranspiration, and streamflow for four segments of the Contoocook River basin in central New Hampshire.

Table 9B9.1

Watershed segment, *i*	Stream Gauge at	Area, *A* (km^2)	Average Streamflow (m^3/s)	Precipitation, *P* (mm/yr)	Evapotranspiration, *ET* (mm/yr)
1	Peterboro	176	3.31	1,300	500
2	Henniker	777	18.0	1,180	500
3	W. Hopkinton	153	10.7	1,020	550
4	Penacook	878	35.5	1,070	550

We want to estimate the ground-water outflow, G_i from each segment using the method and assumptions of section 9.5.5.2.1. For the first (upstream-most) segment, we assume no stream or ground-water inflow, and equation (9.53) gives

$$G_1 = [(1{,}300 - 500)\ \text{mm/yr}] \times (176\ \text{km}^2) \times [3.17\times10^{-5}\ \text{m}^3/\text{yr}/(\text{mm}\cdot\text{km}^2\cdot\text{s})] + 0\ \text{m}^3/\text{s} + 0\ \text{m}^3/\text{s} - 3.31\ \text{m}^3/\text{s} = 1.15\ \text{m}^3/\text{s}.$$

For the second segment, we have

$$G_2 = [(1{,}180 - 500)\ \text{mm/yr}] \times (777\ \text{km}^2) \times [3.17\times10^{-5}\ \text{m}^3/\text{yr}/(\text{mm}\cdot\text{km}^2\cdot\text{s})] + 1.15\ \text{m}^3/\text{s} + 3.31\ \text{m}^3/\text{s} - 18.0\ \text{m}^3/\text{s} = 3.21\ \text{m}^3/\text{s}.$$

Similarly, the third and fourth segments yield the results in table 9B9.2.

Table 9B9.2

Segment, *i*	G_i (m^3/s)	G_i/Q_i
1	1.15	0.35
2	3.21	0.18
3	3.76	0.19
4	2.50	0.07

These computations suggest that deep seepage is a significant component of the water balance in the Contoocook River basin. Note that the calculated proportion of outflow occurring as ground water decreases downstream, as would be expected as larger watersheds capture more ground water. The uncertainties in these estimates should be assessed (section 1.11.2) before accepting these conclusions (see exercise 9.12).

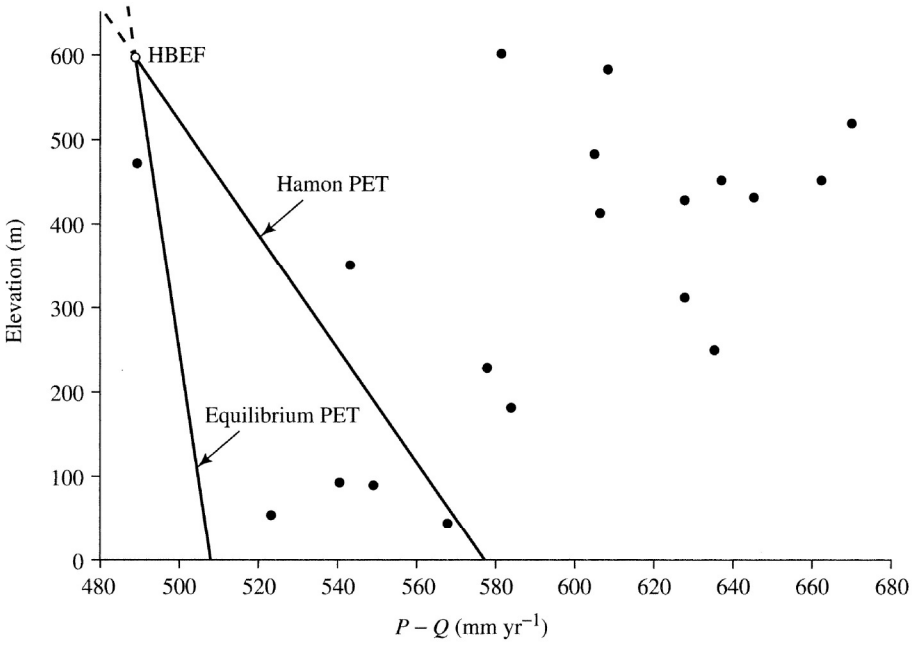

Figure 9.38 Long-term average precipitation (*P*) minus streamflow (*Q*) versus mean basin elevation for 19 small gauged basins in New Hampshire and Vermont. The lines are estimates of potential evapotranspiration (*PET*) using the Hamon and equilibrium estimates (see section 6.7.2.2), with the value determined at Hubbard Brook Experimental Forest (HBEF) as control. The existence of deep seepage is suggested for basins that plot to the right of the *PET* lines [reproduced from Dingman (1981), Elevation: A major influence on the hydrology of New Hampshire and Vermont, USA. *Hydrological Sciences Bulletin* 26:399–413, courtesy of International Association of Hydrological Sciences].

not characterized geologically or examined regionally, and doing so might have brought out that relation.

Although unaccounted for, artificial water transfers and uncertainty in the estimates of precipitation and evapotranspiration could have affected Schaller and Fan's (2009) Q/R values. However, their results suggest that ground-water outflow or inflow can be a significant portion of a watershed's water budget and emphasize the need for careful assessment of watershed water-budget components.

9.6 Impacts of Ground-Water Development on Areal Hydrology

Ground water is of course a major source of water for domestic, industrial, and agricultural uses. In many regions, the extraction of ground water has major impacts on local and regional hydrology, affecting streamflow, lake and wetland levels, coastal ecology, water quality, and land subsidence (box 9.2). The goal of this section is to provide a basic understanding of these impacts.

We focus on unconfined aquifers, because they have the most direct connections with other portions of the land phase of the hydrologic cycle and their exploitation as water sources has the most direct impacts on regional hydrology. However, we will use the mathematically simpler but essentially similar behavior of confined aquifers to illustrate the most basic features of the effects of the extraction of ground water on drainage-basin hydrology. This is justified because the behavior of unconfined aquifers is nearly identical to that of confined aquifers as long as the changes in water-table elevation are small relative to the saturated thickness.

To further simplify the discussion we consider only homogeneous, isotropic aquifers, simple aquifer configurations, and fully-penetrating wells. General ground-water texts such as Bear (1979), Freeze and Cherry (1979), and Fetter (2001) explore more exact models of ground-water development in unconfined flows and in more complex boundary conditions.

9.6.1 Hydraulics of Ground-Water Development

9.6.1.1 Radial Flow to a Well

Consider the highly idealized case of a well completely penetrating a homogeneous unconfined aquifer of infinite extent resting on a horizontal impermeable base (figure 9.40 on p. 443). The water table is initially horizontal everywhere at a height h_0 above the base and there is no recharge or capillary rise.

When the well is pumped at a constant rate Q_w, water is withdrawn from aquifer storage, the water table declines toward the well, and flow is induced toward the well from all directions. Thus the flow has radial symmetry, and if we approximate the unconfined case by equivalent confined conditions (i.e., assume negligible water-table decline and horizontal streamlines and ignore a transient initial period prior to the establishment of gravity drainage), it can be described by transforming the two-dimensional form of the general ground-water equation [equation (9B1.8)] to polar coordinates (Freeze and Cherry 1979):

$$\frac{\partial^2 h}{\partial r^2} + \frac{1}{r} \cdot \frac{\partial h}{\partial r} = \frac{S_y}{K_h \cdot h_0} \cdot \frac{\partial h}{\partial t}, \qquad \textbf{(9.56)}$$

where r is the radial distance measured outward from the well.

Theis (1935) showed that an analytical solution for equation (9.56) is

$$h_0 - h(r,t) = \frac{Q_w}{4 \cdot \pi \cdot K_h \cdot h_0} \cdot W[u(r,t)], \qquad \textbf{(9.57)}$$

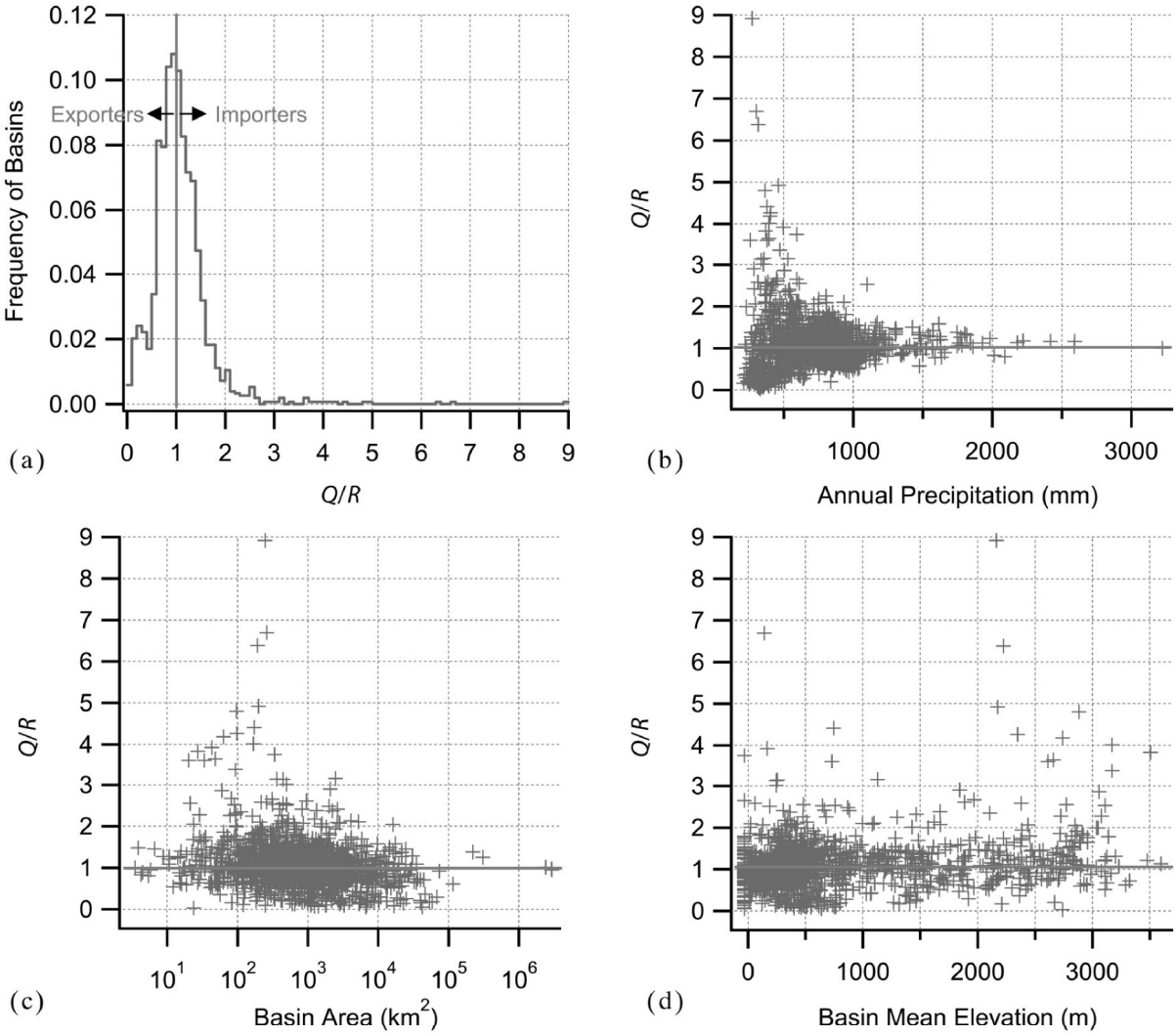

Figure 9.39 (a) The frequency of basins found at a given *Q/R* ratio, (b) the ratio as a function of annual precipitation, (c) the ratio as a function of basin area, and (d) the ratio as a function of mean basin elevation [Schaller and Fan (2009). River basins as groundwater exporters and importers: Implications for water cycle and climate modeling. *Journal of Geophysical Research* 114, with permission of the American Geophysical Union].

where

$$W[u(r,t)] \equiv \int_{u(r,t)}^{\infty} \frac{\exp[-u(r,t)]}{u(r,t)} \cdot \mathrm{d}u(r,t) \qquad \textbf{(9.58)}$$

and $u(r,t)$ is a measure of the aquifer response time similar to equation (9.12):

$$u_{r,t} \equiv \frac{S_y \cdot r^2}{4 \cdot K_h \cdot h_0 \cdot t}. \qquad \textbf{(9.59)}$$

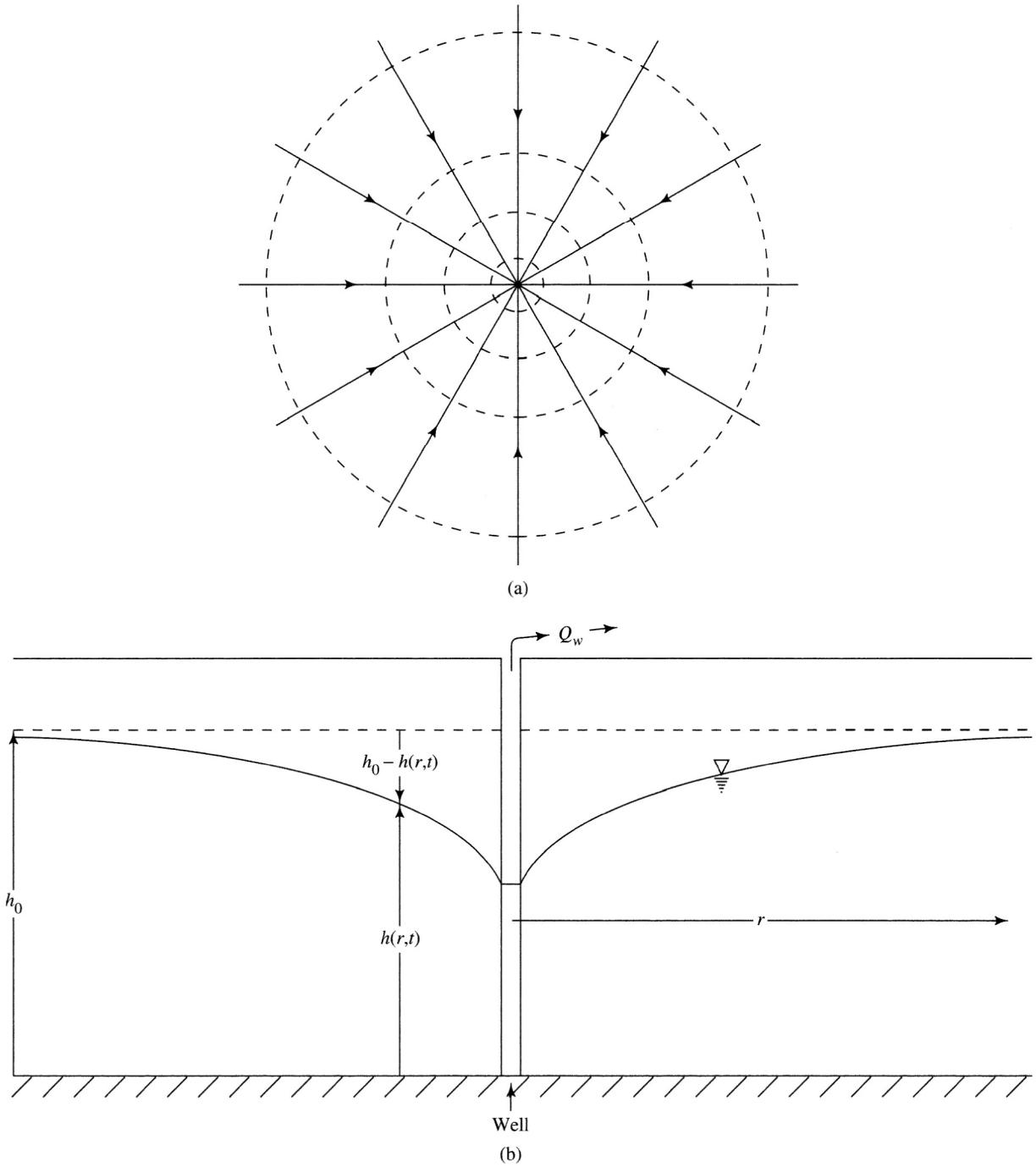

Figure 9.40 Definitions of terms for equations describing radial flow to a well in an unconfined aquifer [equations (9.56)–(9.59)]. (a) Plan view; dashed lines are equipotentials, arrows show flow directions. (b) Cross section.

The function $W[u(r,t)]$ is known as the **well function**; its values are tabulated in table 9.3. The quantity $[h_0 - h(r,t)]$ is the **drawdown**, and when its values are plotted as a function of distance at any time they define a **drawdown curve** or, in three dimensions, a **cone of depression** that is asymptotic to h_0. Box 9.10 shows how this relation is applied.

The area over which the pumping causes drawdown is called the **area of influence**. For the idealized situation of figure 9.40, the lines of equal drawdown and the extent of the cone of depression are circular in plan view and the area of influence coincides with the projected area of the cone.

Clearly, the drawdown is proportional to pumping rate, and it decreases with distance at any time and increases with time at any distance. For a given pumping rate and a given duration of pumping, the rates of change are controlled by the aquifer properties. At a given time,

- lower $K_h \rightarrow$ larger drawdown spread over a smaller area
- higher $K_h \rightarrow$ smaller drawdown spread over a greater area
- lower $S_y \rightarrow$ larger drawdown spread over a greater area
- higher $S_y \rightarrow$ smaller drawdown spread over a smaller area

An interesting and useful property of the solution to equation (9.56) is that the drawdown at any location due to the pumping of more than one well is equal to the sum of the drawdowns that would be produced at that location by each of the wells individually.

9.6.1.2 Contributing Areas

The **contributing area** of a well is the area on the land surface above the portion of aquifer from which water is flowing to the well. Identification of this area for unconfined aquifers receiving recharge from infiltration and/or surface-water bodies is important because (1) the levels of ground-water-fed lakes or streams in the contributing area will be affected by pumping and (2) any water-contaminating substances introduced into the contributing area will eventually reach the well. The delineation of these areas by analytical and numerical methods was reviewed by Morrissey (1987).

Table 9.3 Values of $W[u(r,t)]$ for Various Values of $u(r,t)$.[a]
Example: For $u(r,t) = 4.0\times10^{-5}$, $W[u(r,t)] = 9.55$.

$u(r,t)$	1.0	2.0	3.0	4.0	5.0	6.0	7.0	8.0	9.0
$\times 1$	0.219	0.049	0.013	0.0038	0.0011	0.00036	0.00012	0.000038	0.000012
$\times 10^{-1}$	1.82	1.22	0.91	0.70	0.56	0.45	0.37	0.31	0.26
$\times 10^{-2}$	4.04	3.35	2.96	2.68	2.47	2.30	2.15	2.03	1.92
$\times 10^{-3}$	6.33	5.64	5.23	4.95	4.73	4.54	4.39	4.26	4.14
$\times 10^{-4}$	8.63	7.94	7.53	7.25	7.02	6.84	6.69	6.55	6.44
$\times 10^{-5}$	10.94	10.24	9.84	9.55	9.33	9.14	8.99	8.86	8.74
$\times 10^{-6}$	13.24	12.55	12.14	11.85	11.63	11.45	11.29	11.16	11.04
$\times 10^{-7}$	15.54	14.85	14.44	14.15	13.93	13.75	13.60	13.46	13.34
$\times 10^{-8}$	17.84	17.15	16.74	16.46	16.23	16.05	15.90	15.76	15.65
$\times 10^{-9}$	20.15	19.45	19.05	18.76	18.54	18.35	18.20	18.07	17.95
$\times 10^{-10}$	22.45	21.76	21.35	21.06	20.84	20.66	20.50	20.37	20.25
$\times 10^{-11}$	24.75	24.06	23.65	23.36	23.14	22.96	22.81	22.67	22.55
$\times 10^{-12}$	27.05	26.36	25.96	25.67	25.44	25.26	25.11	24.97	24.86
$\times 10^{-13}$	29.36	28.66	28.26	27.97	27.75	27.56	27.41	27.28	27.16
$\times 10^{-14}$	31.66	30.97	30.56	30.27	30.05	29.87	29.71	29.58	29.46
$\times 10^{-15}$	33.96	33.27	32.86	32.58	32.35	32.17	32.02	31.88	31.76

[a]Interpolated values can be estimated using the method of Barry et al. (2000).

Source: Wenzel (1942).

Box 9.10 Example Calculations: Drawdown and Stream Depletion

Example Drawdown Calculation

Here we compute the drawdown at various distances from a well (r = 1, 5, 10, 50, and 100 m) at various times after pumping begins (t = 1, 2, 40, and 80 hr). We assume an ideal homogeneous horizontal aquifer with $K_h = 10^{-5}$ m/s, $h_0 = 20$ m, $S_y = 0.20$, a constant pumping rate $Q_w = 0.001$ m^3/s (= 86.4 m^3/day), and no interaction with surface-water bodies. For the first values of time and distance we use equation (9.59) to find $u(r,t)$ as

$$u(1\text{ m},\ 3{,}600\text{ s}) = \frac{0.2\times(1\text{ m})^2}{4\times\left(10^{-5}\text{ m/s}\right)\times(20\text{ m})\times(3{,}600\text{ s})} = 0.07. \qquad \textbf{(9B10.1)}$$

Repeating this for all combinations of time and distance gives the values of $u(r,t)$ in table 9B10.1.

Table 9B10.1 $u(r, t)$

t (s)	r = 1 m	r = 5 m	r = 10 m	r = 50 m	r = 100 m
3,600	0.07	1.74	6.94	173.61	694.44
7,200	0.03	0.87	3.47	86.81	347.22
144,000	0.00	0.04	0.17	4.34	17.36
288,000	0.00	0.02	0.09	2.17	8.68

From table 9.3 we find the values of $W[u(r,t)]$ that correspond to the above values of $u(r,t)$ [table 9B10.2; interpolated using approximation of Barry et al. (2000)].

Table 9B10.2 $W[u(r,t)]$

t (s)	r = 1 m	r = 5 m	r = 10 m	r = 50 m	r = 100 m
3,600	2.16	0.07	0.00	0.00	0.00
7,200	2.82	0.28	0.01	0.00	0.00
144,000	5.78	2.60	1.34	0.00	0.00
288,000	6.47	3.27	1.96	0.04	0.00

Finally, the drawdown is calculated by multiplying the above values of $W[u(r,t)]$ by

$$\frac{Q_w}{4\cdot\pi\cdot K_h\cdot h_0} = \frac{0.001\text{ m}^3/\text{s}}{4\times 3.14\times\left(10^{-5}\text{ m/s}\right)\times(20\text{ m})} = 0.398\text{ m} \qquad \textbf{(9B10.2)}$$

to give $h_0 - h(r,t)$ in m. The results are found in table 9B10.3.

Table 9B10.3 Drawdown, $h_0 - h(r,t)$ (m)

t (s)	r = 1 m	r = 5 m	r = 10 m	r = 50 m	r = 100 m
3,600	0.86	0.03	0.00	0.00	0.00
7,200	1.12	0.11	0.00	0.00	0.00
144,000	2.30	1.04	0.53	0.00	0.00
288,000	2.58	1.30	0.78	0.02	0.00

(continued)

Example Stream-Depletion Calculation

Consider a well in an aquifer with the same properties as in the previous example, except it is located 20 m from a stream. To determine the streamflow depletion rate D_w at 1, 10, 30, 60, 180, and 365 days of continuous pumping, refer to equation (9.64) and calculate

$$\frac{K_h \cdot h_0}{x^2 \cdot S_y} = \frac{\left(10^{-5}\ \text{m/s}\right) \times (20\ \text{m})}{(20\ \text{m})^2 \times (0.20)} = 2.5 \times 10^{-6}\ \text{s}^{-1}. \qquad \textbf{(9B10.3)}$$

Table 9B10.4 shows the arguments of $D(\ )$ obtained by multiplying the value of equation (9B10.3) by the times of interest. The values of $D_w(t)/Q_w$ are then found from the curve in figure 9.43, and D_w is found by multiplying those values by Q_w.

Table 9B10.4 Argument of Depletion Function

Quantity	t = 1 day = 8.64×10^4 s	t = 10 days = 8.64×10^5 s	t = 30 days = 2.59×10^6 s	t = 60 days = 5.18×10^6 s	t = 180 days = 1.56×10^7 s	t = 365 days = 3.15×10^7 s
argument	0.216	2.16	6.48	13.0	38.9	78.8
$D_w(t)/Q_w$	0.11	0.62	0.77	0.82	0.90	0.92
D_w (m^3/s)	1.1×10^{-4}	6.2×10^{-4}	7.7×10^{-4}	8.2×10^{-4}	9.0×10^{-4}	9.2×10^{-4}

For the ideal, infinite, homogeneous aquifer with an initially horizontal water table described in the preceding section all the water extracted from the cone of depression eventually arrives at the well, and the contributing area at any time is identical to the area of influence. However, actual aquifers do not have horizontal water tables (which would imply no flow) and do not extend infinitely. If the water table is initially sloping, the cone of depression is no longer circular and the contributing area does not coincide with the area of influence (figure 9.41). If the aquifer is in a river valley, the contributing area may extend to or even beyond the river (figure 9.42 on pp. 448–449).

9.6.2 Effects of Ground-Water Extraction

9.6.2.1 Effects on Natural Recharge and Discharge

Consider the ground-water system of a drainage basin in which there is no ground-water flow in or out. Under natural (no development) conditions, the long-term average recharge and discharge for this system must be in balance, and from equation (9.23):

$$R_{nat} - Q_{GWnat} = 0, \qquad \textbf{(9.60)}$$

where the subscript "*nat*" denotes the natural recharge and discharge rates.

If one or more wells begins pumping from the system, water will be removed from aquifer storage as the cones of depression develop. In addition, the natural rates of recharge and/or discharge will in general be changed as the water-table configuration is altered by the pumping. Thus, during development, the water-balance for the system becomes

$$\left(R_{nat} + \Delta R\right) - \left(Q_{GWnat} + \Delta Q_{GW}\right) - \Sigma Q_w = \frac{\Delta S}{\Delta t}, \qquad \textbf{(9.61)}$$

where ΔR and ΔQ_{GW} are the changes in recharge and discharge, respectively, due to the water-table lowering induced by the pumping; ΣQ_w is the total pumping rate; and $\Delta S/\Delta t$ is the rate of change of aquifer storage ($\Delta S/\Delta t < 0$). Combining equations (9.60) and (9.61) yields

$$\Sigma Q_w = \Delta R - \Delta Q_{GW} - \frac{\Delta S}{\Delta t}. \qquad \textbf{(9.62)}$$

Equation (9.62) states that ground-water extraction must be balanced by a decrease in storage ($-\Delta S$, which always occurs) and, in general, by some combination of increased (induced) recharge ($+\Delta R$) and/or decreased ground-water discharge ($-\Delta Q_{GW}$). We now examine how water tables lowered by pumping affect ΔR and ΔQ_{GW}.

From the definition of recharge [equation (9.22)], we see that ΔR must be due to some combination of: (1) increased recharge from infiltration, R_I; (2) increased recharge from surface-water bodies,

R_{SW}; and (3) decreased capillary rise, CR. Lowered water tables due to pumping affect these components in the following ways:

R_I: As shown in figure 9.26, net recharge from infiltration tends to increase with water-table depth up to a point, beyond which there is little change.

R_{SW}: As shown in figure 9.42, the cone of depression from wells near streams can extend to the stream, locally reverse the

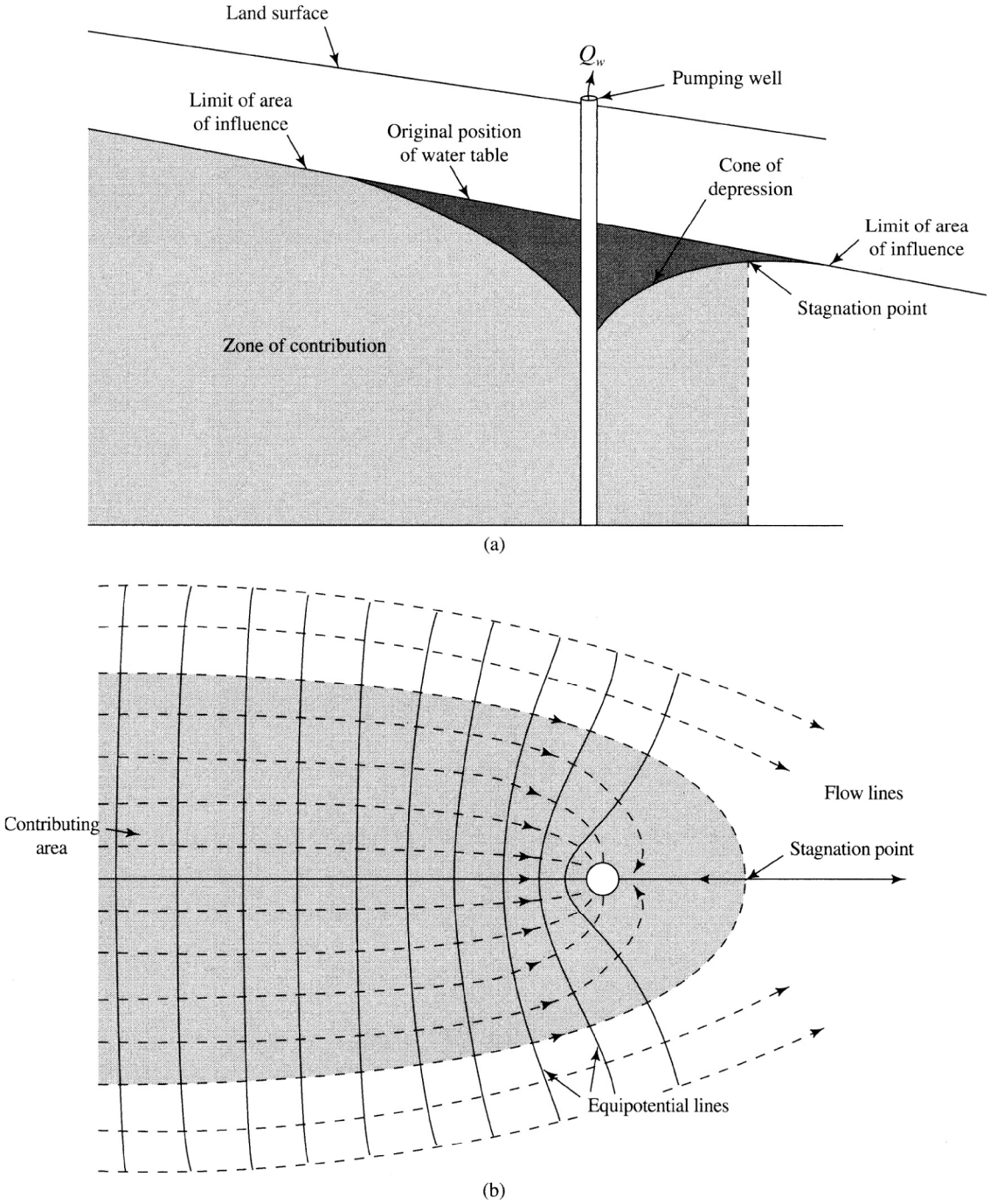

Figure 9.41 The cone of depression, area of influence, and contributing area for an aquifer with a sloping water table. (a) Cross section. (b) Plan view [adapted from Morrissey (1987)].

potential gradient, and induce recharge from the stream. (This effect is discussed further in the next section.)

CR: Again from figure 9.26, lowered water tables tend to decrease capillary rise by lowering the capillary fringe beyond the reach of plant roots.

Thus the overall effect of ground-water development tends to be a net increase in recharge; the magnitude of the effect will be highly dependent on the drainage-basin geology, topography, and climate and the placement and pumping rates of wells. In humid regions with gaining streams, lakes, and wetlands, much of this will be due to water loss from surface water (ΔR_{SW}).

It should be clear from the preceding discussion that some "mining"—i.e., removal of water from aquifer storage—occurs with any extraction rate. However, if a constant rate of ground-water extraction is imposed on a region for a sufficient time, a new equilibrium state *may* eventually be reached in which there is no further change in storage ($\Delta S/\Delta t = 0$); if this occurs, the extraction rate (ΣQ_w) is supplied by increased recharge ($\Delta R_I + \Delta R_{SW} > 0$) and/or reduced discharge ($\Delta CR + \Delta Q_{GW} < 0$). Bredehoeft et al. (1982) pointed out that the time required to reach this equilibrium may be very long indeed (hundreds of years), depending on the region's size, hydrology, and geology and on the locations and pumping rates of wells. In some situations, it is not possible to reach an equilibrium state before drawdown at wells equals its maximum value, i.e., the water table is drawn down to the bottom of the deepest well. Only detailed ground-water modeling studies can evaluate a given situation.

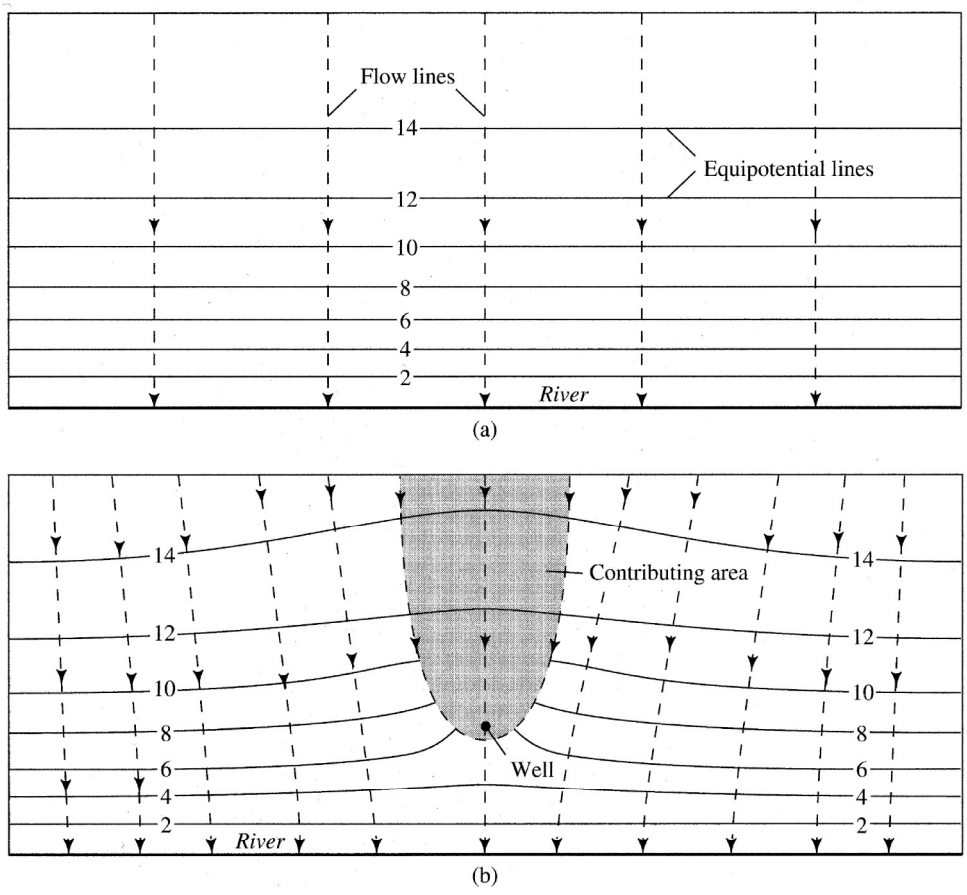

Figure 9.42 Contributing areas and water-table contours for wells near a river. (a) Natural condition before pumping. (b) Well intercepts water that was flowing to the river. (c) Well intercepts water and extracts flow from the river. (d) Well intercepts water from both sides of the valley and extracts water from the river. Existence of conditions (b), (c), or (d) depends on pumping rate and aquifer configuration and properties [Morrissey (1987)].

9.6.2.2 Effects on Streams

As shown in figure 9.42, ground-water extraction can reduce streamflow by: (1) inducing local recharge from a gaining stream ($\Delta R_{SW} > 0$) and (2) intercepting water that would naturally discharge to streams ($\Delta Q_{GW} < 0$). The net of these two effects is called **stream depletion**, D_w:

$$D_w \equiv \Delta R_{SW} - \Delta Q_{GW}. \qquad \textbf{(9.63)}$$

Jenkins (1968) showed that, under the same idealized aquifer conditions used to solve equation (9.56), the ratio of stream depletion rate to a constant rate of pumping, Q_w, from a well located a distance x from a stream is given by a **depletion function**, D, where

$$\frac{D_w(t)}{Q_w} = D\left(\frac{K_h \cdot h_0 \cdot t}{x^2 \cdot S_y}\right). \qquad \textbf{(9.64)}$$

Figure 9.43 gives the form of this depletion function; note that depletion rate is a function of the aquifer properties (K_h, S_y, h_0) and the distance of the well from the stream (x), and that the function is asymptotic to $D_w(t)/Q_w = 1$. Thus the fraction of pumpage that comes from the river increases with time until ultimately all the water withdrawn by the well comes from streamflow.

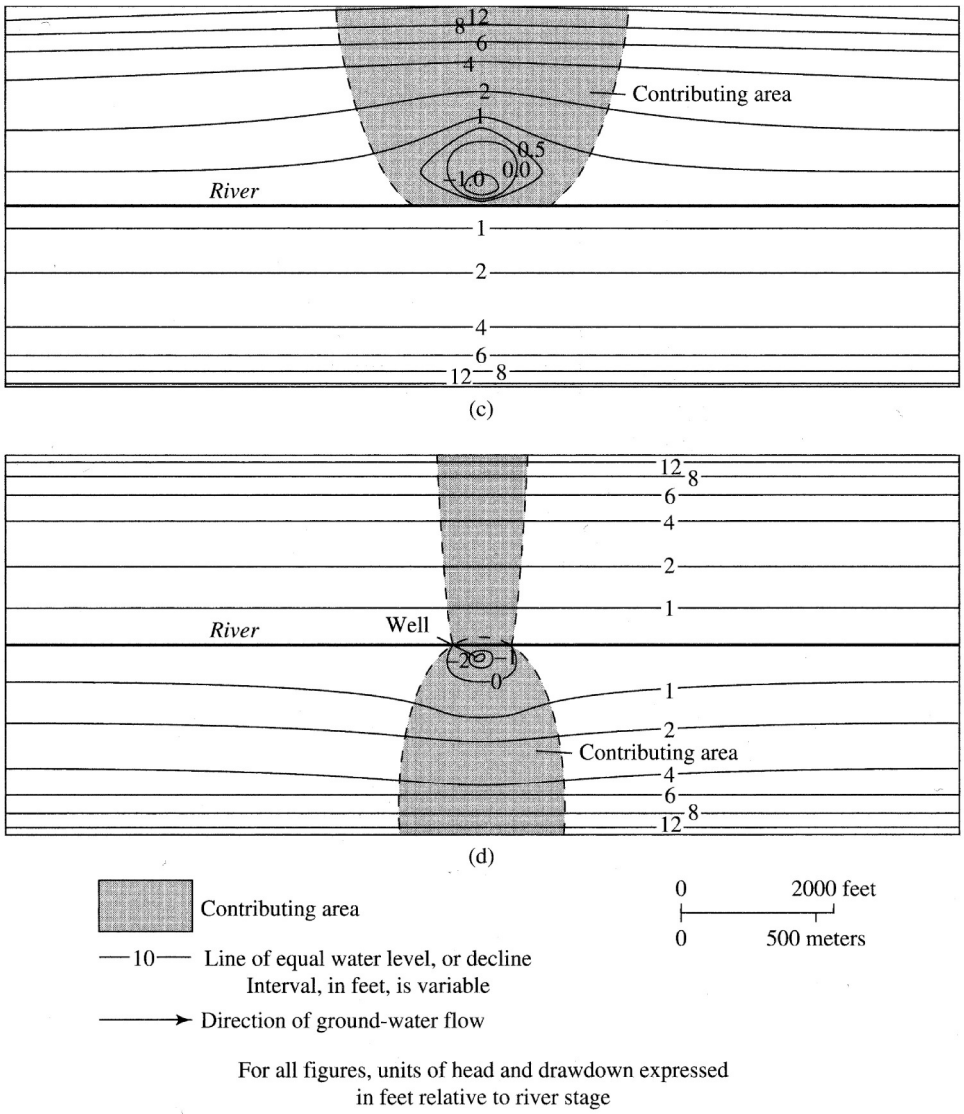

Figure 9.42 *(continued)*

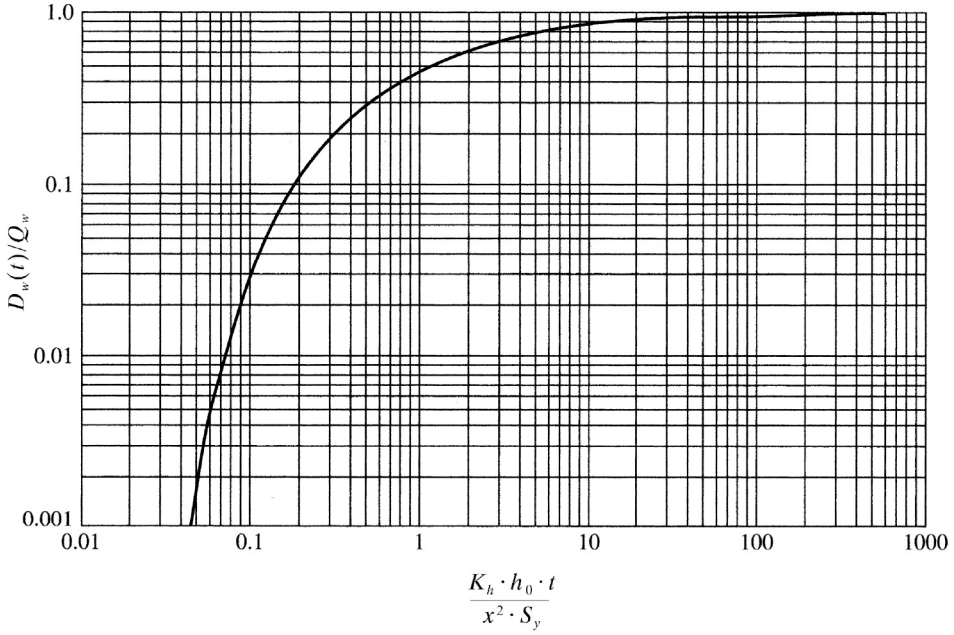

Figure 9.43 The stream-depletion function, $D_w(t)/Q_w$, as a function of $K_h \cdot h_0 \cdot t/(x^2 \cdot S_y)$. See example in box 9.10 [reproduced from Jenkins (1968), Techniques for computing rate and volume of stream depletion by wells. *Ground Water* 6(2):37–46, with permission from Wiley].

Box 9.10 gives an example of the application of this relation to estimating streamflow depletion rates. Jenkins (1968) gave additional examples, and showed how the relation can be used to estimate depletion rates and volumes due to continual and intermittent pumping.

9.6.2.3 Salt-Water Intrusion

Consider a well located above the fresh-salt interface in a coastal aquifer like that shown in figure 9.23. By the Ghyben–Herzberg principle (box 9.5), the elevation of the interface will increase by 40 m for every 1 m in drawdown caused by pumping. Thus if the drawdown at the well approaches 1/40th of the vertical distance between the bottom of the well and the interface, the well is likely to pump salt water.

To the extent that the idealized conditions assumed in deriving them are not satisfied, equations (9.57)–(9.59) will not exactly predict the drawdown in a coastal aquifer. This may occur when the aquifer is not quasi-infinite, the well is not fully penetrating, or the interface between fresh and salt water is not sharp. Modified versions of those equations are available to account for these complicating conditions (Freeze and Cherry 1979).

9.6.3 "Safe Yield"

It is widely believed, even by many hydrologists and water-resource managers, that the sustainable rate of extraction—or "**safe yield**"—of ground water from a basin equals the rate of natural recharge, R_{nat}. It should be clear from the preceding discussion that this is not true: Equation (9.62) shows that the rate of extraction is supplied by a decrease in storage and, in general, by *changes* in recharge and/or discharge. R_{nat} itself does not enter into that equation, and in fact is relevant to the determination of safe yield only to the extent that it should be accounted for in ground-water models (Bredehoeft et al. 1982; Bredehoeft 1997, 2002; Zhou 2009). Instead,

> **Safe yield** (or **sustainable yield**) is best defined as the rate at which ground water can be withdrawn without producing undesirable effects (Lohman 1979).

The preceding discussion has identified the most important hydrologic impacts of ground-water extraction, and most of these have potentially undesirable effects:

- Reductions of streamflow may seriously reduce surface water available for instream (e.g., wildlife habitat, waste dilution, hydropower, recreation, navigation) and withdrawal (water supply, irrigation) uses.
- Levels and/or extents of lakes and wetlands may be reduced, with consequent loss of valued habitat and recreational value.

- Extent of areas where water is available to plants that exploit the capillary fringe (phreatophytes) may be reduced, with consequent loss of habitat.
- Ground-water outflow to the ocean may be reduced, with consequent effect on coastal wetlands and/or nearshore benthic marine habitats.
- Lowered water table may cause land subsidence as some of the overburden stresses formerly supported by ground water are transferred to the mineral grains (box 9.2). Land subsidence of up to 9 m has occurred due to extraction of ground water for irrigation in the Central Valley of California.
- Costs of pumping, which are proportional to depth of water table, rise.
- Water tables lowered by one developer may fall below depths of nearby wells belonging to others, perhaps resulting in legal action.
- The fresh-salt interface may be raised, increasing the likelihood of salt-water intrusion.

Because of the varying importance of all these hydrologic effects and their economic, social, environmental, and legal consequences in different regions, and within a given region, there is no general formula for computing "safe yield." Acceptable rates of development can only be determined by: (1) determining the likely hydrologic effects of various combinations of rates, timing, and location of ground-water extraction, which requires ground-water modeling; (2) assessing the environmental, economic, legal, and social impacts of these effects; and (3) balancing the benefits afforded by the ground water against the undesirable consequences of the various schemes.

▼ EXERCISES

1. Given the following measurements at individual piezometers, calculate (a) the hydraulic head, (b) the pressure head, (c) the elevation head, and (d) the pressure:

Piezometer→	**A**	**B**	**C**	**D**	**E**
Ground surface elevation (m)	450	100	320	65	210
Piezometer depth (m)	150	100	80	120	20
Depth to water surface (m)	27	65	55	40	10

2. Piezometers A, B, and C are located 1,000 m apart in a horizontal aquifer. A is due south of B, and C is due east of a line between A and B. Given the data in the table below, determine (a) the direction of ground-water through the triangle ABC and (b) the hydraulic gradient.

Piezometer→	**A**	**B**	**C**
Ground surface elevation (m)	95	110	135
Depth to water surface (m)	5	30	35

3. A horizontal aquifer with a thickness of 45 m is subjected to pumping that lowers the pressure head by 25 m. Assuming an aquifer compressibility of $\alpha = 1.8\times10^{-8}$ m^2/N, how much does the aquifer compact?
4. Obtain information about the general geology and ground-water environment of your region. For the United States, information can be accessed at http://water.usgs.gov/ogw/gwrp/activities/regional.html. Write a brief report summarizing the general geology and regional ground-water flow, including:
   a. Typical values of ground-water residence times [equation (9.14)].
   b. Which of the fundamental hydrologic landscape units (FHLUs) shown in figure 9.15 most closely applies to your region?
   c. Likely typical values of the water-table ratio (*WTR*) [equation (9.16)].
   d. The implication of regional *WTR* values for computation of watershed water budgets.

5. Which of the stream types shown in figure 9.17 characterizes streams in your region? Are different types associated with streams of different sizes?
6. a. To what extent do streams in your area seem to conform to the Dupuit approximation (box 9.4)?
   b. Locate a stream-gauging station in your region and obtain annual flow data with which to estimate long-term average discharge, Q. In the United States, gauging stations can be located via the USGS website (http://www.usgs.gov/water) and average discharge data can be directly obtained through the WaterWatch website (http://waterwatch.usgs.gov) by clicking on "Toolkit," followed by entering the name or number of the stream-gauging station of interest. Estimate the proportion of streamflow from ground water, Q_{GW}/Q, via equation (9.18), using topographic maps or Google Earth to estimate a regional value of interstream spacing X and stream length L for the selected gauge.
7. It is often stated that riparian wetlands reduce downstream flooding by acting as "sponges" that absorb flood water from upstream. Evaluate that belief based on the discussion in section 9.3.2.
8. Compute the base-flow index (*BFI*) for one year for a USGS stream gauge as specified by your instructor, following the instructions in box 9.8 to download the data and compute the *BFI* in a spreadsheet. (Ideally, different students could compute values for different streams for the same year and compare *BFI* values.)
9. A series of observation wells (piezometers) are installed in a straight line at varying distances from the edge of a small reservoir in Durham, New Hampshire. The table below gives the distances from the reservoir, the heights of the top of the well casing (TOC) above the ground surface, the ground-surface elevations, and the depth to water table from TOC as measured in October 2000 and October 2001.

Location →	**Reservoir**	**Well 1**	**Well 2**	**Well 3**	**Well 4**	**Well 5**
Distance from reservoir (m)	——	4.79	32.62	53.87	75.03	105.88
Ground elevation (m.a.s.l.)	24.16	25.35	26.18	26.28	26.23	27.98
TOC elevation (m.a.s.l.)		25.95	26.82	27.08	26.93	29.20
Depth to water table from TOC (m) in 2000	0.87*	0.88	1.38	1.38	1.11	2.76
Depth to water table from TOC (m) in 2001	0.38*	1.40	2.27	2.51	2.35	4.49
*Depth of water above point of ground-elevation measurement at edge of reservoir.						

   a. Calculate the water-table elevations at each well and the reservoir water-surface elevations for the two years.
   b. Graph the ground and water-table elevations along the profile for the two years. Use an appropriate degree of vertical exaggeration. Show the locations of all measurements and the calculated elevations.
   c. Write a paragraph summarizing your observations. Is the relation of ground water to surface water typical of humid regions?
10. Outer Cape Cod at Eastham, Massachusetts, is a 4,800-m wide north/south-trending peninsula consisting of glacially deposited sands and gravels. Ground water discharges into the Atlantic Ocean to the east and Cape Cod Bay to the west. Recharge from precipitation = 0.46 m/yr; the aquifer specific yield is 0.15 and hydraulic conductivity is 75 m/day.
   a. Calculate and graph the water-table profile and depth to salt-water/fresh-water interface from the center of the peninsula to either coast, accounting for the outflow face.
   b. Calculate the width of the outflow face.
   c. Calculate the discharge per length of coastline through the outflow face.
11. Figure 9.32 shows a portion of a flow net adjacent to one-half a symmetrical stream. Assume that the flow net is spatially and temporally representative of a reach of length L = 1,500 m, that the aquifer is homogeneous and isotropic with a hydraulic conductivity K_h =

10^{-5} m/s, and that the equipotentials are drawn at Δh = 1 m intervals. What is the ground-water contribution to streamflow Q_{GW} for this reach?

12. Construct a spreadsheet program to explore the effects of various degrees of relative uncertainty in estimates of precipitation and evapotranspiration on the G terms estimated in the example in box 9.9 (see section 1.11.2). Typical 95% confidence levels for relative errors are 5% for streamflow and 10% for precipitation and evapotranspiration. Does your analysis tend to confirm or cast doubt on the hypothesis that deep seepage is important in this region?
13. Find a drainage basin in your region in which an analysis like that of box 9.9 can be done. Carry out the analysis and test for the effects of uncertainty on your estimates of deep seepage.
14. Using the WellFunc.xls spreadsheet on the disk accompanying the text, compute the drawdown for a well pumping 3,000 m^3/day for distances up to 3 km and times up to 10 yr from an aquifer with a hydraulic conductivity of K_h = 30.5 m/day and a specific yield of S_y = 0.15.
15. Use the spreadsheet program WellFunc.xls to compute drawdowns as a function of distance and time for an aquifer typical of your region. How well do the assumptions involved in deriving the well function apply for this case?
16. Use WellFunc.xls to explore the effects of varying at least two of the variables Q_w, K_h, S_y, and h_0 on drawdown for a typical aquifer in your region and write a paragraph describing your results.
17. What are the most important potential adverse impacts of ground-water development in your region? Is there evidence that any of these impacts have occurred? What studies would you recommend for determining safe yield in your region?

▼ NOTES

[1] Ground-water hydrologists often distinguish between the **primary porosity**, which is the original intergranular porosity of a soil or sedimentary deposit, and the **secondary porosity**, which is due to void spaces developed subsequently by fracturing and/or dissolution.

[2] The effect of pumping on the ground-water balance is considered in the last section of this chapter.

[3] As described in sections 7.4.1 and 8.1.4, this water movement occurs in response to pressure gradients created by evapotranspiration that reduces the liquid water content in the vadose zone. Capillary rise can be a significant portion of basin evapotranspiration in many semiarid and arid regions where a class of vascular plants called **phreatophytes** grows near streams and obtains water via roots that extend to the capillary fringe. Saltcedar, arrowweed, cottonwood, cattails, and willows are common phreatophytes.